الجمهورية الجزائرية الديمقراطية الشعبية

République Algérienne Démocratique et Populaire
Ministère de L'Enseignement Supérieur et de la Recherche Scientifique

UNIVERSITÉ SETIF 1-Ferhat ABBAS

FACULTÉ DE TECHNOLOGIE

THÈSE

Présentée au Département de Génie des Procédés

Pour l'obtention du diplôme de

DOCTORAT

Domaine: Sciences et Technologie

Filière : Génie des Procédés **Option : Génie Chimique**

Par

KABOUB DOUNYA

THÈME

Caractérisation de biomatériaux à base de déchets agricoles en vue de l'élimination des polluants en solutions aqueuses.

Soutenue le 29/11/2025 devant le Jury :

OUARI Kamel	**Professeur**	**Univ. Sétif1-FerhatABBAS**	**Président**
KHELILI Hinda	**Professeur**	**Univ. Sétif1-FerhatABBAS**	**Directrice de thèse**
GUELLAL Messaoud	**Professeur**	**Univ. Sétif1-FerhatABBAS**	**Co-Directeur**
KAABI Ilhem	**MCA**	**Univ. Sétif1-FerhatABBAS**	**Examinateur**
OUNOKI Samira	**Professeur**	**Univ. Biskra**	**Examinateur**
ADAIKA Kaltoum	**MCA**	**Univ. Biskra**	**Examinateur**

الجمهورية الجزائرية الديمقراطية الشعبية

DEMOCRATIC AND POPULAR REPUBLIC OF ALGERIA
MINISTRY OF HIGHER EDUCATION AND SCIENTIFIC RESEARCH

Setif 1 University-Ferhat ABBAS

Faculty of technology

Thesis submitted to the Process Engineering Department for a Doctorate Degree

Domain: Science and Technology

Option: Chemical Engineering

Section :Process Engineering

BY

KABOUB DOUNYA

TITLE OF THE THESIS

Characterization of biomaterials based on agricultural waste for the elimination of pollutants in aqueous solutions.

Defended on 29/11/ 2025 in front of the Jury:

OUARI Kamel	**Professor**	**SETIF1University-Ferhat ABBAS**	**Chairman**
KHELILI Hinda	**Professor**	**SETIF1University-Ferhat ABBAS**	**Supervisor**
GUELLAL Messaoud	**Professor**	**SETIF1University-Ferhat ABBAS**	**Co-Supervisor**
KAABI Ilhem	**MCA**	**SETIF1University-Ferhat ABBAS**	**Examinator**
OUNOKI Samira	**Professor**	**Univ. Biskra**	**Examinator**
ADAIKA Kaltoum	**MCA**	**Univ. Biskra**	**Examinator**

Acknowledgements

First and foremost, I would like to express my deepest gratitude to Allah, the Almighty, for granting me the strength, patience, and foresight necessary to carry out this research work. Without His mercy and blessings, none of this would have been possible.

My sincere thanks go to my thesis supervisor, Pr. Hinda KHELILI, for her attentive supervision, insightful guidance, and unwavering support throughout this journey. Her scientific expertise and kindness were instrumental in the successful completion of this research.

I also extend my heartfelt gratitude to my co-supervisor, Pr. Messaoud GUELLAL, for his generosity, rigorous follow-up, and consistently valuable feedback, all of which greatly contributed to the advancement of my work.

I am particularly honored by the acceptance of Pr. Kamel OUARI to chair the jury for my defense. I warmly thank him for the time he has generously dedicated to evaluating this work and for the thoroughness and care he brings to this role.

I would like to sincerely thank all the members of the jury: Pr. Samira OUNOKI, Dr. Ilham KAABI, and Dr. Kaltoum ADAIKA. I am deeply grateful for your careful review, constructive feedback, and insightful comments, which will undoubtedly enhance the quality of this research.

Finally, my sincere thanks go to the entire team at the Chemical Process Engineering Laboratory (LGPC) of Setif 1 University, whose technical support and valuable collaboration were essential to the successful completion of my experiments.

Dedications

I would like to express my deep gratitude to my family, whose unconditional love, understanding and unwavering support have been an essential pillar for me. Their patience, their kindness and their constant faith in my abilities have provided me with invaluable strength and lasting motivation throughout this journey.

List of figures

List of tables

Summary

Chapter I : bibliographic review

Chapter II: Materials, Experimental methodology and characterization techniques

Chapter III: Enhanced bio-adsorbent derived from Turnip leaves for crystal violet removal in aqueous solutions: Experimental investigation, characterization, and machine learning modeling

General introduction

General Introduction

Water is an essential resource for human existence and natural ecosystems. Despite the Earth's surface being predominantly water, merely 3% comprises freshwater appropriate for human use [1,2]. The restricted availability is exacerbated by the rising global pollution of aquatic systems with diverse contaminants, posing significant issues in contemporary times[3].

In recent years, environmental contamination by hazardous materials has emerged as a significant global issue. A multitude of studies has focused on the efficient elimination of these contaminants to reduce the threats they present to living creatures[4]. Diverse categories of organic contaminants have been identified in multiple water sources. Synthetic organic dyes are notably ubiquitous, being extensively utilised as pigments across several industries, including textiles, cosmetics, pharmaceuticals, polymers, food processing, and paper manufacture[5]. These dyes resist natural degradation, and their persistence in aquatic systems substantially hinders light penetration, consequently altering aquatic ecosystems by restricting photosynthesis in aquatic plants [6]. Dyes are primarily categorised into two types: azo and non-azo dyes, with azo dyes comprising approximately 70% of industrial usage[7]. The dyeing and textile industries manufacture around 10,000 kg of fabric daily, utilise up to 18,000 kg of water, and employ around 2 million kg of dye each day. Disturbingly, almost 15% of these colors are discarded as trash during industrial operations[8]. The existence of dyes in the environment, even at minimal concentrations, presents significant hazards to health and the ecosystem. These chemicals can interfere with biological processes in aquatic environments, and many are recognised as mutagenic and carcinogenic, presenting substantial risks to human health if not adequately managed [7,9].

Among the diverse techniques employed for dye elimination such as biological membranes, chemical precipitation, sedimentation, ultrafiltration, electrowinning, electrocoagulation, cementation, ion exchange, reverse osmosis, redox reactions, electrochemical treatment, and distillation adsorption is distinguished as a notably advantageous method for the extraction of synthetic dyes owing to its cost-effectiveness, high efficiency, practical applicability, and environmental safety[10].

According to the literature, various materials have been used as adsorbents for the treatment of effluents, among which mention may be made of activated carbon , zeolites , clays , silica , agricultural waste and hydrogels [11]. Each of these materials has specific advantages and

disadvantages in terms of efficiency, cost and environmental impact[11]. Commercial activated carbon (AC) is widely used due to its excellent adsorption properties with respect to organic and inorganic substances, which makes it one of the most popular adsorbents [12]. However, the high cost of this element represents a significant obstacle to its large-scale deployment. In reality, activated carbon is usually made from non-renewable and rather expensive resources, such as mineral coal[13]. The high cost of this product restricts its availability, especially in developing nations or in cases where large quantities of adsorbent are required. Faced with these constraints, research is increasingly turning to the design of alternative adsorbents that are both ecological, locally available, effective and economical. This trend is attracting increasing interest within the scientific community[14]. Residues from agriculture are attracting more and more attention due to their abundance, their moderate cost, their renewable nature and their potential effectiveness when subjected to adequate treatments. They represent an ecological and sustainable option as a replacement for conventional adsorbents.

During this research, adsorbents were developed using frequently rejected agricultural waste such as turnip leaves, pumpkin peels and pomegranate peels. These biomasses have been used as raw materials in the manufacture of adsorbents for the treatment of water polluted by synthetic dyes.

The main purpose of this study is to highlight some recently mentioned agricultural residues, turnip leaves, pumpkin peels and pomegranate crusts, as adsorbent materials. These materials can be used either in their natural state, or after chemical activation using phosphoric acid (H_3PO_4) for the elimination of organic dyes «crystal violet, congo red and methyl red » present in aqueous effluents. This study is part of a perspective that combines environmental and economic considerations, with the aim of developing an effluent treatment solution while highlighting underutilized local biomass.

The current thesis is structured in five chapters.

The first chapter is devoted to an in-depth bibliographic analysis of the fundamental concepts and essential definitions related to our field of study. It is structured as follows:

- Dyes: general presentation, definitions, types, classifications, and a state of knowledge concerning the three dyes targeted in this work (crystal violet, congo red and methyl red), as well as their toxicity and the different methods of elimination available.

- Adsorption: definitions, types, mechanisms, mathematical models used for the analysis of experimental results, different types of adsorbents, the adsorbents used during our experimental tests and methods of treatment or activation of adsorbents.
- Bibliographic review of previous studies: synthesis of work on the adsorption of crystal violet, congo red and methyl red dyes on various materials.

The second chapter presents in detail the method of preparation of the various precursor materials used, as well as the dyes targeted for elimination. It also defines the different experimental conditions implemented. This chapter brings together all the physicochemical characterization techniques applied to adsorbents, in particular Fourier transform infrared spectroscopy (FTIR), X-ray diffraction (XRD), UV-Visible spectroscopy (UV-Vis), scanning electron microscopy (SEM), thermogravimetric and differential thermal analysis (TGA/DTA), as well as the determination of the isoelectric point.

The third chapter presents the results of the various physico-chemical analyses carried out on the turnip leaves used as adsorbent material. It presents in detail the structural, morphological and thermal characteristics of this precursor. This chapter also deals with the adsorption of crystal violet (CV) by these sheets, by evaluating the adsorption performances as a function of various experimental parameters such as the pH, the initial concentration of the dye, the contact time and the adsorbent mass. To model the multicomponent dynamic adsorption of this organic pollutant (CV) on our adsorbent, a hybrid approach was adopted, combining the SVM-Discriminate optimization method with the SVM-DA hybrid model. This modeling is based on a large and representative dataset, guaranteeing the reliability of the predictions.

The fourth chapter is devoted to the study of the adsorption of congo red (CR) by pumpkin peels**.**

The fifth chapter is dedicated to the study of the adsorption of methyl red (MR) using pomegranate crusts used as adsorbent material.

References

[1] S. S. Emmanuel, M. O. Idris, C. O. Olawoyin, A. A. Adesibikan, A. A. Aliyu, et A. I. Suleiman, « Biosynthesized Metallic Nanoarchitecture for Photocatalytic Degradation of Emerging Organochlorine and Organophosphate Pollutants: A Review », ChemistrySelect, vol. 9, nº 14, p. e202304956, avr. 2024, doi: 10.1002/slct.202304956.

[2] I. U. Islam et al., « Parthenium hysterophorus-derived iron-coated biochar: a sustainable solution for nitrate and phosphate removal from water », Biomass Convers. Biorefinery, vol. 15, nº 7, p. 10773-10790, avr. 2025, doi: 10.1007/s13399-024-05821-w.

[3] J. O. Ighalo et al., « Recent advances in hydrochar application for the adsorptive removal of wastewater pollutants », Chem. Eng. Res. Des., vol. 184, p. 419-456, 2022.

[4] A. Jahanban-Esfahlan, R. Jahanban-Esfahlan, M. Tabibiazar, L. Roufegarinejad, et R. Amarowicz, « Recent advances in the use of walnut (Juglans regia L.) shell as a valuable plant-based bio-sorbent for the removal of hazardous materials », RSC Adv., vol. 10, nº 12, p. 7026-7047, 2020.

[5] P. Monash, R. Niwas, et G. Pugazhenthi, « Utilization of ball clay adsorbents for the removal of crystal violet dye from aqueous solution », Clean Technol. Environ. Policy, vol. 13, nº 1, p. 141-151, févr. 2011, doi: 10.1007/s10098-010-0292-6.

[6] A. Mittal, J. Mittal, A. Malviya, D. Kaur, et V. K. Gupta, « Adsorption of hazardous dye crystal violet from wastewater by waste materials », J. Colloid Interface Sci., vol. 343, nº 2, p. 463-473, 2010.

[7] M. Haris, M. W. Khan, J. Paz-Ferreiro, N. Mahmood, et N. Eshtiaghi, « Synthesis of functional hydrochar from olive waste for simultaneous removal of azo and non-azo dyes from water », Chem. Eng. J. Adv., vol. 9, p. 100233, 2022.

[8] S. S. Emmanuel, A. A. Adesibikan, et O. D. Saliu, « Phytogenically bioengineered metal nanoarchitecture for degradation of refractory dye water pollutants: A pragmatic minireview », Appl. Organomet. Chem., vol. 37, nº 2, p. e6946, févr. 2023, doi: 10.1002/aoc.6946.

[9] J. G. da Silva Andrade, C. E. Porto, W. M. Moreira, V. R. Batistela, et M. H. N. O. Scaliante, « Production of hydrochars from Pinus caribaea for biosorption of methylene blue and tartrazine yellow dyes », Clean. Chem. Eng., vol. 5, p. 100092, 2023.

[10] P. Barooah, N. Mushahary, B. Das, et S. Basumatary, « Waste biomass-based graphene oxide decorated with ternary metal oxide (MnO-NiO-ZnO) composite for adsorption of methylene blue dye », Clean. Water, vol. 2, p. 100049, 2024.

[11] A. Guediri, A. Bouguettoucha, H. Tahraoui, D. Chebli, A. Amrane, et J. Zhang, « Thermodynamic study and the development of a support vector machine model for predicting adsorption behavior of orange peel-derived beads in wastewater treatment », J. Mol. Liq., vol. 403, p. 124860, 2024.

[12] A. Mittal, R. Jain, J. Mittal, S. Varshney, et S. Sikarwar, « Removal of Yellow ME 7 GL from industrial effluent using electrochemical and adsorption techniques », Int. J. Environ. Pollut., vol. 43, nº 4, p. 308, 2010, doi: 10.1504/IJEP.2010.036929.

[13] R. Subramaniam et S. K. Ponnusamy, « Novel adsorbent from agricultural waste (cashew NUT shell) for methylene blue dye removal: Optimization by response surface methodology », Water Resour. Ind., vol. 11, p. 64-70, 2015.

[14] F. Benamraoui, « Synthèses et caractérisations de nouveaux matériaux composites », PhD Thesis, 2024. Consulté le: 9 mai 2025. [En ligne]. Disponible sur: http://dspace.univ-setif.dz:8888/jspui/handle/123456789/4866

Chapter I
Bibliographic review

I.1. Introduction

Dyes represent chemical compounds frequently used in different industrial fields such as the textile industry, the leather industry, the food industry and the cosmetics industry. However, their discharge into wastewater represents an important source of pollution due to their high chemical stability, their potential toxicity and their low biodegradability[1]. These dyes, even when present in low concentrations, have the potential to cause damage to aquatic life as well as human health[2]. Adsorption is considered one of the most effective and economical methods for the treatment of colored water. It is highly valued for its simplicity, flexibility and effectiveness at low concentrations of pollutants[3]. Activated carbon is widely used as an adsorbent due to its high specific surface area and its ability to adsorb various molecules[4].However, due to their relatively high cost, many studies are turning to the use of natural biomass or agricultural residues as substitute adsorbent materials. These different biomasses such as sawdust, walnut shells, or even corn stalks, can be exploited for the production of effective, durable and economical adsorbents, following a physical or chemical activation treatment[5,6].

In this context, the objective of this chapter is to present an in-depth bibliographic study on dyes, by addressing their types, their classification, as well as their impacts on human health and the environment. A specific state of knowledge will then be devoted to the three dyes that are the subject of our work, namely crystal violet (CV), congo red (CR) and methyl red (MR). The chapter continues with a general presentation of the adsorption phenomenon, in order to better understand its importance, its mechanism and its ability to eliminate pollutants. A theoretical study of the different types of adsorbents is also proposed, with particular emphasis on the biomass used in this research. Finally, a review of previous work devoted to the adsorption of the mentioned dyes on various materials will be presented.

I.2. Dyes

Dyes are substances that are very stable to light, chemicals, biological exposures and other conditions[7].The majority of dyes are organic substances, either synthetic or natural, that can adhere to surfaces or textiles to create a brilliant and long-lasting color[8].

I.2.1. Types of dyes

The dyes can be divided into a number of categories based on the classifications made by various research teams, as illustrated in Figure I.1.

Nowadays, it is crucial to classify dyes according to their chemical characteristics and intended uses. Previously, chemists employed classifications mostly based on the chromophore groups found in molecules. Auxochromes, which supply electrons (such as -NHR, -NH2, -OH, -NR2, -COOH, -CSOH, -OCH3), and chromophores, which attract electrons (such as C=C, C=N, C=O, N=N, NO2), are important components of dye structures. The dyes are divided into 20 to 30 groups according to their chromophore structures; the primary groups are triarylmethanes, azo compounds, anthraquinones, and phthalocyanins [9]. Furthermore, the Color Index (IC)'s classification by usage or application has emerged as the industry standard for dye producers and consumers.

Category	Description
Source of Materials	- Natural dyes: derived from plants, invertebrates, or minerals. - Synthetic dyes: chemically prepared (e.g., Acid dyes, Azo dyes).
Nature of Chromophore Groups	- Nitro / Nitroso dyes: contain NO or NO_2 groups. - Azo dyes: contain the –N=N– azo group. - Triarylmethane dyes: triphenylmethane backbone.
Nuclear Structure	- Cationic dyes: e.g., Methylene Blue. - Anionic dyes: e.g., Congo Red.
Industrial Classification – Cellulose Textile Dyes	- Direct dyes: mostly acidic azo dyes. - Basic dyes: contain cationic groups such as $–NR_2^+$. - Vat dyes: strong affinity for cotton fibers (e.g., indigo).
Synthetic Textile Dyes	- Disperse dyes: low water solubility. - Solvent dyes: stain by dissolving in the target substrate.
Protein Textile Dyes	- Acid dyes: highly soluble with good fastness. - Mordant dyes: form coordination complexes with fibers.

Figure I.1. Classification of dyes [10].

I.2.1.1. Anionic dyes

Anionic dyes are of paramount importance in the textile industry sector, being widely used for the coloring of natural and synthetic fibers. Due to their high affinity for cellulose fibers such as cotton, as well as for protein fibers such as silk and wool, these dyes are considered coloring agents of choice. During their dissolution in an aqueous solution, these dyes separate into anion

ions carrying a negative charge[11]. Anionic dyes are highly acidic and reactive dyes, often defined by the presence of an azo group in their chromophore. Mention may be made, among the dyes currently used, of Methyl red[12], Acid Orange 7 (AO7)[13], Methyl Orange (MO)[14] and Congo Red (CR)[15].

Congo red dye (CR)

Congo red (CR), chemically designated as 1-naphthalene sulfonic acid, disodium salt of 3,3'-(4,4'-biphenylene bis(azo)) bis(4-amino), is a dye classified among benzidine-based dyes Figure I.2. It poses a considerable toxicological hazard, as it can be metabolised into benzidine, a compound identified as carcinogenic to humans. Congo Red is likely to induce skin irritation and allergic dermatitis[16]. Table I.1 lists the physico-chemical characteristics of congo red (CR). The removal of CR from the environment is particularly difficult because it is a negatively charged dye that is insoluble in acidic and alkaline media. When discharged, it can have various degrees of negative effects on the human digestive and circulatory systems and can hinder the growth of plants and animals[17].

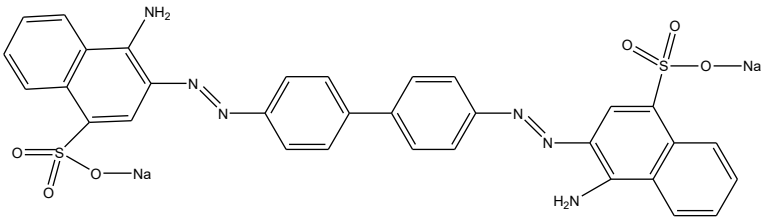

Figure I.1. Molecular structure of CR day[18].

Table I.1. Main physico-chemical characteristics of the CR dye [19]

NAME	Congo Red
FAMILY	azoïque
RAW FORMILLA	C32H22N6Na2O6S2
CHEMICAL APPEAL	Benzidinediazo-bis-1-naphthylamine-4-sulfonic acid
Molecular weight (g\mol)	696.66 g /mol
Solubility in water	25 g/l à 20 C
λ max	498 nm
pKa	4.1

Methyl red dye (MR)

Methyl red is an azo dye widely used as a pH indicator due to its property of changing color depending on the acidity of the medium: it has a red tint in acidic medium (pH < 4.4) and yellow in basic medium (pH > 6.2). However, once released into industrial wastewater, this compound turns into a toxic pollutant, not very biodegradable, likely to cause damage to aquatic fauna and compromise water quality. Due to its chemical stability, the elimination of this substance requires the use of special methods such as adsorption or biological degradation[20-22].

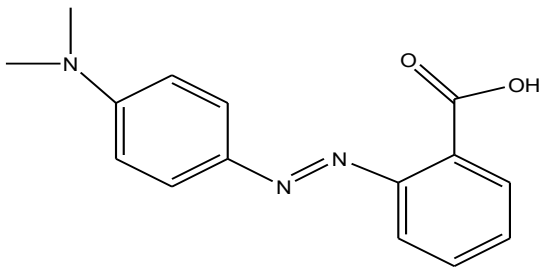

Figure I.2: Molecular structure of MR dye [23].

Table I.2: Main physico-chemical characteristics of the MR dye [23].

NAME	Methyl red
FAMILY	Monoazo
RAW FORMILLA	C15H15N3O2
CHEMICAL APPEAL	4-dimethylamino-2-phenylazobenzoic acid
Molecular weight (g\mol)	269.3 g /mol
Solubility in water	0,2 g/L
λ max	410–526 nm
pKa	5 (28 °C)

I.2.1.2. Cationic dyes

Cationic dyes are characterized by the release of positive ions (cations) during their dissolution in an aqueous solution. They hold fundamental groups, such as ammonium ions. In contrast, the anionic dyes contain acid groups such as carboxylic anions. Methylene Blue (MB) is a classic example of a cationic dye[24].Crystal violet (CV)[25], Rhodamine B (RhB)[26] and Malachite Green (MG)[27] are among the cationic dyes most commonly present in wastewater effluents from the textile industry. These dyes have a high affinity for synthetic fibers that are negatively charged, which makes them very effective for coloring nylon and acrylic fibers[28].

Crystal violet (CV)

Crystal violet is a synthetic cationic dye, also known as Gentian violet or Methyl violet 10B. It is part of the triarylmethanes family. Used in various fields, it is used in particular as a dermatological agent, as a treatment in veterinary medicine, or even as an additive in poultry feed to prevent parasitic and fungal infections. This dye is also widely used in the textile industry and for printing on paper[29].

Crystal violet is a toxic substance that has the ability to be absorbed by the skin, thus causing skin irritation. It also carries risks if inhaled or swallowed. In exceptional circumstances, it can lead

to kidney failure, severe eye irritation that can lead to permanent blindness, as well as an increased risk of cancer [30,31]. Thus, the removal of this dye from wastewater and water represents a top environmental priority.

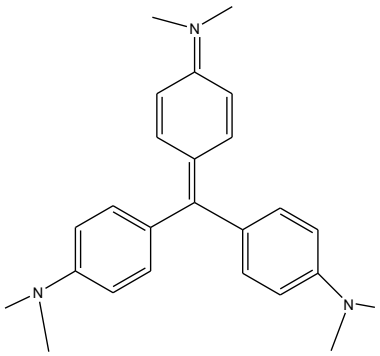

Figure I.3: Molecular structure of CV dye.

.

Table I.3. Main physico-chemical characteristics of the CV dye [32].

NAME	Crystal violet
FAMILY	Basic dye
RAW FORMILLA	C25H30N3Cl
CHEMICAL APPEAL	méthylrosaniline Violet basique 3
Molecular weight (g\mol)	407.98 g /mol
Solubility in water	4
λ max	590 nm

I.2.2. Toxic effects of dyes

Synthetic dyes were created to overcome the constraints of natural dyes, such as the scarcity of resources and the problems associated with their harvesting. Nevertheless, almost 40% of the

synthetic dyes used around the world contain chlorine, a compound recognized for its potential to induce cancer. These chemicals have the ability to evaporate or absorb through the skin, triggering allergies and posing a health hazard, especially in children, including during the prenatal period[33]. However, synthetic dyes carry significantly higher ecotoxicological risks than natural dyes such as indigo, turmeric, cochineal, madder, acorns, black tea, campeche wood or coffee, due to their molecular complexity and their low biodegradation capacity[34]. These characteristics lead to a sustainable contamination of water sources over the long term. Artificial dyes, such as crystal violet and its derivatives , contain carcinogenic and mutagenic substances. They disrupt aquatic ecosystems by decreasing the amount of dissolved oxygen and hindering the photosynthesis process. On the other hand, natural dyes are generally biodegradable and have a lower environmental impact. The transition to more environmentally friendly solutions, whether of natural or synthetic origin, offers a promising prospect for reducing the consequences on the environment. However, there are still challenges to overcome with regard to costs, availability and performance, in order to guarantee the effective sustainability of dyeing practices[35].

I.2.3. Wastewater treatment methods for the removal of dyes

In general, dyes are divided into anionic, cationic, and nonionic categories based on their chemical makeup[36,37]. There are several dye removal processes available, each with a different success rate, as shown in Figure I.5. Reverse osmosis, solvent extraction, flocculation, membrane separation, filtration, electrolysis, evaporation, adsorption, reduction, oxidation, coagulation, ion exchange, and chemical precipitation are some of these methods. Toxic pollutants from industrial effluents have been removed and recovered using these techniques [38,39]. However, as shown in Table I.4, each of these methods has unique benefits and drawbacks that necessitate careful consideration for the best use in dye removal procedures.

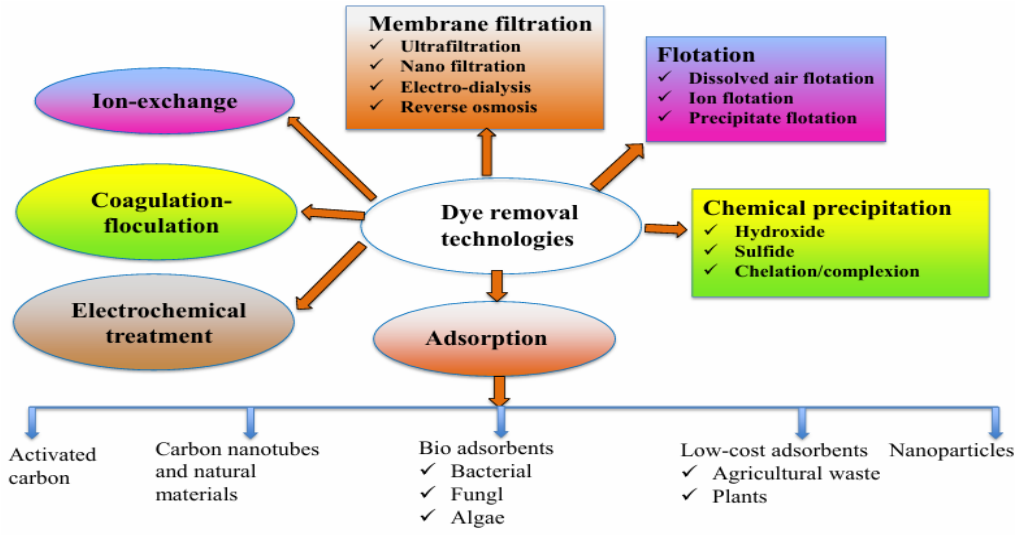

Figure I.5. Schematic representations of available dye removal [40].

Table I.4. Advantage and disadvantages of the dye removal process technologies [41].

Treatment Technology	Advantages	Disadvantages	References
Advanced Oxidation Process	•Direct production of reactive radicals on site •Rapid degradation of contaminants	•Technology still at the laboratory stage •Possible formation of by-products	[42]
Ion Exchange	• Wide choice of commercial products available •Procedures already well mastered	•Large volumes requiring large columns •Limited effectiveness for disperse dyes	[42,43]
Chemical Precipitation	•Simple to implement technology •Economically profitable solution	•Significant consumption of chemicals •Additional costs related to sludge disposal	[42,43]
Coagulation/Flocculation	• Simple to implement process •Low investment cost •Good sludge settling	•Requires the addition of non-reusable chemicals •Low efficiency for arsenic removal	[42,43]
Membrane Technologies	•Elimination of all types of dyes •Resistance to temperature variations and chemical	•Investment costs that are often too high for small and medium-sized industries •Limited service life due to	[42,43]

	environments	fouling of the membranes	
Electrochemical Techniques	•Effective removal of toxins, oils, fats, dyes and metals. •Faster and more efficient separation of organic matter compared to traditional coagulation.	•Periodic maintenance. •Cost	[42,43]
Adsorption	•The dyes possess a strong adsorption capacity. •Simple technology. •Practical, easy to use, simple design and cost-effectiveness.	•Non-destructive processes. •Cost of regeneration. •Generation of sludge.	[42,43]

I.3. Adsorption

I.3.1. Dye removal adsorbent

Adsorption is an efficient technique for eliminating colors from industrial waste effluent. This method has numerous advantages compared to other techniques, notably its operation without sludge generation and its capacity to eradicate pigments entirely. The adsorption processes fall into two categories: physical or chemical, depending on the mechanism by which the adsorbate attaches to the surface of the adsorbent, as shown in Figure I.6 [44].The adsorbate is bound to the adsorbent by weak physical forces such as Van der Waals forces, hydrogen bonds, polarity, hydrophobicity, static interactions, dipole interactions and π-π interactions. Conversely, chemical adsorption happens when an adsorbate and the adsorbent surface exchange electrons[45]. Zeolites, alumina, silica gel, activated carbon and biomass are commonly used as adsorbents for the removal of dyes present in wastewater. Among them, activated carbon and certain biomasses stand out for their superior efficiency in the adsorption of organic molecules, making them adsorbents of choice.[46]. Figure I.7 illustrates the schematic representation of the adsorption process for dye-contaminated wastewater, employing agricultural biomass as the adsorbent. Various ways are employed to utilize agricultural biomass as an adsorbent, including the conversion of biomass into activated carbon[47,48], chemical activation and modification of biomass[49,50], hybridization[51], impregnation[52], and more techniques. Numerous prior

studies have investigated a range of natural and synthetic adsorbents, specifically wool and cotton fibers[53], banana pith[54,55], carbonized coconut pith[56], coconut pith[57], mahogany sawdust, chitosan[58], hardwood[59], rice husk[60], neem husk (Azadirachtaindica)[61], silk cotton husk, coconut palm sawdust[62], tuberose sticks[63],gypsum[64], tamarind fruit shell[65].

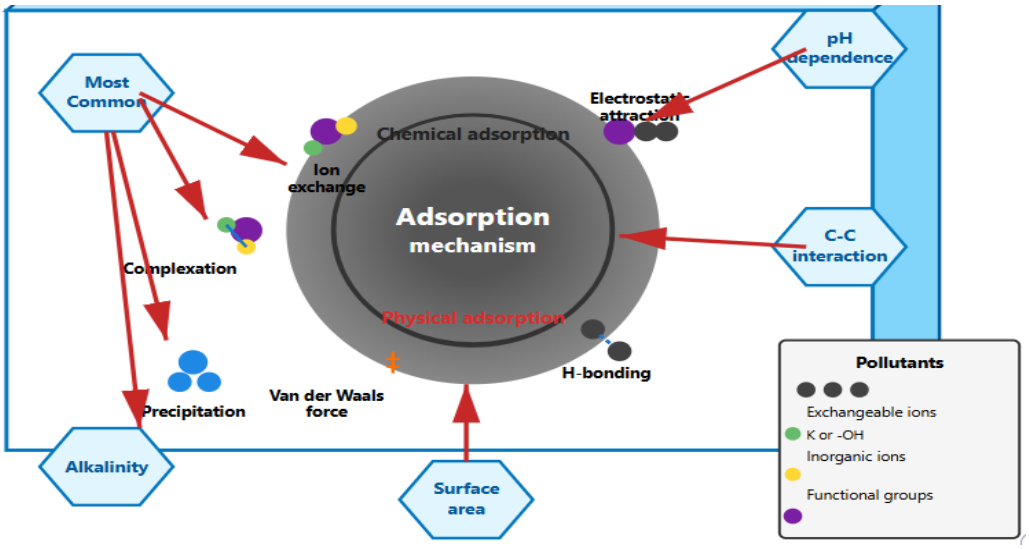

Figure I.6. Physical and chemical adsorption mechanism [44].

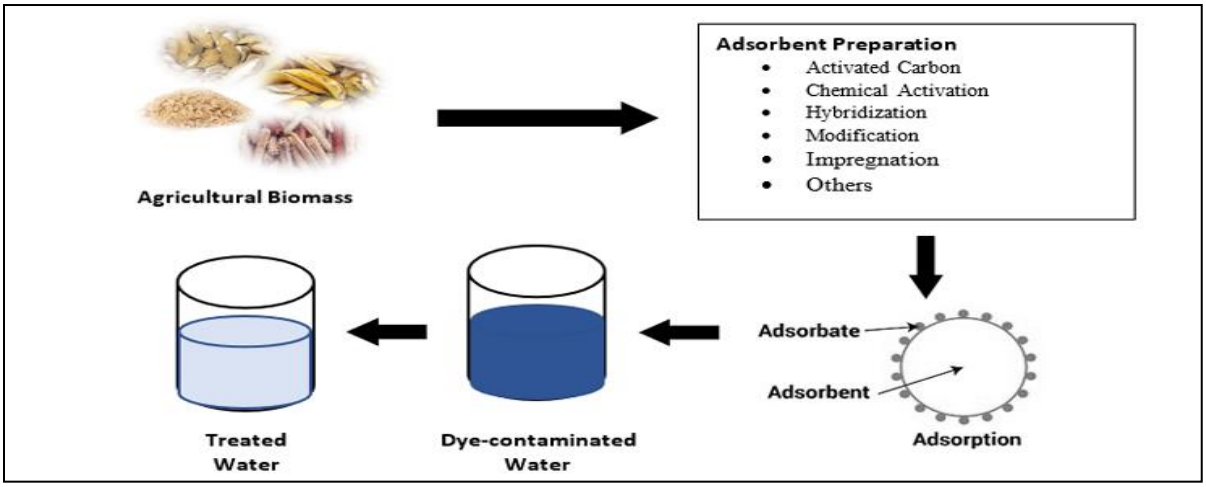

Figure I.7. An overview of dye adsorption in polluted water using biomass derived from agriculture [41].

I.3.2. Adsorption mechanisms

The adsorption mechanism generally comprises three primary steps Figure I.8 [66,67]:

- **Bulk diffusion**: Adsorbate molecules migrate from the bulk solution to the exterior surface of the adsorbent. This process is affected by concentration gradients and agitation conditions.
- **Film or boundary layer diffusion:** The adsorbate traverses a boundary layer that develops adjacent to the adsorbents surface. This phase may become a rate-limiting issue if the border layer is either dense or inadequately blended.
- **Intraparticle or pore diffusion**: Upon reaching the surface, the adsorbate penetrates the interior pores of the adsorbent, where it engages with accessible active sites.
- **Surface interaction (adsorption):** Ultimately, the adsorbate adheres to the surface through physisorption (weak van der Waals forces) or chemisorption (strong covalent or ionic bonding), contingent upon the nature of the interaction.

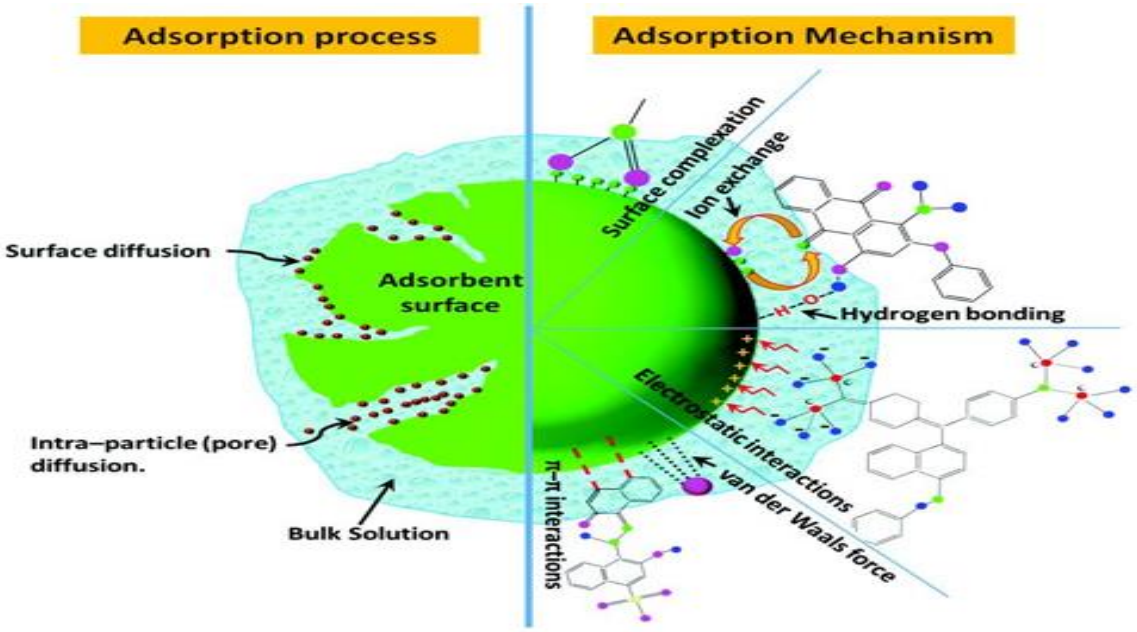

Figure I.8. Mechanism of adsorption process [68].

I.3.3. Modeling of adsorption kinetics (non-linear forms)

The adsorption kinetics models were used to determine the speed of the adsorption process, an essential data for the design and optimization of an efficient adsorption system[69]. Previous research[70] exposes the kinetic mechanism of adsorption in two distinct phases. The first phase consists of the migration of the substance to be adsorbed, also called adsorbate, from the bulk solution to the surface of the adsorbent material. Subsequently, during the second phase, the

adsorbate gradually penetrates into the pores of the adsorbent material and is deposited there. In general, it is the slowest step, also called the limit step, which determines the overall speed of the process. The recognition of this phase allows a better understanding of the adsorption process involved[71]. Different models, such as the pseudo-first order, the pseudo-second order, the Elovich model and the intraparticle diffusion, have been used to calculate the adsorbed amount and to study the adsorption kinetics and describe the process.

Table I.5. Kinetic models used to describe the adsorption process [72].

Models	Equations	Parameters
Pseudo-first-order	$q_t = q_e\left(1 - e^{-k_1 t}\right)$ (I.1)	q_e,q_t(mg/g): the quantities of solute adsorbed by the adsorbent at equilibrium and time (t). k_1 (min^{-1}): the rate constants for PFO.
Pseudo-second-order	$q_t = \frac{q_e^2 k_2 t}{1 + q_e k_2 t}$ (I.2)	k_2 (mg/g. min): the rate constants for PSO
Elovich	$q = \frac{1}{\beta}\ln\beta\alpha + \frac{1}{\beta}\ln t$ (I.3)	β ($g.mg^{-1}$) : is the desorption constant associated with the surface area coverage, and chemisorption activation energy α($mg.g^{-1}.min^{-1}$) : is the initial adsorption rate ($mg.g^{-1}.min^{-1}$)
intraparticle diffusion	$q_t = k_{diffusion} \times t^{1/2} + C$ (I.4)	$k_{diffusion}$ ($mg/g\,min1/2$): is the adsorption rate constant of the intraparticle diffusion model. C: is the layer's thickness

I.3.4. Modeling of adsorption isotherms

The adsorption isotherms describe the way in which a substrate behaves during its transfer from the solution to the surface of the adsorbent. These isotherms make it possible to correlate the amount adsorbed per unit mass of adsorbent with the concentration (or pressure) of the substrate in solution, at a given temperature. The temperature exerts a significant influence on the nature

and intensity of the adsorption, which makes it possible to evaluate the favorability of the process[70].

There are four main categories of isotherms, classified according to their low adsorbent concentration profile[73] :

- The S type corresponds to a cooperative adsorption, characterized by more intense interactions between the adsorbate molecules than with the adsorbent, which favors their agglomeration on the surface.
- The L value of testifies to a high affinity between the adsorbate and the adsorbent, characteristic of chemisorption.
- The H type represents an extreme version of the L type, indicating almost complete adsorption of the adsorbent in dilute solution.
- Type C is characterized by a constant and proportional affinity between the adsorbed molecules and the adsorbent, a phenomenon generally observed at low concentration.

To adequately describe the experimental data of adsorption at equilibrium, three models were used: Langmuir, Freundlich and Sips Table I.6. The Langmuir model, with two parameters (K_L and Q_{max}), is based on the assumption of a monolayer adsorption on the homogeneous surface, without interaction between the adsorbed molecules[74]. the Freundlich isotherm, characterized by its two parameters (n and K_F), postulates a multilayer adsorption process on a heterogeneous surface, involving interactions between the adsorbed molecules. The index 1/n expresses the intensity of the adsorption or the variability of the surface, indicating that the more this value tends to zero, the more the surface has a high diversity of adsorption sites. In addition, an adsorption is considered favorable when the adsorption coefficient is less than 1[75]. The three-parameter Sips model (q_S, K_S and n_S) exhibits a behavior similar to a Freundlich isotherm at low concentrations of the adsorbate, but it converges towards monolayer adsorption at high concentrations, which is a characteristic of the Langmuir model[76].

Table I.6. Isotherm models used to describe the adsorption process [73].

Models	Equations	Parameters
Langmuir	$q_e = \frac{q_m k_L Ce}{1+k_L C_e}$	q_e(mg/g): is the quantity of dye adsorbed per gram of the adsorbent at equilibrium.

	(I.5)	q_m (mg/g): is the maximal monolayer coverage capacity. K_L **:** is the Langmuir isotherm constant (L/mg).
Freundlich	$q_e = k_f c_e^{\frac{1}{n}}$ (I.6)	C_e (mg/L): is the equilibrium concentration of the adsorbate. K_f : is the Freundlich constant indicative of the relative adsorption capacity of the adsorbent. n: is adsorption intensity related to the surface heterogeneity.
Sips	$qe = \frac{qsksCe^{1/ns}}{1+ksCe^{1/ns}}$ (I.7)	Ks (L/g) and ns are Sips constants.

I.3.5. Adsorption thermodynamics

Different thermodynamic parameters have been calculated to evaluate the feasibility and spontaneity of the adsorption, as well as to determine whether the process is exothermic or endothermic. The CV, CR and MR adsorption experiments were carried out at three distinct temperatures, 25 °C., 30 °C. and 40 °C. Each material was subjected to a specific concentration, while the amount of adsorbent used was fixed at 1 g/L. The thermodynamic quantities evaluated include the Gibbs free energy (ΔG°, in kJ/mol), the enthalpy (ΔH°, in kJ/mol) and the entropy (ΔS°, in J/mol K). These quantities have been calculated using the relevant thermodynamic equations in order to study the influence of temperature on the adsorption process[77].

$$\Delta G = -RT \ln Kc \quad (I.8)$$

$$\Delta G° = \Delta H° - T\Delta S° \quad (I.9)$$

K_L is the Langmuir equilibrium parameter, converted from the unit (L/mg) to the unit (L/mol)

According to the following formula[78]:

$$k_L\,(L/mol) = k_L(L/mg) * 1000\,(mg/g) * M_{adsorbate}\,(g/mol) \quad (I.10)$$

where $M_{adsorbate}$(g/mol) is the molecular weight of the adsorbate. Subsequently, the dimensionless adsorption equilibrium constant (K_c) is estimated as Conforming to the following formula[79]:

$$Kc = k_L\ (\ L/\ mol\ )\ *\ Cref(mol/\ L) *\ 1/\Upsilon \quad (I.11)$$

Based on the ionic strength, the activity coefficient is denoted by γ, and the molar concentration of the reference state is indicated by C_{ref}. It is widely acknowledged in the standard method that the concentration of the adsorbate or pollutant in the reference state is 1 M, or C_{ref} = 1 mol/L[80].

R: universal gas constant (8.314 J/mol K); and T: absolute temperature (K).

Error analysis

The coefficient of determination (R^2) and the chi-square (χ^2) test are statistical parameters used to evaluate how well the models fit the experimental data, as illustrated by the following equations[76] :

$$R^2 = 1 - \frac{\sum_{i=1}^{n}(qe,exp - qe,cal)^2}{\sum_{i=1}^{n}(qe,exp - qe,mean)^2} \quad (I.12)$$

$$x^2 = \sum_{i=1}^{n}\frac{(qe,exp\ - qe,cal)^2}{qe,cal} \quad (I.13)$$

Where n is the number of experiments, q_e,mean is the average of the experimental q_e,exp values, q_e,cal is the model-predicted value corresponding to C_e, and q_e,exp is the experimentally determined equilibrium adsorption capacity

I.3.6. Agricultural waste and residues as adsorbents for the treatment of wastewater contaminated with dyes.

In order to find cheaper alternatives to activated charcoal, many researchers have been interested in the use of agricultural waste as raw materials for the manufacture of adsorbents, these being produced in large quantities in the food sectors due to global population growth. Thanks to their availability, their low cost and their ecological character, these biomasses have been widely studied and used as effective adsorbents in wastewater treatment [81,82]. Several types of plant residues show a high potential for the elimination of dyes present in contaminated water, thus making it possible to recover them rather than eliminate them. In this context, our study focuses

on three biomass selected for their adsorption performance: turnip leaves, pumpkin peels [56,83,84,] and the pomegranate crusts [57,85,86,], which retain the dye molecules on their surface and contribute effectively to the purification of water.

I.3.6.1. Turnip leaves

The turnip (Brassica rapa L.), a biennial herbaceous plant of the Brassicaceae family, is native to Europe, Russia, Central Asia and the Near East, but today it is widely cultivated around the world for food and oil production, with two main distinguished breeds: western (oilseed) and oriental (vegetable) [87]. Although sometimes avoided in Asia for its flatulent effects, it occupies an important place in the Western diet and has recognized medicinal uses, especially in the traditional treatment of liver diseases, kidneys and other ailments [88]. Often neglected, turnip leaves nevertheless present a significant nutritional richness in vitamins A, C and K, as well as calcium, iron and magnesium, and their high fiber and bioactive compound content is generating increasing interest in environmental applications, in particular water purification by adsorption [89]. In this perspective, our study was interested in the valorization of these sheets as an adsorbent material for the treatment of colored water, a promising approach given their accessibility, their renewability and their functional potential.

Figure I.9. the turnip and its leaves.

I.3.6.2. Pumpkin peels

The pumpkin, which is in the Cucurbitaceae family is a type of vegetable plant Figure I.10, is one of the most popular veggies to grow and eat. In 2022, the world produced about 23 million tons of pumpkin[90]. Pumpkin is esteemed for its abundant nutritional composition, comprising carotenoids, minerals, and polysaccharides, and is frequently utilized as a fundamental component in medicinal and culinary applications[91]. The composition of the pumpkin includes about 93.64% water, 0.63% protein, 0.09% fat, 66% fiber and 17.5 g / g of beta-carotene, with a dietary fiber content varying between 15.5% and 26.5% [63]. Thanks to their richness in fibers, polysaccharides and functional groups such as hydroxyls and carboxyls, pumpkin peels have a high potential as natural adsorbents, offering numerous active sites capable of fixing various pollutants, in particular heavy metals, dyes and other organic contaminants. Their porous structure and their large specific surface give them a high adsorption capacity, while their low cost, their biodegradability and their ecological character make them a sustainable and advantageous alternative compared to synthetic adsorbents. Thus, the use of pumpkin peels constitutes an effective and environmentally friendly solution for water treatment and sanitation.

Figure I.10. the Pumpkin and its peels.

I.3.6.3. Pomegranate crusts

Pomegranate Figure I.11 is considered a superfruit due to its richness in antioxidants and health-promoting compounds, which can serve as a natural food additive. The pomegranate processing chain produces considerable quantities of co-products, in particular the peels (representing 50% of the weight of fresh fruits), which have a negative environmental impact in the event of improper disposal[92]. In this context, pomegranate peels have been used as effective natural adsorbents for the purification of various pollutants present in aqueous solutions.

Figure I.11. Pomegranate.

I.3.7. Preparation of sorbents from biomass

The transformation of biomass into adsorbents involves various physical, physico-chemical and chemical processes [93,94]: physical activation consists of carbonization under an inert atmosphere followed by activation with CO_2, steam or air between 800 and 1100 ° C, although temperatures ≥1200 ° C reduce the carbon yield and cause the collapse of porous structures [95,96], requiring precise control to develop porosity [97]. The physico-chemical activation combines impregnation of an agent and heating in the presence of an oxidizer, but remains expensive and inefficient when the agent cannot be removed by simple washing [98-100]. The chemical activation is based on a pretreatment (washing, drying at 65-105 °C., grinding) followed by the incorporation of an acidic, basic or saline agent (k_2CO_2, $ZnCl_2$) before or after carbonization at 400-800 °C., which makes it particularly suitable for lignocellulosic biomass [99,101]. The activation in a single step (impregnation then heating) is fast but can induce excessive combustion, while microwaves make it possible to considerably reduce the treatment time [102]. The two-step method, including carbonization and then activation, makes it possible to obtain a porous carbonaceous material without prior grinding but increases the duration, the energy consumed and the costs, and is not always more efficient even when coupled with microwaves [103,104]. The microwave activation, more ecological, improves energy efficiency thanks to the selective absorption of certain biomass and limits self-gasification by rapid and homogeneous heating [105-108]. The activating agents strongly modulate the final structure: acid treatments depolymerize cellulose and hemicellulose, promote deligification and the formation of symmetrical pores, in particular with HCl or H_3PO_4, the latter generating large specific surfaces (up to 1218 m2 /g from olive pits) [109-111]. Basic treatments, in particular with KOH, fragment the fibers, develop microporosity and can reach high surfaces, such as 2300 m2/g for cane

bagasse [76,112,113]. The salts influence the hydrolysis of hemicelluloses, can cause a Leidenfrost effect generating steam explosions and catalyze gasification above 400 °C [109]. The $ZnCl_2$ is very efficient, giving for example 1836 m2 / g for the seeds of Elaeagnus angustifolia or 1489 m2 / g for potato peels activated at 400 ° C [114,115]. Finally, although little studied, $FeCl_2$ and $fecl_2$ show a notable efficiency, $fecl_2$ making it possible to obtain up to 1680 m2/g from Tara gum between 400 and 1000 °C. [116,117].

I.4. Bibliographic review on the adsorption of CV, CR and MR

In recent years, the issue of wastewater treatment containing dyes has aroused increasing interest among researchers. Among the various treatment approaches, absorption is generally considered the most effective and frequently used method for removing dyes. The current section presents a synthesis of various studies on the adsorption of crystal violet (CV), congo red (CR) and methyl red (MR) on various adsorbent materials.

I.4.1. The adsorption of crystal violet

In 2023, research was published describing the development by researchers of an activated carbon made from bamboo fibers, used for the adsorption of crystal violet. The material demonstrated an exceptional adsorption capacity, amounting to 1353.09 mg/g. Under optimal conditions (0.04 g of adsorbent, 600 mg/L of CV, 25 °C., 30 min), the removal rate of the dye was 99.96%. The adsorption was in accordance with the Langmuir isothermal model and pseudo-second-order kinetics, which suggests a monomolecular process regulated by the interactions between the functional groups of the coal and the dye[118].

Two varieties of biochar, produced at temperatures of 350 °C and 450 °C respectively from banana stems, were examined in terms of CV adsorption efficiency. The biochar produced at a temperature of 350 °C (BSB-350) demonstrated a maximum adsorption capacity of 208.33 mg/g, while the one manufactured at 450 °C (BSB-450) presented a capacity of 153.50 mg/g. Both obeyed the Langmuir model, which suggests monomolecular adsorption[119].

Radish leaves were used as a biosorbent in a previous study, demonstrating an adsorption capacity of 48.7 mg/g for CV. The pseudo-second-order kinetic model, with a coefficient of determination R^2 of 0.999, demonstrated a strong affinity for the dye[120].

I.4.2. The adsorption of congo red

Research has shown that orange peel biochar treated with cetyltrimethylammonium bromide (CTAB) exhibits a significant adsorption capacity towards congo red. The modified biochar (NOBC) has a maximum adsorption capacity of 290.1 mg/g after 60 minutes, while the unmodified biochar displays a capacity of 155.2 mg/g after 210 minutes. The adsorption is described by the Langmuir isothermal model and the pseudo-second-order kinetic model, which suggests a monomolecular adsorption mainly governed by electrostatic interactions[121].

Cowpea seed husks, a by-product of agriculture, have been used as a biosorbent in order to remove the Congo red from aqueous solutions. The maximum adsorption capacity reached amounts to 161.29 mg/g, after an equilibrium time of 60 minutes. The experimental results show a good agreement with the Langmuir isothermal model as well as with the pseudo-second-order kinetic model, which suggests chemical adsorption on homogeneous sites[122].

The seeds of the date palm have been used as a biosorbent for congo red. The maximum adsorption capacity reached is 51.245 mg/g. The adsorption is described by the Langmuir isothermal model and the pseudo-second-order kinetic model, which suggests chemical adsorption on homogeneous sites. The thermodynamic parameters reveal that the process is both spontaneous and endothermic[123].

I.4.3. The adsorption of methyl red

Research has shown that biochar made from Rumex abyssinicus stems exhibits a maximum adsorption capacity of 42.34 mg/g for Methyl Red. The adsorption conforms to the isothermal Freundlich model (R^2 = 0.99), which suggests the presence of a heterogeneous surface and a multilayer adsorption. Kinetics is characterized by the pseudo-second-order model, which implies adsorption of a chemical nature. The adsorption process involves electrostatic interactions, hydrogen bonds and π-π interactions between the functional groups of the biochar

and the Methyl Red molecules. A maximum yield of 99.2% was obtained at a pH of 6, using an initial concentration of 70 mg/L and an amount of adsorbent of 0.2 g/100 mL[124].

An activated carbon, made from coffee grounds treated with silver, was used for the adsorption of Methyl Red. At a pH of 4, the maximum adsorption capacity reaches 9.86 mg/g. The adsorption conforms to the Langmuir isothermal model, while the kinetics are represented by the pseudo-first order model, which suggests adsorption of a chemical nature[125].

Biochars derived from the pyrolysis of fennel seeds and activated by physical and chemical methods have been studied as to their adsorption capacity of methyl red. The adsorption capacities vary from 26 to 135 mg/g. The adsorption is described by the isothermal Freundlich model, which implies a multilayer adsorption process on a surface exhibiting heterogeneity. Kinetics is characterized by the pseudo-second-order model. The efficiency of adsorption increases with increasing temperature, and thermodynamic analyses reveal a spontaneous and endothermic process[126].

I.5. Bibliographic review on the use of pumpkin peels, and pomegranate crusts as adsorbents

I.5.1. Pumpkin Peels as Adsorbents

Sharma et al. (2018) used KOH-modified pumpkin peels for the adsorption of Cu2 ions. The optimal conditions were pH = 5, contact time = 60 min and adsorbent dose = 0.1 g. The maximum adsorption capacity (Q_{max}) reached is 73.16 mg /g, showing that this activated alkaline biochar constitutes an effective adsorbent for copper in aqueous solution.[127]

Allende et al. (2025) have developed an ecological method for converting pumpkin peels into carbon nanomaterials via microwave-assisted pyrolysis under nitrogen, without chemical agents. The biochar obtained has a specific surface area of 29.1 m2/g, a pore volume of 0.13 cm3/g and average pores of 3.7 nm, with hydroxyl and carbonyl functional groups favorable to adsorption and electrochemical reactivity. When used to modify a printed carbon electrode, it reduces the charge transfer resistance from 10 kΩ to 563 Ω and allows the detection of nitrite with a detection limit of 10 µM. This fast, sustainable and simple process recovers agricultural waste and paves the way for applications in water treatment or electrochemical sensors[128].

In the Eco-friendly Biochar from Pumpkin Peel study (2021), a biochar from pumpkin peels was used for the adsorption of the dye Methylene Blue (MB). The optimal conditions were pH ≈ 7-9, contact time ≈ 40-60 min and dose = 1 g /L. The maximum adsorption capacity (Q_{max}) reached is 208.3 mg / g, demonstrating that this biochar constitutes an effective, economical and ecological adsorbent for the treatment of colored water[129].

I.5.2. Pomegranate Crusts as Adsorbents

The sulfonated pomegranate peel biochar (SPPBC) is obtained by carbonization of the peels followed by a treatment with sulfuric acid to introduce SO_3H groups. It has a high affinity for cationic dyes such as Blue Methylene, with a maximum adsorption capacity (Q_{max}) of 161.9 mg / g. The optimal conditions are: dose 0.18 g, pH ~ 9.7, temperature 49 ° C, contact time 4.3 h. This simple and ecological process allows a effective adsorption thanks to the porosity of the biochar and the sulfonated functional groups.[130]

In this study, the authors prepared a biochar from pomegranate peels (PP biochar) via carbonization (pyrolysis) then characterization (BET, FTIR, SEM, pHPZC). This biochar has a very porous structure with a specific surface SBET = 508.9 m2/g, a total pore volume VT = 0.19 cm3/g, distributed between micropores (~50.8%) and mesopores (~49.2%), and a pH of charge point pH_{PZC} = 6.42. When used for the adsorption of cationic dyes (crystal violet CV and methylene blue - MB), the maximum capacity determined by the Langmuir model (q_{max}) reaches 201.2 mg/g for CV and 320.6 mg/g for MB (in simple systems). The adsorption kinetics follow a pseudo-second-order model (and sometimes the Avrami model), which suggests that the adsorption is controlled chemically or via surface interactions[131]

I.6. Conclusion

This chapter presents a comprehensive overview of the phenomena of adsorption, which is currently an effective and straightforward therapeutic strategy. Activated carbon is the standard adsorbent; nevertheless, its expense compels researchers to explore other materials, particularly those derived from plant biomass or agricultural byproducts. This plentiful and renewable biomass presents a promising ecological and economic alternative for wastewater treatment.

This chapter concludes with an overview of current investigations on the adsorption of crystal violet, congo red, and red methyl, which constitute the primary focus of our research.

References

[1] T. Robinson, G. McMullan, R. Marchant, et P. Nigam, « Remediation of dyes in textile effluent: a critical review on current treatment technologies with a proposed alternative », Bioresour. Technol., vol. 77, nº 3, p. 247-255, 2001.

[2] E. Forgacs, T. Cserháti, et G. Oros, « Removal of synthetic dyes from wastewaters: a review », Environ. Int., vol. 30, nº 7, p. 953-971, 2004.

[3] G. Crini, « Non-conventional low-cost adsorbents for dye removal: a review », Bioresour. Technol., vol. 97, nº 9, p. 1061-1085, 2006.

[4] R. C. Bansal et M. Goyal, Activated carbon adsorption. CRC press, 2005. Consulté le: 3 décembre 2025. [En ligne]. Disponible sur: https://www.taylorfrancis.com/books/mono/10.1201/9781420028812/activated-carbon-adsorption-roop-chand-bansal-meenakshi-goyal

[5] A. Demirbas, « Agricultural based activated carbons for the removal of dyes from aqueous solutions: a review », J. Hazard. Mater., vol. 167, nº 1-3, p. 1-9, 2009.

[6] S. Babel et T. A. Kurniawan, « Low-cost adsorbents for heavy metals uptake from contaminated water: a review », J. Hazard. Mater., vol. 97, nº 1-3, p. 219-243, 2003.

[7] E. N. El Qada, S. J. Allen, et G. M. Walker, « Adsorption of basic dyes from aqueous solution onto activated carbons », Chem. Eng. J., vol. 135, nº 3, p. 174-184, 2008.

[8] L. Giraldo et J. C. Moreno-Piraján, « Synthesis of Activated Carbon Mesoporous from Coffee Waste and Its Application in Adsorption Zinc and Mercury Ions from Aqueous Solution », J. Chem., vol. 9, nº 2, p. 938-948, janv. 2012, doi: 10.1155/2012/120763.

[9] M. Roy et R. Saha, « Dyes and their removal technologies from wastewater: A critical review », Intell. Environ. Data Monit. Pollut. Manag., p. 127-160, 2021.

[10] M. Roy et R. Saha, « Dyes and their removal technologies from wastewater: A critical review », Intell. Environ. Data Monit. Pollut. Manag., p. 127-160, 2021.

[11] T. Chinedu Egbosiuba, « Application of Agricultural Waste in Anionic Dyes Removal from Wastewater », in Textile Wastewater Treatment, S. S. Muthu et A. Khadir, Éd., in Sustainable Textiles: Production, Processing, Manufacturing & Chemistry. , Singapore: Springer Nature Singapore, 2022, p. 111-141. doi: 10.1007/978-981-19-2852-9_7.

[12] E. Yılmaz, E. Sert, et F. S. Atalay, « Synthesis, characterization of a metal organic framework: MIL-53 (Fe) and adsorption mechanisms of methyl red onto MIL-53 (Fe) », J. Taiwan Inst. Chem. Eng., vol. 65, p. 323-330, 2016.

[13] A. Eleryan et al., « Kinetic and isotherm studies of Acid Orange 7 dye absorption using sulphonated mandarin biochar treated with TETA », Biomass Convers. Biorefinery, vol. 14, nº 9, p. 10599-10610, mai 2024, doi: 10.1007/s13399-023-04089-w.

[14] M. I. Din, R. Khalid, Z. Hussain, M. Arshad, et S. A. Khan, « A critical review on application of organic, inorganic and hybrid nanophotocatalytic assemblies for photocatalysis of methyl orange dye in aqueous medium », Rev. Chem. Eng., vol. 40, nº 1, p. 67-91, janv. 2024, doi: 10.1515/revce-2022-0026.

[15] N. Siddique, M. I. Din, R. Khalid, et Z. Hussain, « A comprehensive review on the photocatalysis of Congo red dye for wastewater treatment », Rev. Chem. Eng., vol. 40, nº 4, p. 481-510, mai 2024, doi: 10.1515/revce-2022-0076.

[16] P. Parthasarathy, S. Sajjad, J. Saleem, M. Alherbawi, et G. Mckay, « A review of the removal of dyestuffs from effluents onto biochar », Separations, vol. 9, nº 6, p. 139, 2022.

[17] Z. Hua, Y. Pan, et Q. Hong, « Adsorption of Congo red dye in water by orange peel biochar modified with CTAB », RSC Adv., vol. 13, nº 18, p. 12502-12508, 2023.

[18] A. Debnath, K. Deb, N. S. Das, K. K. Chattopadhyay, et B. Saha, « Simple Chemical Route Synthesis of Fe_2 O_3 Nanoparticles and its Application for Adsorptive Removal of Congo Red from Aqueous Media: Artificial Neural Network Modeling », J. Dispers. Sci. Technol., vol. 37, nº 6, p. 775-785, juin 2016, doi: 10.1080/01932691.2015.1062772.

[19] A. Eleryan et al., « Kinetic and isotherm studies of Acid Orange 7 dye absorption using sulphonated mandarin biochar treated with TETA », Biomass Convers. Biorefinery, vol. 14, nº 9, p. 10599-10610, mai 2024, doi: 10.1007/s13399-023-04089-w.

[20] E. Forgacs, T. Cserháti, et G. Oros, « Removal of synthetic dyes from wastewaters: a review », Environ. Int., vol. 30, nº 7, p. 953-971, 2004.

[21] A. Bhatnagar et A. K. Minocha, « Conventional and non-conventional adsorbents for removal of pollutants from water-A review », Indian J. Chem. Technol., vol. 13, nº 3, p. 203-217, 2006.

[22] R. G. Saratale, G. D. Saratale, J.-S. Chang, et S. P. Govindwar, « Bacterial decolorization and degradation of azo dyes: a review », J. Taiwan Inst. Chem. Eng., vol. 42, nº 1, p. 138-157, 2011.

[23] A. Strebel, M. Behringer, H. Hilbig, A. Machner, et B. Helmreich, « Anionic azo dyes and their removal from textile wastewater through adsorption by various adsorbents: a critical review », Front. Environ. Eng., vol. 3, p. 1347981, 2024.

[24] H. Kumari et al., « A Review on Photocatalysis Used For Wastewater Treatment: Dye Degradation », Water. Air. Soil Pollut., vol. 234, nº 6, p. 349, juin 2023, doi: 10.1007/s11270-023-06359-9.

[25] G. Derafa et H. Zaghouane-Boudiaf, « Urtica dioica leaves-calcium alginate as a natural, low cost and very effective bioadsorbent beads in elimination of dyes from aqueous medium: Equilibrium isotherms and thermodynamic studies », Int. J. Biol. Macromol., vol. 124, p. 915-921, 2019.

[26] V. Yalasangi, N. Mayilswamy, et B. Kandasubramanian, « Biochar-derived adsorbents for removal of Rhodamine B from wastewater », Bioresour. Technol. Rep., p. 101987, 2024.

[27] L. Dutta, G. K. Sethi, et S. Dey, « A Comprehensive and Critical Assessment on the Efficiency of Natural and Synthetic Adsorbents for the Removal of Recalcitrant Malachite Green from Water: Present Level and Future Perspectives », Korean J. Chem. Eng., vol. 41, nº 3, p. 589-607, mars 2024, doi: 10.1007/s11814-024-00114-4.

[28] A. P. Periyasamy, « Recent advances in the remediation of textile-dye-containing wastewater: prioritizing human health and sustainable wastewater treatment », Sustainability, vol. 16, nº 2, p. 495, 2024.

[29] A. Adak, M. Bandyopadhyay, et A. Pal, « Removal of crystal violet dye from wastewater by surfactant-modified alumina », Sep. Purif. Technol., vol. 44, nº 2, p. 139-144, 2005.

[30] R. Ahmad, « Studies on adsorption of crystal violet dye from aqueous solution onto coniferous pinus bark powder (CPBP) », J. Hazard. Mater., vol. 171, nº 1-3, p. 767-773, 2009.

[31] A. A. Oladipo et M. Gazi, « Enhanced removal of crystal violet by low cost alginate/acid activated bentonite composite beads: optimization and modelling using non-linear regression technique », J. Water Process Eng., vol. 2, p. 43-52, 2014.

[32] A. Mittal, J. Mittal, A. Malviya, et V. K. Gupta, « Removal and recovery of Chrysoidine Y from aqueous solutions by waste materials », J. Colloid Interface Sci., vol. 344, nº 2, p. 497-507, 2010.

[33] A. E. Gahrouei, S. Vakili, A. Zandifar, et S. Pourebrahimi, « From wastewater to clean water: Recent advances on the removal of metronidazole, ciprofloxacin, and sulfamethoxazole antibiotics from water through adsorption and advanced oxidation processes (AOPs) », Environ. Res., p. 119029, 2024.

[34] B. Pizzicato, S. Pacifico, D. Cayuela, G. Mijas, et M. Riba-Moliner, « Advancements in sustainable natural dyes for textile applications: a review », Molecules, vol. 28, nº 16, p. 5954, 2023.

[35] S. I. Ichetaonye, K. K. Ajekwene, U. K. Ugo, C. K. Oguzie, et F. A. Opara, « A review of the characteristics and prospective applications of cola acuminata (cola nut) dye extract on textile materials », Discov. Mater., vol. 4, nº 1, p. 32, août 2024, doi: 10.1007/s43939-024-00095-5.

[36] M. R. Heidari et al., « Photo-Fenton like catalyst system: activated carbon/CoFe2O4 nanocomposite for reactive dye removal from textile wastewater », Appl. Sci., vol. 9, nº 5, p. 963, 2019.

[37] Y. Dai et al., « Utilizations of agricultural waste as adsorbent for the removal of contaminants: A review », Chemosphere, vol. 211, p. 235-253, 2018.

[38] S. Afroze et T. K. Sen, « A Review on Heavy Metal Ions and Dye Adsorption from Water by Agricultural Solid Waste Adsorbents », Water. Air. Soil Pollut., vol. 229, nº 7, p. 225, juill. 2018, doi: 10.1007/s11270-018-3869-z.

[39] T. Ahmad, M. Rafatullah, A. Ghazali, O. Sulaiman, et R. Hashim, « Oil Palm Biomass–Based Adsorbents for the Removal of Water Pollutants—A Review », J. Environ. Sci. Health Part C, vol. 29, nº 3, p. 177-222, juill. 2011, doi: 10.1080/10590501.2011.601847.

[40] M. Roy et R. Saha, « Dyes and their removal technologies from wastewater: A critical review », Intell. Environ. Data Monit. Pollut. Manag., p. 127-160, 2021.

[41] V. I. Mabayo et R. Orale, « Agricultural-based Biomass as an Efficient Adsorbent in the Removal of Dyes in Dye-contaminated Wastewater: A Mini Review », Curr. Appl. Sci. Technol., p. e0257011-e0257011, 2024.

[42] G. Crini et E. Lichtfouse, « Advantages and disadvantages of techniques used for wastewater treatment », Environ. Chem. Lett., vol. 17, nº 1, p. 145-155, mars 2019, doi: 10.1007/s10311-018-0785-9.

[43] T. A. Aragaw et F. M. Bogale, « Biomass-based adsorbents for removal of dyes from wastewater: a review », Front. Environ. Sci., vol. 9, p. 764958, 2021.

[44] G. Liu, Z. Dai, X. Liu, R. A. Dahlgren, et J. Xu, « Modification of agricultural wastes to improve sorption capacities for pollutant removal from water – a review », Carbon Res., vol. 1, nº 1, p. 24, nov. 2022, doi: 10.1007/s44246-022-00025-1.

[45] M. Sardar, M. Manna, M. Maharana, et S. Sen, « Remediation of Dyes from Industrial Wastewater Using Low-Cost Adsorbents », in Green Adsorbents to Remove Metals, Dyes and Boron from Polluted Water, vol. 49, Inamuddin, M. I. Ahamed, E. Lichtfouse, et A. M. Asiri, Éd., in Environmental Chemistry for a Sustainable World, vol. 49. , Cham: Springer International Publishing, 2021, p. 377-403. doi: 10.1007/978-3-030-47400-3_15.

[46] A. A. Attia, W. E. Rashwan, et S. A. Khedr, « Capacity of activated carbon in the removal of acid dyes subsequent to its thermal treatment », Dyes Pigments, vol. 69, nº 3, p. 128-136, 2006.

[47] A. Lim, J. J. Chew, S. Ismadji, D. S. Khaerudini, N. Darsono, et J. Sunarso, « Kinetic and equilibrium adsorption study of anionic dyes using oil palm trunk-derived activated carbon », Mater. Today Proc., vol. 64, p. 1627-1638, 2022.

[48] S. K. Yadav, S. R. Dhakate, et B. P. Singh, « Carbon nanotube incorporated eucalyptus derived activated carbon-based novel adsorbent for efficient removal of methylene blue and eosin yellow dyes », Bioresour. Technol., vol. 344, p. 126231, 2022.

[49] M. Sultana, M. H. Rownok, M. Sabrin, M. H. Rahaman, et S. N. Alam, « A review on experimental chemically modified activated carbon to enhance dye and heavy metals adsorption », Clean. Eng. Technol., vol. 6, p. 100382, 2022.

[50] G. Feiqiang, L. Xiaolei, J. Xiaochen, Z. Xingmin, G. Chenglong, et R. Zhonghao, « Characteristics and toxic dye adsorption of magnetic activated carbon prepared from biomass waste by modified one-step synthesis », Colloids Surf. Physicochem. Eng. Asp., vol. 555, p. 43-54, 2018.

[51] A. Yadav, N. Bagotia, S. Yadav, A. K. Sharma, et S. Kumar, « Adsorptive studies on the removal of dyes from single and binary systems using Saccharum munja plant-based novel functionalized CNT composites », Environ. Technol. Innov., vol. 24, p. 102015, 2021.

[52] S. A. Shah et al., « Biomass impregnated zero-valent Ag and Cu supported-catalyst: Evaluation in the reduction of nitrophenol and discoloration of dyes in aqueous medium », J. Organomet. Chem., vol. 938, p. 121756, 2021.

[53] [5 6] B. Noroozi, G. A. Sorial, H. Bahrami, et M. Arami, « Equilibrium and kinetic adsorption study of a cationic dye by a natural adsorbent—Silkworm pupa », J. Hazard. Mater., vol. 139, nº 1, p. 167-174, 2007.

[54] A. R. Khan, F. U. HAJIRA TAHIR, et U. HAMEED, « Adsorption of methylene blue from aqueous solution on the surface of wool fiber and cotton fiber », J. Appl. Sci. Environ. Manag., vol. 9, nº 2, p. 29-35, 2005.

[55] S. Wang, Y. Boyjoo, A. Choueib, et Z. H. Zhu, « Removal of dyes from aqueous solution using fly ash and red mud », Water Res., vol. 39, nº 1, p. 129-138, 2005.

[56] C. Namasivayam et N. Kanchana, « Removal of Congo red from aqueous solution by waste banana pith », Pertanika J. Sci. Technol. Malays., vol. 1, nº 1, 1993, Consulté le: 14 novembre 2024. [En ligne]. Disponible sur: https://agris.fao.org/search/en/providers/122640/records/64775900bc45d9ecdbc1b1f1

[57] C. Namasivayam, N. Kanchana, et R. T. Yamuna, « Waste banana pith as adsorbent for the removal of rhodamine-B from aqueous solutions », Waste Manag., vol. 13, nº 1, p. 89-95, 1993.

[58] R. Juang, R. Tseng, F. Wu, et S. Lin, « Use of chitin and chitosan in lobster shell wastes for color removal from aqueous solutions », J. Environ. Sci. Health Part Environ. Sci. Eng. Toxicol., vol. 31, nº 2, p. 325-338, févr. 1996, doi: 10.1080/10934529609376360.

[59] H. M. Asfour, O. A. Fadali, M. M. Nassar, et M. S. El-Geundi, « Equilibrium studies on adsorption of basic dyes on hardwood », J. Chem. Technol. Biotechnol. Chem. Technol., vol. 35, nº 1, p. 21-27, janv. 1985, doi: 10.1002/jctb.5040350105.

[60] D. K. Singh et B. Srivastava, « Basic dyes removal from wastewater by adsorption on rice husk carbon », 2001, Consulté le: 14 novembre 2024. [En ligne]. Disponible sur: https://nopr.niscpr.res.in/handle/123456789/22874

[61] K. K. Alau, C. E. Gimba, et J. A. Kagbu, « Removal of dyes from aqueous solution using neem (Azadirachta indica) husk as activated carbon », Arch. Appl. Sci. Res., vol. 2, nº 5, p. 456-461, 2010.

[62] V. Subburam, « Activated parthenium carbon as an adsorbent for the removal of dyes and heavy metal ions from aqueous solution », Bioresour. Technol., vol. 85, nº 2, p. 205-206, 2002.

[63] A. Habib, Z. Hasan, A. Rahman, et A. S. Alam, « Tuberose Sticks as an Adsorbent in the Removal of Methylene Bluefrom Aqueous Solution », Pak. J. Anal. Environ. Chem., vol. 7, nº 2, p. 112-115, 2006.

[64] M. A. Rauf, I. Shehadeh, A. Ahmed, et A. Al-Zamly, « Removal of methylene blue from aqueous solution by using gypsum as a low cost adsorbent », Int. J. Chem. Mol. Eng., vol. 3, nº 7, p. 369-374, 2009.

[65] P. Saha, « Assessment on the Removal of Methylene Blue Dye using Tamarind Fruit Shell as Biosorbent », Water. Air. Soil Pollut., vol. 213, nº 1-4, p. 287-299, nov. 2010, doi: 10.1007/s11270-010-0384-2.

[66] C. Cardot, « Les traitements de l'eau, procédés physico-chimiques et biologiques, Cours et problèmes résolus, Génie de l'environnement, Ed ellipses ». France, 2002.

[67] C. Cardot, Les traitements de l'eau pour l'ingénieur: procédés physico-chimiques et biologiques: cours et problèmes résolus. Ellipses, 2010.

[68] A. Essekri et al., « Novel citric acid-functionalized brown algae with a high removal efficiency of crystal violet dye from colored wastewaters: insights into equilibrium, adsorption mechanism, and reusability », Int. J. Phytoremediation, vol. 23, nº 4, p. 336-346, mars 2021, doi: 10.1080/15226514.2020.1813686.

[69] L. C. Lau, N. MohamadNor, K. T. Lee, et A. R. Mohamed, « Adsorption isotherm, kinetic, thermodynamic and breakthrough curve models of H2S removal using CeO2/NaOH/PSAC », Int. J. Petrochem. Sci. Eng., vol. 1, nº 2, p. 36-44, 2016.

[70] V. Bolis, « Fundamentals in Adsorption at the Solid-Gas Interface. Concepts and Thermodynamics », in Calorimetry and Thermal Methods in Catalysis, vol. 154, A. Auroux, Éd., in Springer Series in Materials Science, vol. 154. , Berlin, Heidelberg: Springer Berlin Heidelberg, 2013, p. 3-50. doi: 10.1007/978-3-642-11954-5_1.

[71] Y.-S. Ho et G. McKay, « Sorption of dye from aqueous solution by peat », Chem. Eng. J., vol. 70, nº 2, p. 115-124, 1998.

[72] N. N. Abd Malek, A. H. Jawad, K. Ismail, R. Razuan, et Z. A. ALOthman, « Fly ash modified magnetic chitosan-polyvinyl alcohol blend for reactive orange 16 dye removal: Adsorption parametric optimization », Int. J. Biol. Macromol., vol. 189, p. 464-476, 2021.

[73] C. H. Giles, D. Smith, et A. Huitson, « A general treatment and classification of the solute adsorption isotherm. I. Theoretical », J. Colloid Interface Sci., vol. 47, nº 3, p. 755-765, 1974.

[74] I. Langmuir, « THE ADSORPTION OF GASES ON PLANE SURFACES OF GLASS, MICA AND PLATINUM. », J. Am. Chem. Soc., vol. 40, nº 9, p. 1361-1403, sept. 1918, doi: 10.1021/ja02242a004.

[75] H. Freundlich, « Über die Adsorption in Lösungen », Z. Für Phys. Chem., vol. 57U, nº 1, p. 385-470, oct. 1907, doi: 10.1515/zpch-1907-5723.

[76] M. Chebbi, S. Ounoki, L. Youcef, et A. Amrane, « Synthesis and characterization of pine cones biochar for the removal of an antibiotic (Metronidazole) from aqueous solutions », J. Ind. Eng. Chem., vol. 126, p. 327-339, 2023.

[77] N. Boukhalfa, M. Boutahala, N. Djebri, et A. Idris, « Kinetics, thermodynamics, equilibrium isotherms, and reusability studies of cationic dye adsorption by magnetic alginate/oxidized multiwalled carbon nanotubes composites », Int. J. Biol. Macromol., vol. 123, p. 539-548, 2019.

[78] A.-C. Enache, P. Samoila, C. Cojocaru, R. Apolzan, G. Predeanu, et V. Harabagiu, « An eco-friendly modification of a walnut shell biosorbent for increased efficiency in wastewater treatment », Sustainability, vol. 15, nº 3, p. 2704, 2023.

[79] A.-C. Enache et al., « Adsorption of brilliant green dye onto a mercerized biosorbent: kinetic, thermodynamic, and molecular docking studies », Molecules, vol. 28, nº 10, p. 4129, 2023.

[80] S. Azizian, S. Eris, et L. D. Wilson, « Re-evaluation of the century-old Langmuir isotherm for modeling adsorption phenomena in solution », Chem. Phys., vol. 513, p. 99-104, 2018.

[81] M. Kadhom, N. Albayati, H. Alalwan, et M. Al-Furaiji, « Removal of dyes by agricultural waste », Sustain. Chem. Pharm., vol. 16, p. 100259, 2020.

[82] N. El Messaoudi et al., « Regeneration and reusability of non-conventional low-cost adsorbents to remove dyes from wastewaters in multiple consecutive adsorption–desorption cycles: a review », Biomass Convers. Biorefinery, vol. 14, nº 11, p. 11739-11756, juin 2024, doi: 10.1007/s13399-022-03604-9.

[83] J. Rashid, F. Tehreem, A. Rehman, et R. Kumar, « Synthesis using natural functionalization of activated carbon from pumpkin peels for decolourization of aqueous methylene blue », Sci. Total Environ., vol. 671, p. 369-376, 2019.

[84] D. Bal, Ç. Özer, et M. İmamoğlu, « Green and Ecofriendly Biochar Preparation from Pumpkin Peel and Its Usage as an Adsorbent for Methylene Blue Removal from Aqueous Solutions », Water. Air. Soil Pollut., vol. 232, nº 11, p. 457, nov. 2021, doi: 10.1007/s11270-021-05411-w.

[85] W. Abbach, C. Laghlimi, et J. Isaad, « Simultaneous adsorption of cationic and anionic dyes by raw pomegranate peel: Modelling of equilibrium, kinetical and thermodynamical studies », Moroc. J. Chem., vol. 11, nº 3, p. J-Chem, 2023.

[86] B. M. Thamer, F. A. Al-Aizari, et H. S. Abdo, « Enhanced adsorption of textile dyes by a novel sulfonated activated carbon derived from pomegranate peel waste: isotherm, kinetic and thermodynamic study », Molecules, vol. 28, nº 23, p. 7712, 2023.

[87] R. Sun, « Economic/Academic interest of Brassica rapa », Brasica Rapa Genome, p. 1-16, 2015.

[88] S. Gairola, J. Sharma, et Y. S. Bedi, « A cross-cultural analysis of Jammu, Kashmir and Ladakh (India) medicinal plant use », J. Ethnopharmacol., vol. 155, n° 2, p. 925-986, 2014.

[89] A. G. Adeniyi et J. O. Ighalo, « Biosorption of pollutants by plant leaves: An empirical review », J. Environ. Chem. Eng., vol. 7, n° 3, p. 103100, 2019.

[90] F. FAO, « Food and agriculture organization corporate statistical database », Hazelnut Prod. Quant. Ctry., p. 2017, 2017.

[91] E. Buzigi, K. Pillay, et M. Siwela, « Potential of pumpkin to combat vitamin A deficiency during complementary feeding in low and middle income countries: variety, provitamin A carotenoid content and retention, and dietary reference intakes », Crit. Rev. Food Sci. Nutr., vol. 62, n° 22, p. 6103-6112, juill. 2022, doi: 10.1080/10408398.2021.1896472.

[92] N. A. Giri, N. N. Gaikwad, P. Raigond, R. Damale, et R. A. Marathe, « Exploring the Potential of Pomegranate Peel Extract as a Natural Food Additive: A Review », Curr. Nutr. Rep., vol. 12, n° 2, p. 270-289, mars 2023, doi: 10.1007/s13668-023-00466-z.

[93] R. S. Varma, « Biomass-Derived Renewable Carbonaceous Materials for Sustainable Chemical and Environmental Applications », ACS Sustain. Chem. Eng., vol. 7, n° 7, p. 6458-6470, avr. 2019, doi: 10.1021/acssuschemeng.8b06550.

[94] N. Hagemann, K. Spokas, H.-P. Schmidt, R. Kägi, M. A. Böhler, et T. D. Bucheli, « Activated carbon, biochar and charcoal: linkages and synergies across pyrogenic carbon's ABC s », Water, vol. 10, n° 2, p. 182, 2018.

[95] E. M. Calvo-Munoz, F. J. Garcia-Mateos, J. M. Rosas, J. Rodriguez-Mirasol, et T. Cordero, « Biomass waste carbon materials as adsorbents for CO2 capture under post-combustion conditions », Front. Mater., vol. 3, p. 23, 2016.

[96] O. F. Olorundare, T. A. M. Msagati, R. W. M. Krause, J. O. Okonkwo, et B. B. Mamba, « Activated Carbon from Lignocellulosic Waste Residues: Effect of Activating Agent on Porosity Characteristics and Use as Adsorbents for Organic Species », Water. Air. Soil Pollut., vol. 225, n° 3, p. 1876, mars 2014, doi: 10.1007/s11270-014-1876-2.

[97] B. S. Girgis, A. M. Soliman, et N. A. Fathy, « Development of micro-mesoporous carbons from several seed hulls under varying conditions of activation », Microporous Mesoporous Mater., vol. 142, n° 2-3, p. 518-525, 2011.

[98] A. Arami-Niya, W. M. A. W. Daud, F. S. Mjalli, F. Abnisa, et M. S. Shafeeyan, « Production of microporous palm shell based activated carbon for methane adsorption: modeling and optimization using response surface methodology », Chem. Eng. Res. Des., vol. 90, n° 6, p. 776-784, 2012.

[99] C.-H. Ooi, W.-K. Cheah, Y.-L. Sim, S.-Y. Pung, et F.-Y. Yeoh, « Conversion and characterization of activated carbon fiber derived from palm empty fruit bunch waste and its kinetic study on urea adsorption », J. Environ. Manage., vol. 197, p. 199-205, 2017.

[100] Z. Z. Chowdhury et al., « Preparation of carbonaceous adsorbents from lignocellulosic biomass and their use in removal of contaminants from aqueous solution », BioResources, vol. 8, nº 4, p. 6523-6555, 2013.

[101] K. Ahmida, M. Darmoon, F. Al-Tohami, M. Erhayem, et M. Zidan, « Effect of physical and chemical preparation on characteristics of activated carbon from agriculture solid waste and their potential application », Int. Inst. Chem. Biol. Environ. Eng. June, p. 5-6, 2015.

[102] J. Liu, Y. Deng, X. Li, et L. Wang, « Promising Nitrogen-Rich Porous Carbons Derived from One-Step Calcium Chloride Activation of Biomass-Based Waste for High Performance Supercapacitors », ACS Sustain. Chem. Eng., vol. 4, nº 1, p. 177-187, janv. 2016, doi: 10.1021/acssuschemeng.5b00926.

[103] S. Bachrun, N. AyuRizka, S. Annisa, et H. Arif, « Preparation and characterization of activated carbon from sugarcane bagasse by physical activation with CO2 gas », in IOP Conference Series: Materials Science and Engineering, IOP Publishing, 2016, p. 012027. Consulté le: 1 mai 2025. [En ligne]. Disponible sur: https://iopscience.iop.org/article/10.1088/1757-899X/105/1/012027/meta

[104] O. Oginni, K. Singh, G. Oporto, B. Dawson-Andoh, L. McDonald, et E. Sabolsky, « Influence of one-step and two-step KOH activation on activated carbon characteristics », Bioresour. Technol. Rep., vol. 7, p. 100266, 2019.

[105] M. Oghbaei et O. Mirzaee, « Microwave versus conventional sintering: A review of fundamentals, advantages and applications », J. Alloys Compd., vol. 494, nº 1-2, p. 175-189, 2010.

[106] C. Gan et al., « Effect of porous zinc–biochar nanocomposites on Cr (VI) adsorption from aqueous solution », Rsc Adv., vol. 5, nº 44, p. 35107-35115, 2015.

[107] A. Dominguez et al., « Conventional and microwave induced pyrolysis of coffee hulls for the production of a hydrogen rich fuel gas », J. Anal. Appl. Pyrolysis, vol. 79, nº 1-2, p. 128-135, 2007.

[108] B. Fidalgo, H. M. Williams, E. A. Dawson, et G. M. B. Parkes, « Conventional and microwave-heated oxygen pulsing techniques on metal-doped activated carbons », J. Porous Mater., vol. 21, nº 1, p. 81-89, févr. 2014, doi: 10.1007/s10934-013-9750-y.

[109] K. S. Ukanwa, K. Patchigolla, R. Sakrabani, E. Anthony, et S. Mandavgane, « A review of chemicals to produce activated carbon from agricultural waste biomass », Sustainability, vol. 11, nº 22, p. 6204, 2019.

[110] C. Qin, K. Clarke, et K. Li, « Interactive forces between lignin and cellulase as determined by atomic force microscopy », Biotechnol. Biofuels, vol. 7, nº 1, déc. 2014, doi: 10.1186/1754-6834-7-65.

[111] S. M. Yakout et G. S. El-Deen, « Characterization of activated carbon prepared by phosphoric acid activation of olive stones », Arab. J. Chem., vol. 9, p. S1155-S1162, 2016.

[112] H.-M. Lee, K.-H. An, et B.-J. Kim, « Effects of carbonization temperature on pore development in polyacrylonitrile-based activated carbon nanofibers », Carbon Lett., vol. 15, nº 2, p. 146-150, 2014.

[113] A. S. Ello, L. K. de Souza, A. Trokourey, et M. Jaroniec, « Development of microporous carbons for CO2 capture by KOH activation of African palm shells », J. CO2 Util., vol. 2, p. 35-38, 2013.

[114] Ö. Şahin, C. Saka, A. A. Ceyhan, et O. Baytar, « Preparation of High Surface Area Activated Carbon fromElaeagnus angustifoliaSeeds by Chemical Activation with $ZnCl_2$in One-Step Treatment and its Iodine Adsorption », Sep. Sci. Technol., vol. 50, nº 6, p. 886-891, avr. 2015, doi: 10.1080/01496395.2014.966204.

[115] A. C. Arampatzidou et E. A. Deliyanni, « Comparison of activation media and pyrolysis temperature for activated carbons development by pyrolysis of potato peels for effective adsorption of endocrine disruptor bisphenol-A », J. Colloid Interface Sci., vol. 466, p. 101-112, 2016.

[116] K. Fu, Q. Yue, B. Gao, Y. Wang, et Q. Li, « Activated carbon from tomato stem by chemical activation with FeCl2 », Colloids Surf. Physicochem. Eng. Asp., vol. 529, p. 842-849, 2017.

[117] L. Z. Lee et M. A. A. Zaini, « Metal chloride salts in the preparation of activated carbon and their hazardous outlook », Desalination Water Treat., vol. 57, nº 34, p. 16078-16085, 2016.

[118] S. Sun et al., « Adsorption of crystal violet on activated bamboo fiber powder from water: preparation, characterization, kinetics and isotherms », RSC Adv., vol. 13, nº 9, p. 6108-6123, 2023.

[119] S. K. Jadhav et S. R. Thorat, « Adsorption Isotherm Study of Crystal Violet Dye on to Biochar Prepared from Agriculture Waste », Orient. J. Chem., vol. 38, nº 2, p. 475, 2022.

[120] K. Naseem et al., « Raphanus caudatus biomass powder as potential adsorbent for the removal of crystal violet and Rhodamine B dye from wastewater », Z. Für Phys. Chem., vol. 237, nº 11, p. 1863-1883, nov. 2023, doi: 10.1515/zpch-2023-0259.

[121] Z. Hua, Y. Pan, et Q. Hong, « Adsorption of Congo red dye in water by orange peel biochar modified with CTAB », RSC Adv., vol. 13, nº 18, p. 12502-12508, 2023.

[122] A. A. Muhammad et B. Idoko, « Adsorption of Congo red dye from aqueous solution using raw cowpea (Vigna Unguiculata) husk », J. Appl. Surf. Interfaces, vol. 9, nº 1-3, 2021, Consulté le: 4 mai 2025. [En ligne]. Disponible sur: https://revues.imist.ma/index.php/jasi/article/view/24438

[123] R. O. Yakubu, M. N. Yaro, S. Habibu, et S. Nasir, « Efficient removal of Congo red dye from aqueous solution using a biosorbent derived from Phoenix dactylifera seeds: exploring kinetic and thermodynamic parameters », ChemSearch J., vol. 15, nº 1, p. 8-19, 2024.

[124] M. D. Teweldebrihan et M. O. Dinka, « Methyl red adsorption from aqueous solution using Rumex Abyssinicus-derived biochar: Studies of kinetics and isotherm », Water, vol. 16, nº 16, p. 2237, 2024.

[125] H. S. Rafidah, H. Prasetia, et A. Saefumillah, « Adsorption Study of Methylene Blue and Methyl Red on Activated Carbon from Silver Composite Using the Extract of Spent Coffee Grounds », J. Sains Materi Indones., vol. 25, nº 2, p. 77-84, 2024.

[126] D. Paluch, A. Bazan-Wozniak, R. Wolski, A. Nosal-Wiercińska, et R. Pietrzak, « Removal of methyl red from aqueous solution using biochar derived from fennel seeds », Molecules, vol. 28, nº 23, p. 7786, 2023.

[127] A. Çelekli, B. Bozkuş, et H. Bozkurt, « Development of a new adsorbent from pumpkin husk by KOH-modification to remove copper ions », Environ. Sci. Pollut. Res. Int., vol. 26, nº 12, p. 11514-11523, avr. 2019, doi: 10.1007/s11356-017-1160-2.

[128] S. Allende, Y. Liu, M. A. Zafar, et M. V. Jacob, « Eco-friendly synthesis of carbon nanomaterials from pumpkin waste », J. Porous Mater., vol. 32, nº 6, p. 2443-2453, déc. 2025, doi: 10.1007/s10934-025-01844-4.

[129] D. Bal, C. Ozer, et M. Imamoglu, « Green and Ecofriendly Biochar Preparation from Pumpkin Peel and Its Usage as an Adsorbent for Methylene Blue Removal from Aqueous Solutions », Water Aır Soıl Pollutıon, 2021, doi: 10.1007/s11270-021-05411-w.

[130] « KCER ». Consulté le: 3 décembre 2025. [En ligne]. Disponible sur: https://www.kiche.or.kr/

[131] I. Bouchareb, R. Kara, N. Rouahna, A. Ouakouak, et N. Hamdi, « Utilization of Biochar Produced from Pomegranate Peels for the Effective Adsorption of Dyes in Water », déc. 2023, Consulté le: 3 décembre 2025. [En ligne]. Disponible sur: https://dspace.univ-eloued.dz/handle/123456789/33178

Chapter II

Materials, experimental methodology and characterization techniques

II.1. Introduction

The objective of this chapter is to describe the various protocols used for the preparation of the materials examined and evaluated in the process of adsorption of crystal violet (CV), congo red (CR) and methyl red (MR) dyes. Next, we will describe in detail the procedure for the preparation of the selected pollutants, as well as the analysis tool used, namely UV-visible spectroscopy. Subsequently, we will present the analytical methods used to characterize the adsorbent materials, in particular Fourier transform infrared spectroscopy (FTIR), thermal analysis (TGA/DTA), scanning electron microscopy (SEM) and the determination of the isoelectric point. The analysis of adsorbents is of crucial importance in the understanding of the mechanisms related to adsorption and in the evaluation of the influence of the physicochemical properties of materials on the degradation efficiency of dyes.

II.2. Materials and methods

II.2.1. Materials

All the chemicals used in this research, including CV, CR and MR with 99.99% purity, H_3PO_4(85%), HCl(37%), NaOH(99%) , NaCl(99.9%) and ethanol (99%) were obtained from Sigma Aldrich. The turnip leaves, pumpkin peels and pomegranate crusts were harvested in the region of Setif, in Algeria.

II.2.2. Methods

II.2.2.1. Preparation of adsorbents

Turnip leaves and pumpkin peels were collected in the Setif region. They have been thoroughly washed with tap water, then rinsed with distilled water to remove impurities. After washing, the samples were dried, then ground using a mortar until a fine powder was obtained, designated under the name of turnip leaves (TL) and pumpkin peels (PP) .

A portion of this powder was then chemically activated by mixing with phosphoric acid (H_3PO_4) at 1 M, according to a mass ratio of 1:1 (10 g of powder per 10 g of H_3PO_4). The mixture was kept stirring in the open air for 24 hours. Subsequently, the material was washed with distilled water until a neutral pH was reached, then dried at 60 °C. for 24 hours. Finally,

it was ground again to obtain an activated fine powder, designated under the name of TLA and APP. figures II.1 and II.2 represent images of turnip leaves and pumpkin peel respectively

The pomegranate crusts (PC) were prepared according to the same procedure as that used for turnip leaves and pumpkin peels. After drying and grinding, the powder obtained was chemically activated using phosphoric acid (H_3PO_4) at 3 M, keeping the mixture stirring for 10 hours at room temperature.

The mixture was then washed several times with distilled water until neutral (pH ≈ 7), then dried in an oven at 100 ° C. for 24 hours.

After drying, the material was calcined in an oven at 450 °C. for 1 hour in order to complete the activation. The final product, designated under the name of activated carbon based on pomegranate crusts (APC), constitutes an adsorbent material. Figure II.3 illustrates photos on the crusts of pomegranates.

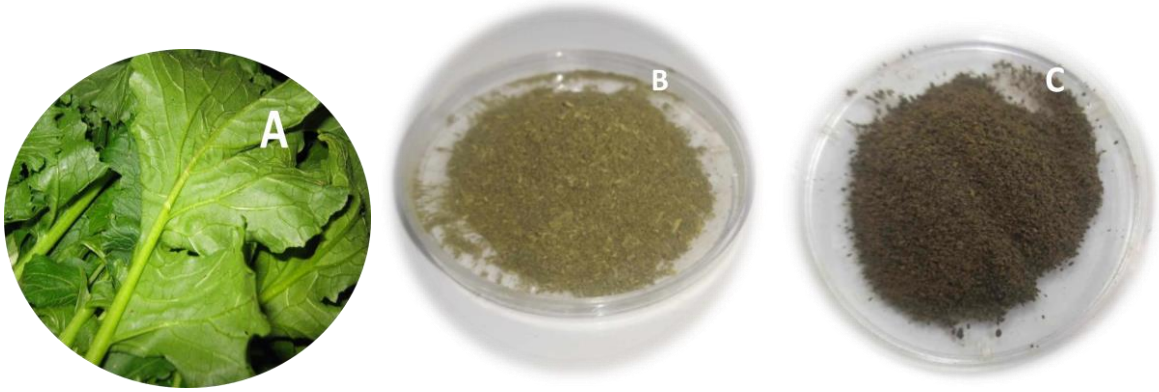

Figure II.1. (A) The turnip leaves, (B) the powder of the raw turnip leaves TL, (C) the activated turnip leaves TLA.

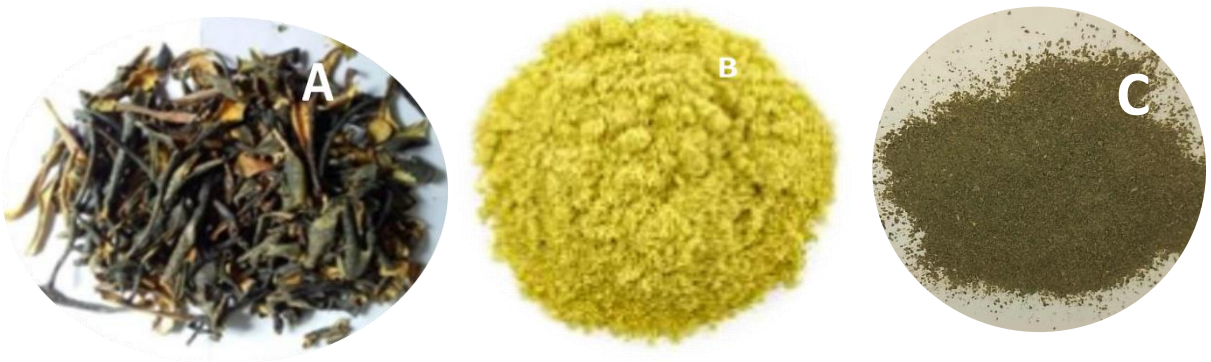

Figure II.2. (A) The pumpkin peels, (B) the powder of the raw pumpkin peels PP, (C) the activated pumpkin peels APP.

Figure II.3. (A) The pomegranate crusts, (B) the powder of the raw pomegranate crusts PC, (C) the activated pomegranate crusts APC.

II.2.2.2. Preparation of adsorbates

In this research work, we used a cationic dye, crystal violet (CV), as well as two anionic dyes, congo red (CR) and methyl red (MR), all obtained from the Sigma-Aldrich company. The stock solutions of each dye were prepared by dissolving 1 g of dye in 1000 mL of distilled water. The daughter solutions were then obtained by appropriate dilution of the mother solutions.

The analysis of the various initial or residual concentrations of the CV, CR and MR solutions was carried out using a UV-Visible spectrophotometer (Shimadzu UV-Vis 1700), at the respective maximum wavelengths of 590, 500 and 520 nm. This device makes it possible to directly measure the optical density (or absorbance) of each solution, which makes it possible to determine the concentrations thanks to the Beer-Lambert law, which establishes a proportionality relationship between the absorbance and the concentration of the analyzed solution[1].The calibration curves of the CV, CR and MR dyes figure II.4 were established by measuring the absorption of the diluted solutions at the maximum absorption wavelength specific to each of the dyes.

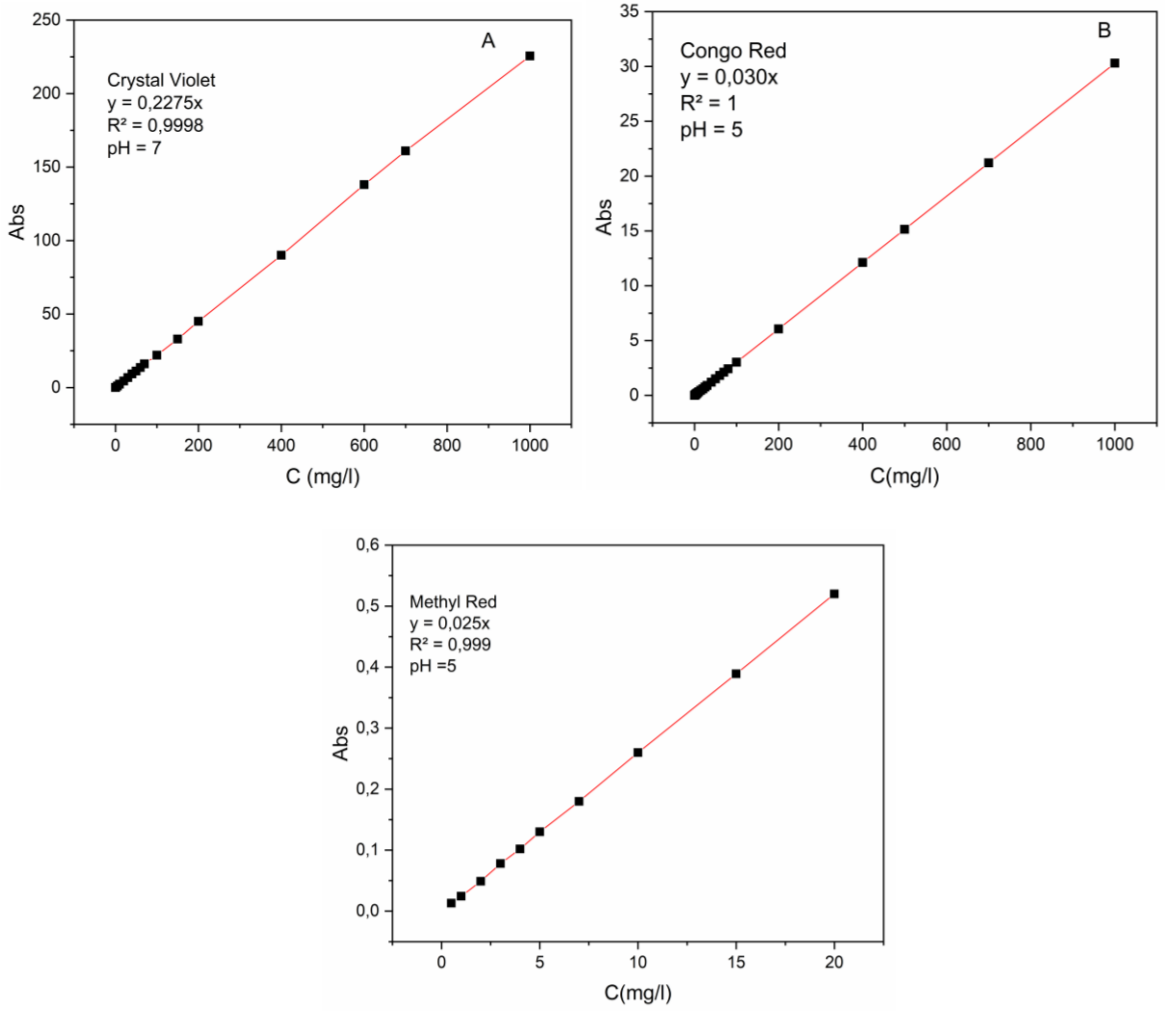

Figure II.4. Calibration curves of : (A) crystal violet, (B) congo red, (C) methyl red.

II.3. Study of adsorption

Each adsorption experiment was carried out in a discontinuous system at ambient temperature (25°C.) with stirring at 250 rpm. In addition to the effect of the adsorbent quality, we also studied the effects of pH (between 2 and 12), dye concentration (3 – 1000 mg/l), contact time (5-4320 min) and temperature (25, 30, 40 ° C) for pumpkin peels and pomegranate crusts and (10,25,30,40 °C) for turnip leaves. In addition to experiments to study the effect of temperature, the samples were separated from the adsorbent by centrifugation and then analyzed using a UV-visible spectrophotometer (model UV-2401PC) . Determine the residual concentration of dye in each suspension using the calibration curve previously established. Equations (II.1), (II.2), and (II. 3) were used to calculate the adsorption capacity (in mg/g) at the desired time (qt), at equilibrium (qe), as well as the percentage (R%) of elimination [2]:

$$\text{Removal percentage} = \frac{Ci - Ce}{Ci} \times 100 \quad \text{(II.1)}$$

$$q_t = \frac{(Ci - Ct) \times V}{m} \quad \text{(II.2)}$$

$$q_e = \frac{(Ci - Ce) \times V}{m} \quad \text{(II.3)}$$

where C_i and C_e ,C_t are the starting and equilibrium concentrations, respectively expressed in (mg/L), and m is the mass of the adsorbent expressed in (g). V is the volume of the solution expressed in (L).

II.4. Method of analysis

II.4.1. UV-Visible (UV-Vis)

UV-Visible Spectrophotometry (UV-Vis) is an analytical technique widely used to study the optical properties of solid materials. It plays an essential role in determining parameters such as the band gap and the absorption coefficient [3]. This method consists in illuminating a sample using monochromatic light, thus generating reflected rays and diffusely scattered rays [4]. The latter are picked up by an integrating sphere, which redirects them unidirectionally towards a detector, while the reflected rays are eliminated. The theory of diffuse reflectance, developed by Kubelka and Munk in 1931, makes it possible to relate diffuse reflectance to the absorption coefficient through the following equation[5] :

$$\frac{K}{S} = \frac{(1-R)^2}{2R} \quad \text{(II.4)}$$

where k represents the absorption coefficient, S the diffusion coefficient, and R the diffuse reflectance.

II.5. Characterization methods

II.5.1. The Brunauer, Emmet and Teller method (BET)

The specific surface area values (SSA) were estimated from the nitrogen adsorption isotherms by applying the BET equation (Brunauer-Emmett-Teller). The isotherms were generated using the Micromeritics ASAP 2020 system. The samples underwent a degassing process at a temperature of 120 °C. for a period of 1 hour before being measured.

II.5.2. Fourier transform infrared (FTIR)

The infrared absorption spectra were recorded using a Fourier Transform Infrared (FTIR) spectrometer (IRAffinity-1S; Shimadzu, Japan) with the potassium bromide (KBr) pellet method, in the wavenumber range of 4000–400 cm^{-1}. Infrared spectroscopy was employed to analyze the chemical structure and identify functional groups present in both the raw materials and the synthesized activated carbons. By comparing the spectra of the raw material with those of the activated samples, the effects of chemical activation on the material's chemical composition were evaluated[6].

II.5.3. Scanning electron microscopy (SEM) analysis:

Scanning electron microscopy (SEM) is an analysis method that makes it possible to acquire high-resolution images of the topography of samples based on the interactions between electrons and matter. It offers the possibility of analyzing the surface of the adsorbent, including its morphology: its shape, its general appearance, its porous structure, etc. These characteristics are of paramount importance in understanding the adsorption process and the interactions between the adsorbent and the adsorbate. This technique is widely used by many researchers to characterize raw, modified, as well as post-adsorption materials[7].

Using the NEOSCOPE JEOL scanning electron microscope (model JCM-5000), SEM images of the surface morphology of TL, TLA, PP, APP, PC and APC samples were obtained.

II.5.4. X-ray diffractometry

X-ray diffraction (XRD) is an analysis technique based on the interaction of X-rays with matter. It is widely used to characterize the structure of materials, including biomass. This method makes it possible to determine whether the structure of the sample is crystalline or amorphous, to evaluate its purity, as well as to measure the interlamellar distance[8].

In this study, the XRD diffractograms were obtained using an X'VERT Pro analytical diffractometer, over an angular range of 2θ comprised between 10° and 60°, with a measurement step of 0.02° and an acquisition time of 1 second per point. The radiation used was the Ka radiation of copper, with a wavelength of λ = 1.5406 Å.

II.5.5. Thermogravimetric analysis (TGA/DTG)

Thermogravimetric analysis (TGA) and its derivative (DTG) are thermal techniques for studying the behavior of materials as a function of temperature. They make it possible in particular to determine thermal properties such as degradation, melting and crystallization temperatures, in particular for small molecules[9].

A gravimetric thermal analysis (TGA) was carried out using a SETSYS national Statistical system, with a heating rate of 10 °C/min up to 1200 °C, in an air atmosphere, The use of the derived DTG curve resulting from the thermogravimetric analysis (TGA) makes it possible to determine more precisely the mass losses, by identifying in a more distinct way the temperatures of beginning and end of the different stages of degradation [10].

II.5.6. Determination of Point of Zero Charge, pH_{PZC}

The point of zero charge pH_{PZC} , corresponds to the pH at which the negative and positive charges on the surface of the adsorbent are balanced. When the pH of the solution is higher than the pH_{PZC} the surface functional groups are predominantly deprotonated due to the presence of OH^- ions. On the other hand, if the pH of the solution is lower than the pH_{PZC}, these groups are protonated under the effect of an excess of protons H^+.

The determination of the Point of Zero Charge was carried out according to the method described by B.K. Nandi [11].

To determine the pH_{PZC} of the adsorbents studied, 20 mL of distilled water were introduced into a series of beakers, the initial pH of which was adjusted between 2 and 12 using solutions of NaOH (0.1 M) or HCl (0.1 M). Then, 20 mg of each prepared adsorbent were added to each beaker. The suspensions were stirred for 24 hours at ambient temperature, then the final pH of each solution was measured[12].

II.6. Conclusion

In this chapter, the protocol of the experimental tests on the elimination of dyes by adsorption on previously prepared biomass has been exposed. The specific polluting substances and the adsorbent materials used, as well as the processes for their preparation, were exposed. In addition, a detailed description of the various methods of material characterization has been provided.

References

[1] F. Benamraoui, “Synthèses et caractérisations de nouveaux matériaux composites”, PhD Thesis,2024. Consulted on: 9 may 2025. Online on: http://dspace.univ setif.dz:8888/jspui/handle/123456789/4866

[2] H. Xue et al., “Adsorption of methylene blue from aqueous solution on activated carbons and composite prepared from an agricultural waste biomass: A comparative study by experimental and advanced modeling analysis”, Chem. Eng. J., vol. 430, p. 132801, 2022.

[3] M. Picollo, M. Aceto, and T. Vitorino, “UV-Vis spectroscopy”, Phys. Sci. Rev., vol. 4, no. 4, p. 20180008, Mar. 2019, doi: 10.1515/psr-2018-0008.

[4] J. Z. Zhang, Optical properties and spectroscopy of nanomaterials. World Scientific, 2009. Consulté le: 13 mai 2025. Disponible sur: https://books.google.com/...

[5] E. L. Simmons, “Diffuse reflectance spectroscopy: a comparison of the theories”, Appl. Opt., vol. 14, no. 6, pp. 1380-1386, 1975.

[6] A. Soudani et al., “High Performance Activated Carbon Based on Date Palm Fibers for Cu2+ Removal in Water”, Chem. Afr., vol. 7, no. 7, pp. 3903-3915, Sep. 2024, doi: 10.1007/s42250-024-00974-7.

[7] S. Thakur, S. Pandey, and O. A. Arotiba, “Development of a sodium alginate-based organic/inorganic superabsorbent composite hydrogel for adsorption of methylene blue”, Carbohydr. Polym., vol. 153, pp. 34-46, 2016.

[8] H. ZAGHOUANE-BOUDIAF, “Préparation et caractérisation de matériaux à base d’argile algérienne. Application à l’adsorption de polluants organiques”, PhD Thesis, 2014. Consulté le: 9 mai 2025. Disponible sur: http://dspace.univ-setif.dz:8888/jspui/bitstream/123456789/81/1/BOUDIAFHASSINA.zip

[9] C. Tiar, “Synthèse et caractérisation des matériaux naturels et mésoporeux. Application à l’élimination des micropolluants”, PhD Thesis, 2018. Consulté le: 9 mai 2025. Disponible sur: http://dspace.univ-setif.dz:8888/jspui/handle/123456789/1556

[10] S. Jebahi, M. Hidouri, and K. Boughzala, “Kinetic and thermodynamic study of the retention of textile effluent by co-products from the phosphate industry”, RHAZES Green Appl. Chem., vol. 14, pp. 76-94, 2022.

[11] B. K. Nandi, A. Goswami, and M. K. Purkait, “Adsorption characteristics of brilliant green dye on kaolin”, J. Hazard. Mater., vol. 161, no. 1, pp. 387-395, 2009.

[12] C. Djama et al., “Statistical physics modelling of azo dyes biosorption onto modified powder of Acorus calamus in batch reactor”, Biomass Convers. Biorefinery, vol. 13, no. 2, pp. 1013-1028, Jan. 2023, doi: 10.1007/s13399-020-01190-2.

Chapter III

Enhanced bio-adsorbent derived from turnip leaves for crystal violet removal in aqueous solutions: experimental investigation, characterization, and machine learning modeling

III.1. Introduction

The manufacturing of textiles is one industry that grows as a result of science and technology progressing more quickly[1]. These effluents pose a threat to human health and aquatic life, and their release into collecting rivers undermines the sustainability of the environment[2].Numerous studies highlight the harmful effects of colorants on the environment, damaging aquatic ecosystems and lowering water quality. They are known for their can crescent properties, genetic mutations, and potential skin issues like dermatitis, allergies, and irritations.[3].one of these dyes is crystal violet that must be eliminated from wastewater due to its toxicity to organisms and its non-biodegradable properties[4]. Adsorption has been identified as one of the most popular techniques for decontaminating aquatic bodies since it is effective and versatile enough to be employed in a wide range of situations. Adsorption is a commonly used process in industry, mostly for recovering solvents, treating contaminated effluents with low concentrations of organic pollutants, and purifying drinking water among other uses[5]. The selection of the adsorbent material and process variable optimization are critical to the effectiveness of adsorption as a separation process[6].Organic, synthetic, and organic materials derived from plants or animals can all be used in the adsorption of organic contaminants. Plant-based materials can take many different forms, such as cellulose from plants that resemble cotton, peanut bark, straw, hay, maize cobs, and bark fibers[7]. The equilibrium of multicomponent adsorption presents intricacies owing to the nonlinearity inherent in the relationships among dependent variables, alongside the intricate interactions prevailing between the adsorbent and the adsorbate, which may manifest as synergistic, antagonistic, or non-interacting phenomena[8].Chemical species undergo simultaneous adsorption with varying degrees of competition, influenced by numerous thermo-physicochemical and morphological parameters[9,10]. As a result, various theoretical and empirical models have been proposed in literature to elucidate this phenomenon, encompassing kinetics such as pseudo-first-order, pseudo-second-order, liquid film diffusion, and isotherms such as competitive Langmuir, Freundlich, Temkin, Sips, and Elovich models[11]. However, the application of these models is constrained due to their reliance on restrictive assumptions concerning the physicochemical nature influencing the adsorption system[12]. Consequently, the complexity of this process has prompted the utilization of

machine learning algorithms as a potent tool, offering advantages over classical methods by directly addressing nonlinear relationships derived from samples without prior knowledge of the chemical or physical characteristics impacting the system[12,13]. Scholarly publications have used a variety of machine learning approaches as complex mathematical techniques to simulate the adsorption capacity of single and multicomponent adsorption systems. Support vector machines (SVM) and artificial neural networks (ANN) are two examples of these techniques[14,15]. In our study, which aims to adsorb the crystal violet (CV) present in an aqueous solution, turnip leaves from local crops were selected as adsorbent material due to their low cost and their high availability.

This chapter presents the results of the various CV adsorption tests, in particular the effect of the adsorbent dose, pH, ionic strength, etc. It also includes the results relating to kinetics, adsorption isotherms as well as thermodynamic parameters., To model the multicomponent dynamic adsorption of this organic dye on our biosorbent, we adopted a hybrid approach combining the SVM-Discriminate optimization method and the SVM-DA model. This modeling is based on a rich and representative set of data.

Finally, a regeneration study of the adsorbent was carried out, followed by a comparison with other biomasses capable of eliminating the violet crystal.

III.2. Study of adsorption

The adsorption experiments were carried out in batch mode by mixing 20 mL of CV solution of known concentration with 20 mg of adsorbent. The effects of adsorbent dosage (2-20 mg), initial CV concentration (5-1000 mg/L), effect of pH (2-10), Effect of particle size(50, 63, 90 and 100 µm)and ionic strength(0.5 M to 3 M of NaCl), contact time (5-1440min) and temperature (10-40 °C) on the adsorption of CV were studied under stirring at 250 rpm. After adsorption, the biosorbent was separated by centrifugation. The solutions were centrifuged at 3000 rpm for 3 min using a centrifuge (SIGMA 2-16P, Germany). The supernatant fraction was analyzed at a wavelength of 590nm using UV–visible spectrophotometer (Shimadzu UV/Vis 1700, Japan).The removal percentage (R%) of the CV and the quantity adsorbed to the surface of the TL and TLA (qt, (mg/g)) were determined using equations Chapter II [16]:

III.3. Results and discussion

III.3.1. Characterization of TL and TLA

The BET method was used to calculate the area, namely for the TL and the TLA. The results indicate specific surface area, of 0.9248 m^2/g for TL, and 4.7386 m^2/g for TLA.

The spectra of the TL and TLA samples are shown in Figure III.1. The peaks in the region (3283 cm^{-1}) were attributed to the hydroxyl (–OH) groups of alcohols, phenols, carboxylic acids and water adsorbed on TL and TLA, confirming the presence of cellulose [17]. The peaks at 2915 and 1410 cm^{-1} were attributed to the CH stretching vibration of $–CH_3–$ or $–CH_2–$[18]. The peak at 1028 cm^{-1} was attributed to the C–O–C and C–O stretching vibrations or O–H bending vibrations in alcohols, phenols, and carboxyl groups[19]. the bands observed at (1584 cm^{-1}) were engendered by amide C=O and NH groups[20]. The peak at 600 cm^{-1} corresponded to the C–N stretching vibration[21].

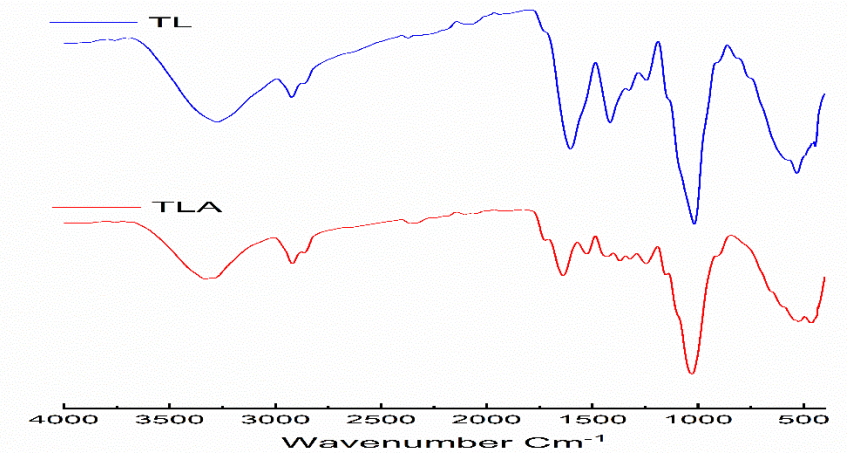

Figure III.1. FTIR spectra of TL and TLA.

From the graph presented in Figure III.2, The TL and TLA's pH_{PZC} value were determined to be 7.2 and 7.4 respectively. which means that the surface of TL and TLA was positively charged when the solution's pH was lower than 7.2 and 7.4 and adversely charged when the solution's pH was more than the 7.2 and 7.4.

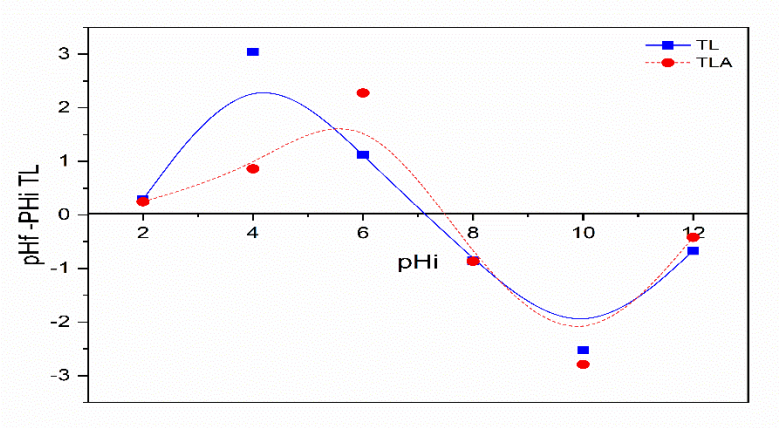

Figure 0.2. Isoelectric points of TL and TLA.

Figure III.3 shows the SEM micrographs of the raw focus the surface of the leaf fibers, while Figure III.4 shows the surface of the turnip leaves after activation. The images clearly show the surface roughness and varied morphology of turnip greens, which are made of fibers. Natural cellulose fibers are multicellular, with lignin and hemicellulose binding together a bundle of individual cells. After the chemical treatment was completed, the cellulose microfibrils in the raw fibers separated from each other and the majority of lignin and hemicellulose were removed, as shown in Figure III.4[23].

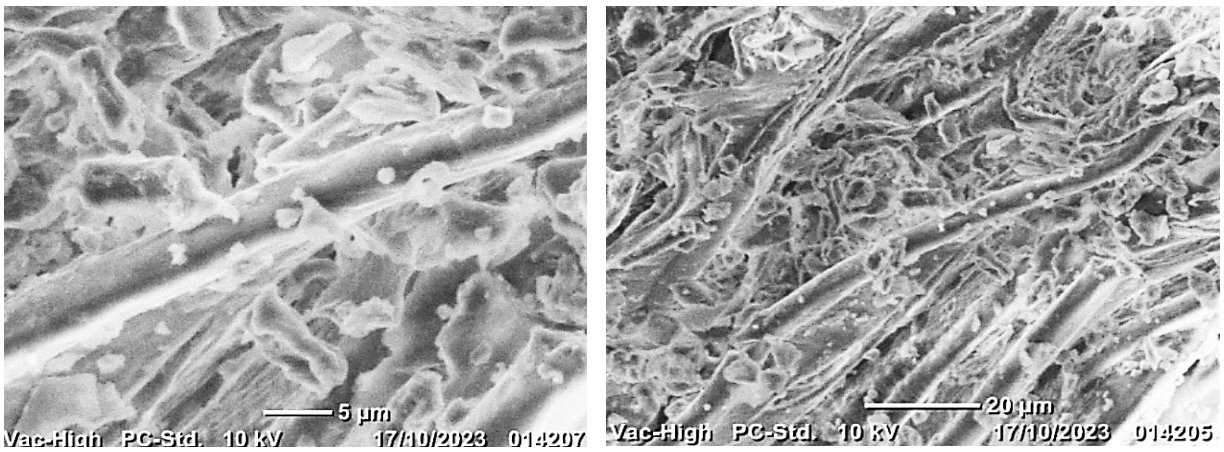

Figure III.3. Scanning electron micrographs of the raw surface of the turnip leaves (TL).

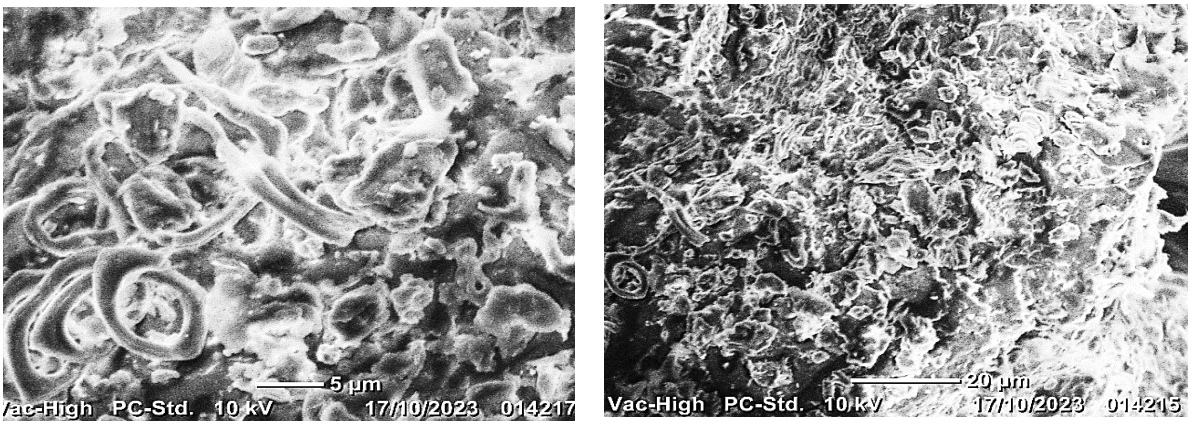

Figure III.4. Scanning electron micrographs of the surface of turnip leaves activated (TLA) with H_3PO_4.

The results of the analysis by X-ray diffraction (XRD) of the turnip leaves before and after treatment are presented in Figure III.5. The diffractograms revealed an amorphous structure for the two samples, indicating that the treatment with orthophosphoric acid did not alter their crystalline organization. Figure III.5 also showed a large and intense peak around 2θ = 22° and 43°, indicating the presence of dehydrated cellulose and hemicelluloses. The amorphous nature of the structure was confirmed by the presence of lignin and hemicellulose, identified by a low intensity peak[22].

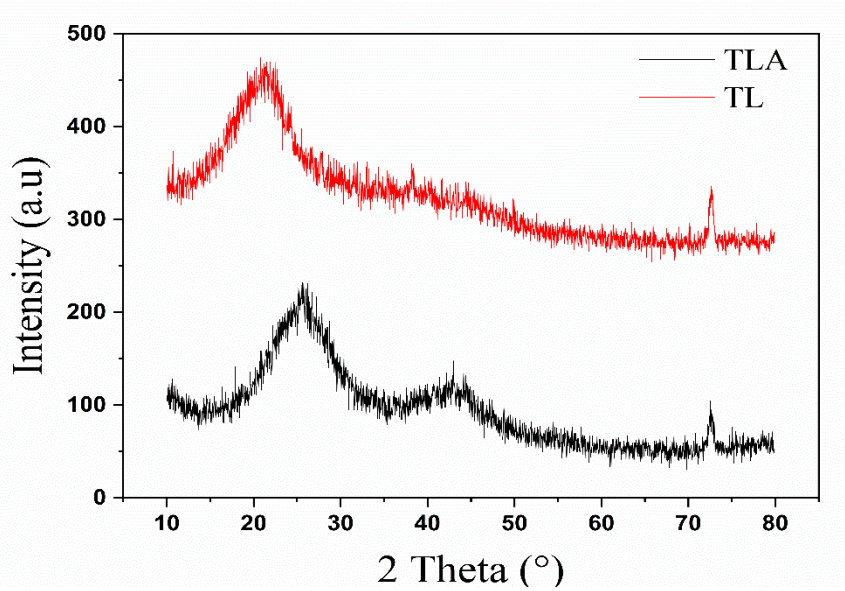

Figure III.5. XRD data of treated and raw Turnip leaves.

The results of the thermogravimetric analysis (TGA) provide information about the temperature range at which the sample remains stable or becomes unstable. Figure III.6 illustrates the thermogravimetric analysis of the TL and TLA samples, carried out in a temperature range between 30 and 1200 °C. It is apparent from this figure that the two samples present similar results, characterized by four distinct steps. The first phase, extending from 30 to 150°C, led to a 10% decrease in the mass of the samples, mainly due to the loss of surface water. The second phase, between 150 and 230°C, corresponded to an equilibrium phase without significant loss of mass. Then, the third stage, between 230 and 365°C. was characterized by a significant loss of mass of about 77%, probably due to the release of gaseous compounds (CO_2, CH_4, CO, H_2) or to the degradation of hemicelluloses[22].

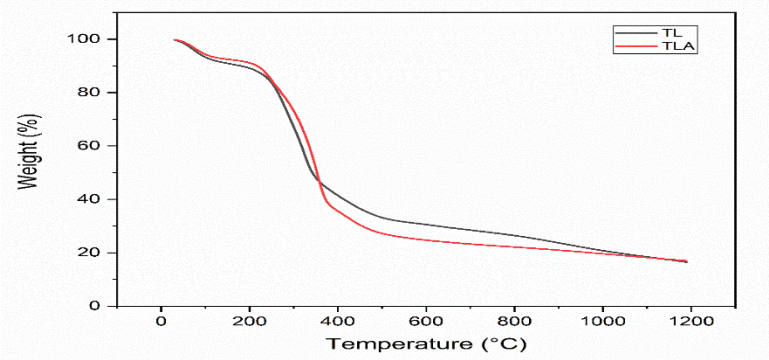

Figure III.6. Thermogravimetric analysis of TL and TLA.

II.3.2. Effect of experimental conditions

III.3.2.1. Effect of adsorbent dosage

The results obtained from the adsorbent dosage experiment are expressed in the Figure III.7 .This figure shows that the adsorption efficiency increased from 41.32% to 92.60% and 49.7% to 97.5% of TL and TLA respectively when the dose of adsorbent increased from1 to 14 mg. After 20 mg, it gradually began to stabilize. on the other hand, the maximum adsorption capacity decreased sharply as the mass of the adsorbent increases from 1 mg to 14mg, then gradually up to 20 mg, at which point it approached a practically constant mass. At low doses of Biosorbent, the pigment CV cations easily access to the adsorption sites of the biosorbent, leadin to a rapid increase in the amount adsorbed with the mass of the biosorbent. Beyond this mass, the number of sites becomes occupied [23].

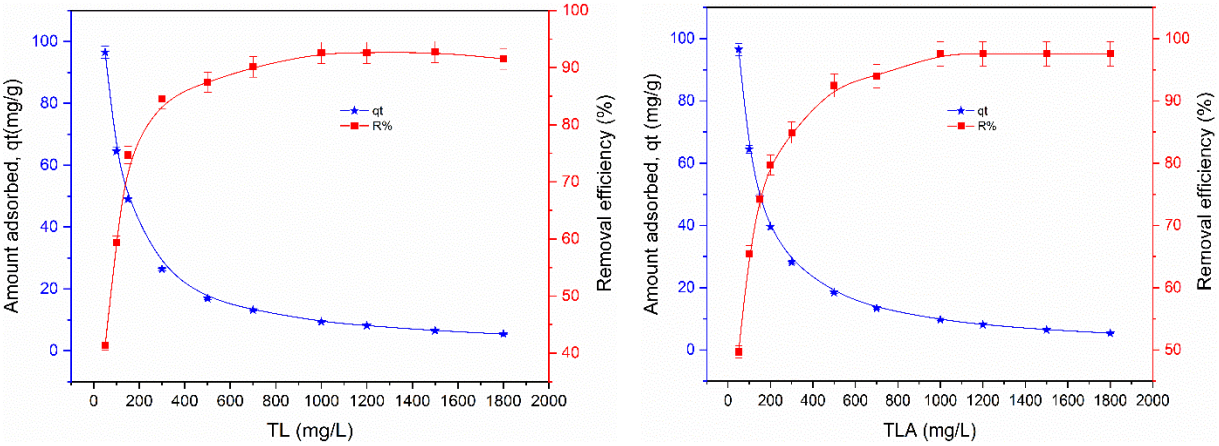

Figure III.7. Effect of the dose of leaf waste from turnips on the amount and percentage of crystal violet dye absorbed.

III.3.2.2. Effect of initial concentration

Figure III.8 shows the results of the initial concentration of TL and TLA effect at 25 ° C with a working range of (5 - 1000 mg / l) and we have drawn the adsorbed amount and the yield as a function of the initial concentration. There is a decrease in the yield from 86% to 39% and 86.81% to 46.54% of TL and TLA respectively with the increase in the concentration of CV due to occupation of the active sites of TL and TLA. This result could be explained by the deficiency of active sites necessary to support the high initial concentration of the dyes. At low concentrations, the adsorption sites absorbed the available solute more quickly[17] .

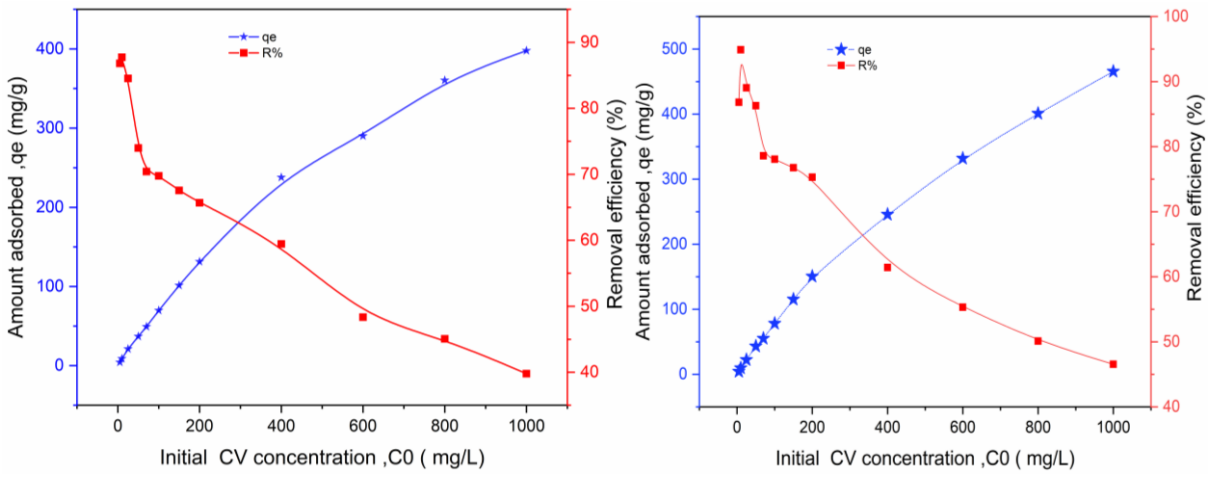

(a) (b)

Figure III.8. Effect of initial concentration of CV by TL(a) and TLA(b).

III.3.2.3. Effect of pH

To evaluate the effect of the pH, suspensions were prepared by dissolving 20 mg of powder in 20 mL of a CV dye solution at a concentration of 100 mg/L. After adjusting the pH between 2 and 9 using HCl or NaOH solutions (1 M) and stirring the mixture, the determination of the supernatant was carried out under the same conditions, as previously. Figure III.9, illustrating the variation in the percentage of elimination as a function of the pH, highlights the influence of the initial pH. A low yield is observed for very low pH values compared to pH_{PZC}, probably due to the repulsion force between the positively charged material and the cationic dye CV. The percentage of elimination (R%) increased gradually with the pH until reaching a maximum at the natural pH of 7. This increase is explained by the increase in the negative charges at the surface of TL and TLA, due to the rise in pH. The increased presence of negative charges on the surface of the biosorbent then favors the adsorption of the cationic dye CV at pH = 7[24].

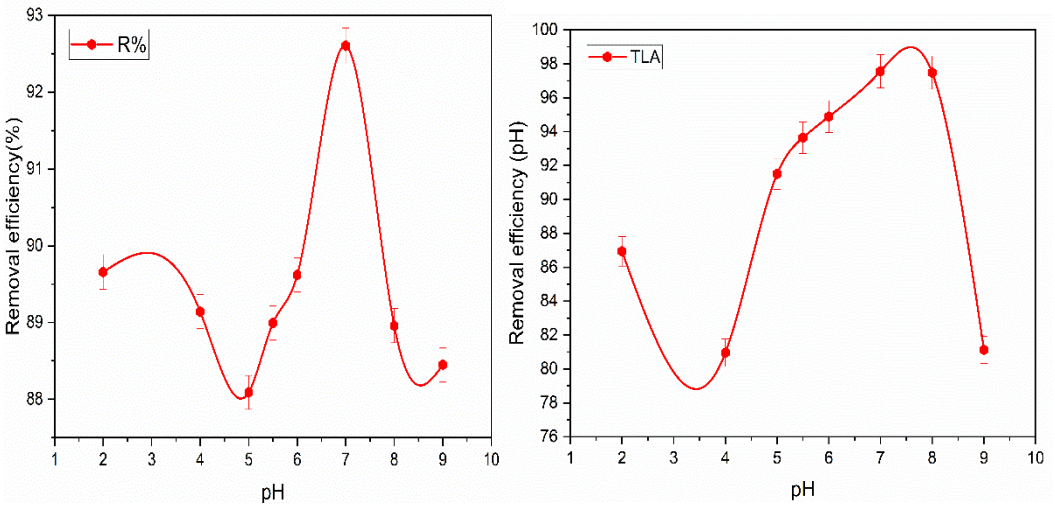

Figure III.9. Effect of pH of TL and TLA.

III.3.2.4. Effect of particle size

The Effect of particle size was carried out by varying the size of the TL and TLA particles (50, 63, 90 and 100 µm), with 20 mg of product and 20 mL of CV solution (100 mg/L) at 25 °C. Figure III.10 represents the percentage of elimination as a function of the NaCl concentration.

It was found that the adsorbed quantity (Q_{ads}) decreased as the particle size increased. In reality, a decrease in the size of the particles leads to an increase in their specific surface area, which favors the adsorption process. On the other hand, larger particles have a smaller specific surface area, which restricts the adsorption process.

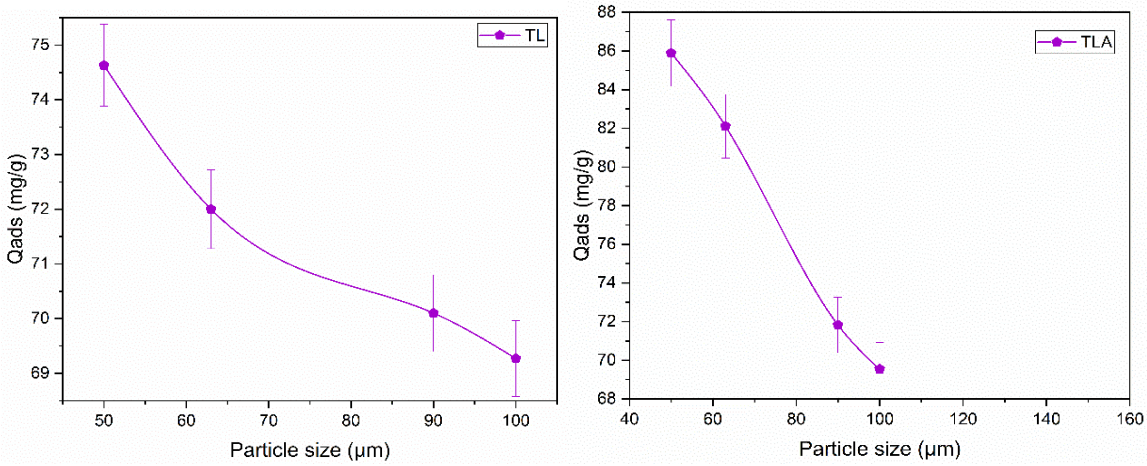

Figure III.10. Effect of particle size.

III.3.2.5. Effect of ionic strength

The influence of the ionic strength was analyzed using NaCl as the reference electrolyte. The study was carried out by varying the NaCl concentrations from 0.5 to 3 mol/L.

a salt, namely sodium chloride (NaCl), was used in this research. The graph presented in Figure III.11 shows how the adsorption of the CV on TL and TLA varies as a function of the salt concentration, which varied from 0.5 M to 3 M. An increase in the adsorption of the CV can be observed as the salt concentration increased, with slight variations depending on the nature of the salt. Consequently, the increase in the ionic strength led to a significant increase in the adsorption capacity of the CV on TL and TLA. This phenomenon can be explained by the creation of charges on the upper surface of our materials by NaCl which promotes adsorption[25].

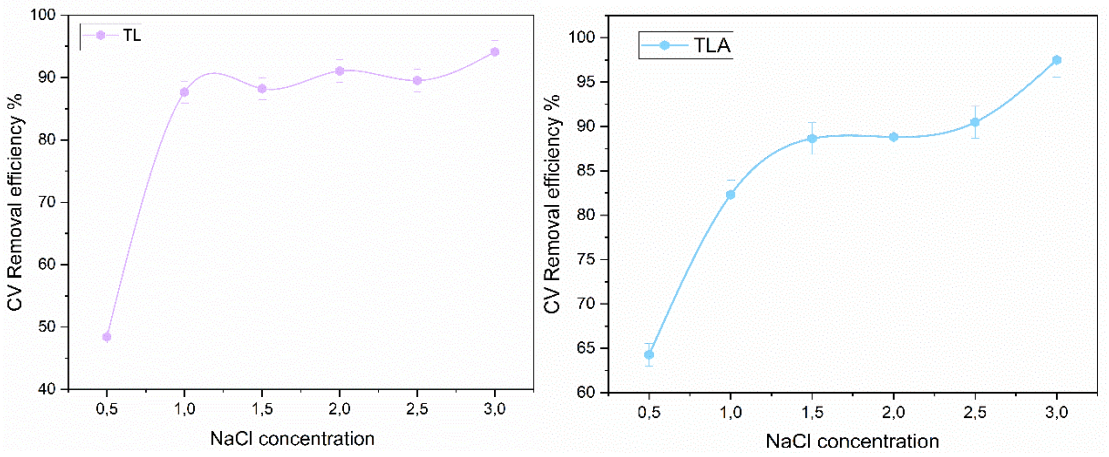

Figure III.11. Effect of ionic strength.

III.3.3. Kinetics of adsorption

Three concentrations (5, 10, 50 mg / l) were used to study the effect of the CV contact time on TL and TLA at pH 7 and at ambient temperature with a mass of 20 mg. According to Figure III.12, adsorption occurs rapidly during the first 30 minutes of contact and then gradually increases until equilibrium is reached in about 120 minutes for TLA and 150 minutes for TL. The rapid absorption at the first stage has been attributed to the availability of free adsorption sites on the surface of the bioadsorbent, These sites gradually become saturated And this is what explains the stability [26].In addition, it is observed that the amount of adsorbed TLA is greater than that of TL because the chemical activation has increased the surface of the hole, thus the adsorption capacity. Four kinetic models, the pseudo-first-order (PFO), the pseudo-second-order (PSO), Elovich kinetics, and intraparticle diffusion models.have been researched in order to completely comprehend the adsorption phenomena and the ratio of adsorbate/adsorbent. The parameters of the referenced models are illustrated in Table III.1 and Table III.2. According to the high values of R^2 for TLA and TL (0.984-0.996 and 0.984-0.998 respectively) and the low values of X^2 (0.005-2.46 and 0.016-0.101), the adsorption of CV on TLA and TL is well described by the pseudo-second-order kinetic model in the range of concentrations studied, compared to the pseudo-first-order model (R^2 of 0.982- 0.992 and 0.935-0.983) and X^2 of (0.016-0.129 and 0.076-2.31) for the two adsorbents. In addition, the adsorption capacities calculated (q_cal) by this model are close to the experimental values (q_exp). The rate constants k_1 and k_2 are also very dependent on the concentration of the CV, decreasing when the initial concentration C_0 increases. A similar kinetic behavior has been

observed for CV adsorption in other studies[27-29]. Elovich modeling, with an R^2 value of 0.914-0.941 for TLA and 0.997-0.968 for TL, supports the kinetic modeling data [30]. The intraparticle diffusion model was also used to verify the effect of the resistance to mass transfer on the binding of the CV to the adsorbents[31]. The plot of qt vs $\sqrt{t}$ in Figure III.13 even describes two steps: the first is the continuous diffusion of CV in the adsorbents at$\sqrt{t}$<8 for TLA and $\sqrt{t}$<6 for TL, and the second is the continuous diffusion (adsorption) at8≤$\sqrt{t}$≤16 for TLA and for TL is 6 ≤$\sqrt{t}$≤17. In addition, the graph in Figure III.13 does not go through the origin (C (mg / g) is not zero),indicating that the diffusion was not only a speed determination process[32].

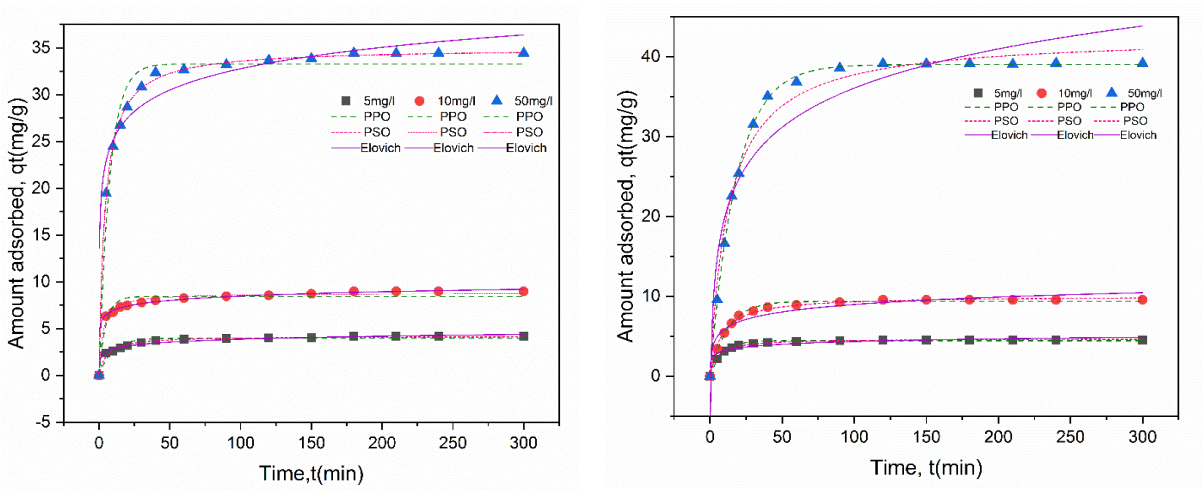

(a) (b)

Figure III.12. Effect of the contact time on the adsorption of CV dyes by TL (a) and TLA (b).

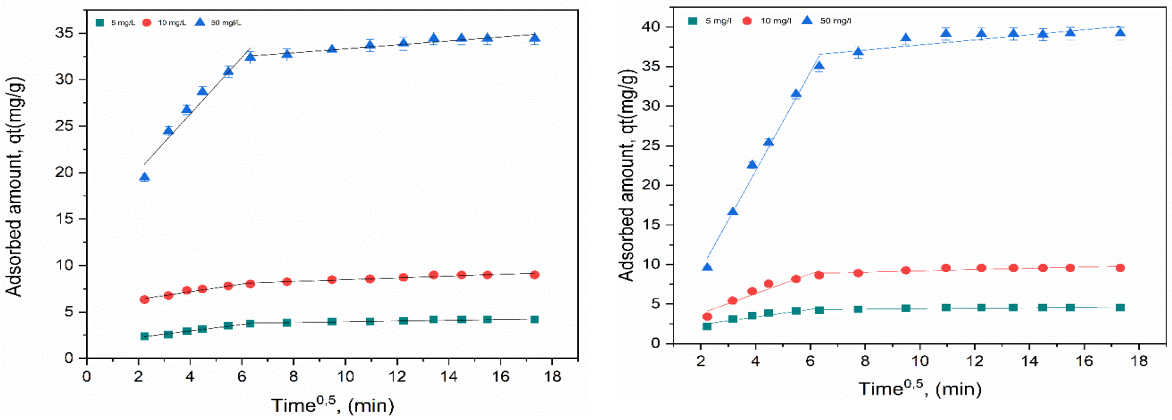

(a) (b)

Figure III.8. Intraparticular diffusion model of the adsorption of CV on TL (a), TLA (b)

Table III.1. Kinetic model parameters of TL.

*C*0 (mg/L)	5		10		50	
qe,exp(mg/g)	4.16		8.98		34.43	
Pseudo-first-order						
qe (mg/g)	3.97		8.43		33.30	
k_1 (min^{-1})	0.107		0.208		0.138	
R^2	0.983		0.935		0.972	
$\boldsymbol{x^2}$	0.07622		0.33007		2.31656	
Pseudo-second-order model						
qe (mg/g)	4.44		9.38		39.02	
k_2(g/mg·min)	0.044		0.042		0.006	
R^2	0.986		0.984		0.998	
$\boldsymbol{x^2}$	0.016		0.076		0.101	
Elovich						
α (mg/g.min)	21.19		19.97		136.75	
β (mg/g)	2.17		1.50		0.30	
R^2	0.979		0.997		0.968	
$\boldsymbol{x^2}$	0.024		0.014		2.63	
Intraparticular diffusion model						
	Step1	Step2	Step1	Step2	Step1	Step2
K_3(mg/g·$min^{0.5}$)	0.348	0.030	0.415	0.095	3.05	0.211
C	1.56	3.68	5.52	7.52	14.10	31.19
R^2	0.987	0.585	0.951	0.902	0.939	0.988

Table III.2. Kinetic model parameters of TLA.

*C*0 (mg/L)	5		10		50	
qe,exp(mg/g)	4.53		9.56		39.14	
Pseudo-first-order						
qe (mg/g)	4.44		9.38		39.02	
k_1 (min^{-1})	0.114		0.081		0.055	
R^2	0.989		0.992		0.999	
$\boldsymbol{x^2}$	0.016		0.061		0.129	
Pseudo-second-order model						
qe (mg/g)	4.69		10.05		42	
k_2(g/mg·min)	0.041		0.012		0.001	
R^2	0.996		0.993		0.984	
$\boldsymbol{x^2}$	0.005		0.048		2.46	
Elovich						
α (mg/g.min)	33.54		10.52		11.52	
β (mg/g)	2.03		0.742		0.141	
R^2	0.941		0.934		0.924	
$\boldsymbol{x^2}$	0.091		0.513		11.91	
Intraparticular diffusion model						
	Step1	Step2	Step1	Step2	Step1	Step2
K_3(mg/g·$min^{0.5}$)	0.482	0.027	1.248	0.081	6.246	0.322
C	1.440	4.14	1.320	8.37	1.64	34.51
R^2	0.844	0.646	0.899	0.678	0.982	0.600

III.3.4. Adsorption isotherms

The pigment fixation data on turnip leaves are processed using the nonlinear Langmuir and Freundlich equation[33]. The purpose of these equations is to validate the model in which adsorption occurs and to be able to draw conclusions about the maximum adsorption capacity and the affinity of the adsorbent for the adsorbent. Figure III.14 shows the expected adjustment curve of the isothermal model, which was recorded to show how temperature

affects the process of biosorption of crystal violet on the surface of TLA and TL. It is noticed that the shape of the isotherm is of type L according to the classification of Limousin et al [34]. this isotherm demonstrates that, particularly at low concentrations, CV has a considerable affinity for the TLA and TL surface., The table III.3 and table III.4 also includes the calculated isothermal parameters. The tests were carried out with CV concentrations ranging from 5 to 1000 mg / L and at 25 °C[35].

III.3.4.1. The Langmuir isotherm

To estimate the maximum adsorption capacity which corresponds to a complete monolayer coverage of the surface of TLA and TL by the CV, the Langmuir isothermal model was selected[36].

In comparison to the Freundlich R^2adj value, the Langmuir model's R^2adj for TLA and TL (0.987–0.995) is superior. Furthermore, the K_L values of TLA and TL, which fall between 0 and 1, are 0.005 and 0.0048, respectively, and show that the two biosorbents have done a decent job of adsorbing the CV[37].

III.3.4.2. The Freundlich isotherm

The adsorbates absorption intensity on the adsorbent surface was estimated using the Freundlich model[38].

The weak correlation with the Freundlich model assumes that multilayers are formed at high concentrations of CV. The type and intensity of the adsorption process both affect the parameter n, which gives information about the adsorption force. The adsorption is physical and advantageous when the value of k_f (16,75 for TLA and 12,52 for TL) is greater than 1 and the value of 1/n (1/n=0.549 for TL and 1/n=0,531 for TLA) less than 1,and what is achieved in our case [39].

III.3.4.3. Sips isotherm

The Sips model is a three-parameter model derived from the combination of Langmuir and Freundlich isotherms. He provided the best estimates for the adsorption of crystal violet (CV), making it possible to conclude that CV adsorption occurs in a heterogeneous system. This model takes into account a heterogeneity factor (ns= 1,071 for TLA and ns= 0,852 for TL)

and avoids the limitation of the Freundlich isotherm, which is not capable of predicting the formation of monolayers[40].

the Langmuir and Sips models represent values of (qm) respectively of (577.24, 621.76mg/g) for TLA (521.05, 635.54 mg/g) for TL. all these results show that our bio-adsorbents have the ability to eliminate micropollutants.

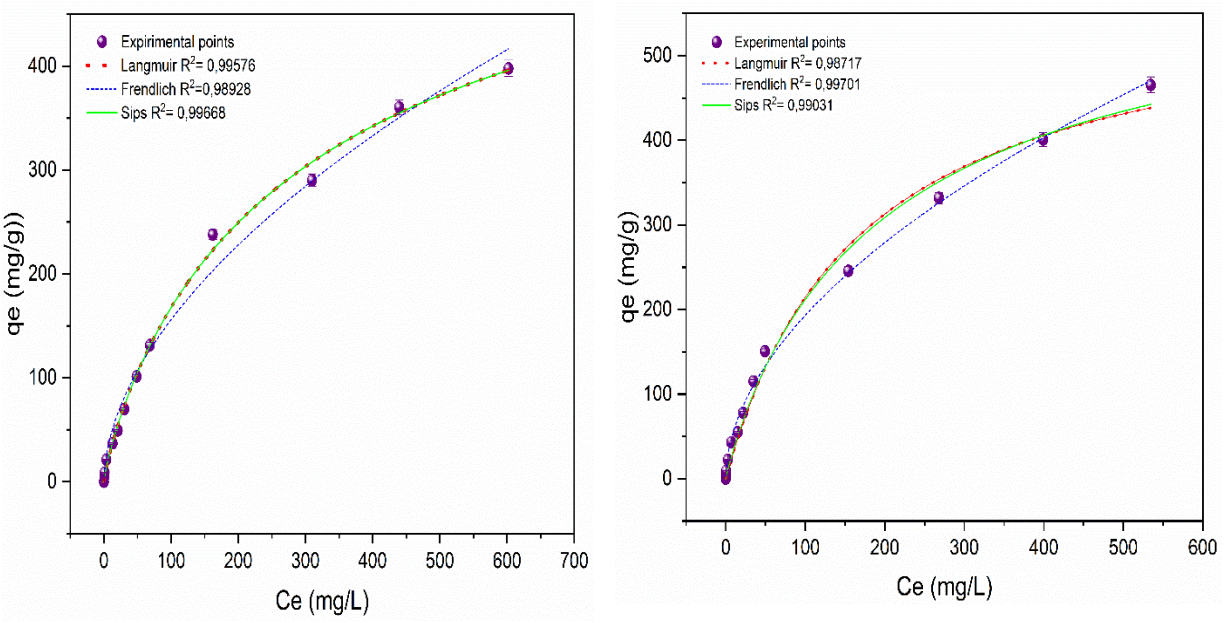

(a) (b)

Figure III.14. CV adsorption isotherm on raw and activated turnip leaves (a) and (b).

Table III.3. Isotherm model parameters of TL.

Two-parameter isotherm models		Three-parameter isotherm models
Langmuir	Freundlich	Sips
q_m=521.05	K_F =12.52	q_m= 635.54
K_L= 0.0048	n_f=1.82	ks=0.007 n =0.852
R^2 = 0.995	R^2 = 0.989	R^2 = 0.996
$\boldsymbol{x^2}$ =85.11	x^2 = 215.20	x^2= 66.64

Table III. 4. Isotherm model parameters of TLA.

Two-parameter isotherm models		Three-parameter isotherm models
Langmuir	Freundlich	Sips
q_m= 577.24	K_F =16 .75	qm = 621.76
K_L= 0.005	n_f= 1.88	ks= O.007 ns= 1.071
R^2 = 0.87	R^2 = 0.997	R^2 = 0.990
$\boldsymbol{x^2}$ =332.7	$\boldsymbol{x^2}$ = 77.49	$\boldsymbol{x^2}$ = **251**.46

III.3.5. Adsorption thermodynamics

Thermodynamic characteristics, such as changes in Gibbs free energy (ΔG), enthalpy (ΔH), and entropy (ΔS), they are investigated and shown in the table III.5 and table III.6, and they are extrapolated from the plot of ln (K_c) vs 1/T Figure III.15. in order to comprehend the nature and viability of the adsorption procss[38], were determined by using the following equations:

$$\Delta G = -RT\ln Kc \quad \text{III.1}$$

$$\Delta G° = \Delta H° - T\Delta S° \quad \text{III.2}$$

K_L is the Langmuir equilibrium parameter, converted from unit (L/mg) to unit (L/mol)

According to the formula (18)[41-42]:

$$k_L\,(L/mol) = k_L(L/mg) * 1000\,(mg/g) * Madsorbate\,(g/mol) \quad \text{III.4}$$

where $M_{adsorbate}$(g/mol) is the molecular weight of the CV contaminant (407.979g/mol). Subsequently, the dimensionless adsorption equilibrium constant (K_c) is estimated as Conforming to formula (19)[41-43]:

$$Kc = k_L\,(L/mol) * Cref(mol/L) * 1/\Upsilon \quad \text{III.5}$$

Based on the ionic strength, the activity coefficient is denoted by γ, and the molar concentration of the reference state is indicated by C_{ref}. It is widely acknowledged in the standard method that the concentration of the adsorbate or pollutant in the reference state is

1 M, or C_{ref} = 1 mol/L[43-45].

R: universal gas constant (8.314 J/mol K); and T: absolute temperature (K).

The negative value of ΔG indicates that the adsorption of CV on the TLA and TL is a spontaneous process. The negative ΔH values confirmed the exothermic character of the adsorption process, The ΔH values are relatively low less than 40 kJ·mol^{-1}, which suggests that the adsorption has a physical effect[46]. Although ΔS is positive, this suggests that the turbulence at the solid-solution interface is reduced. This decrease in the adsorption capacity may be due to a decrease in the strength of the hydrogen bond or to a degradation of the bio sorbent[32].

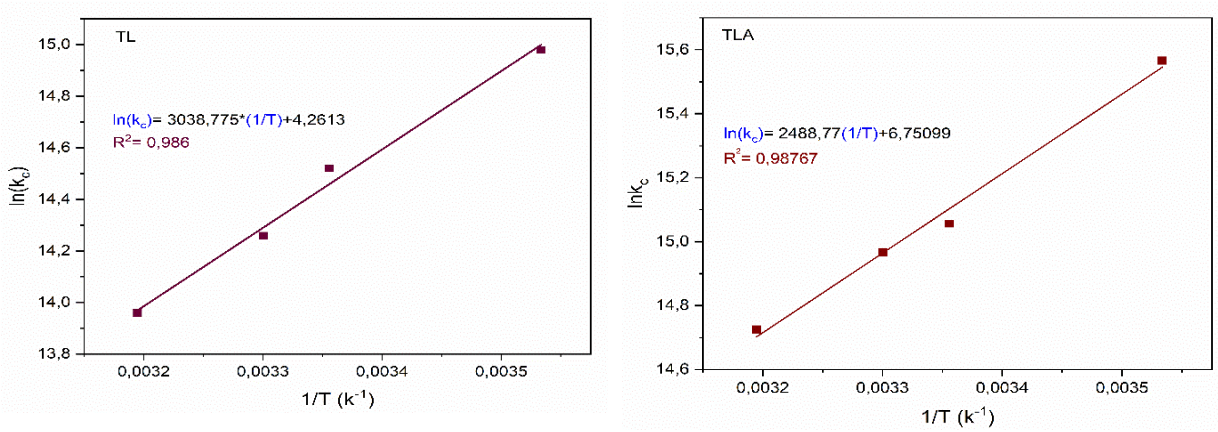

Figure III.15. Thermodynamic of TL and TLA.

Table III.5. Thermodynamic parameters of TL.

Temperature (K)	ΔH° (kJ.mol^{-1})	ΔS° (J.mol^{-1}.K^{-1})	ΔG° (kJ.mol^{-1})	R^2
283	-25.26	35.42	-35.2908	0.986
298			-35.8223	
303			-35.9994	
313			-36.3537	

Table II.6. Thermodynamic parameters of TLA.

Temperature (K)	ΔH° (kJ.mol^{-1})	ΔS° (J.mol^{-1}.K^{-1})	ΔG° (kJ.mol^{-1})	R^2
283	-20.69	56.12	-36.576	0.987
298			-37.4179	
303			-37.6986	
313			-38.2599	

III.3.6. Adsorption mechanism

Understanding the adsorption mechanism or the ratio of adsorbate to adsorbent is crucial. The adsorbent in our case is turnip leaves, which contains cellulose, hemicellulose, lignin, and other minor elements. The CV is a cationic dye, meaning it carries positive charges. The FTIR spectrum confirms that cellulose and hemicellulose comprise the majority of functional groups, such as hydroxyl and carboxyl. The absorption process was carried out at pH > pH_{PZC}, where the CV+ cations and the negative surface charge interact mainly electrostatically. Figure III.16 shows the many methods that have been suggested. The following processes are involved in the mechanism for removing CV via TL and TLA adsorption:

(i) Transfer of the dye from the solution to the adsorbent surface.

(ii) Diffusion of the dye through the interface to the adsorbent surface

(iii) Adsorption of the dye at the TL and TLA surface, which means that two mechanisms may be responsible:

- Electrostatic interactions: (1) between the positively charged nitrogen atoms on the CV and the negatively charged deprotonated carboxylate anions of TLA and TL; and (2) between the hydrogen atoms and the density of delocalized electrons of the CV's aromatic rings.
- The hydrogen atoms on the surface and the hydrogen in the hydroxyl groups of BSW form hydrogen bonds [27,37].
- An interaction of the π-π type can also manifest itself during the process of adsorption of CV dye with TL and TLA. The CV dye is a polycyclic aromatic compound containing several benzene rings. The FT-IR analysis of the biosorbent confirmed the presence of C=C aromatic stretches, indicating the presence of these benzene rings.

Moreover, due to the fact that these benzene rings are electronically rich regions, they are capable of generating donor-acceptor stacking interactions with CV, TL and TLA. Figure III.17 illustrates the CV biosorption process.

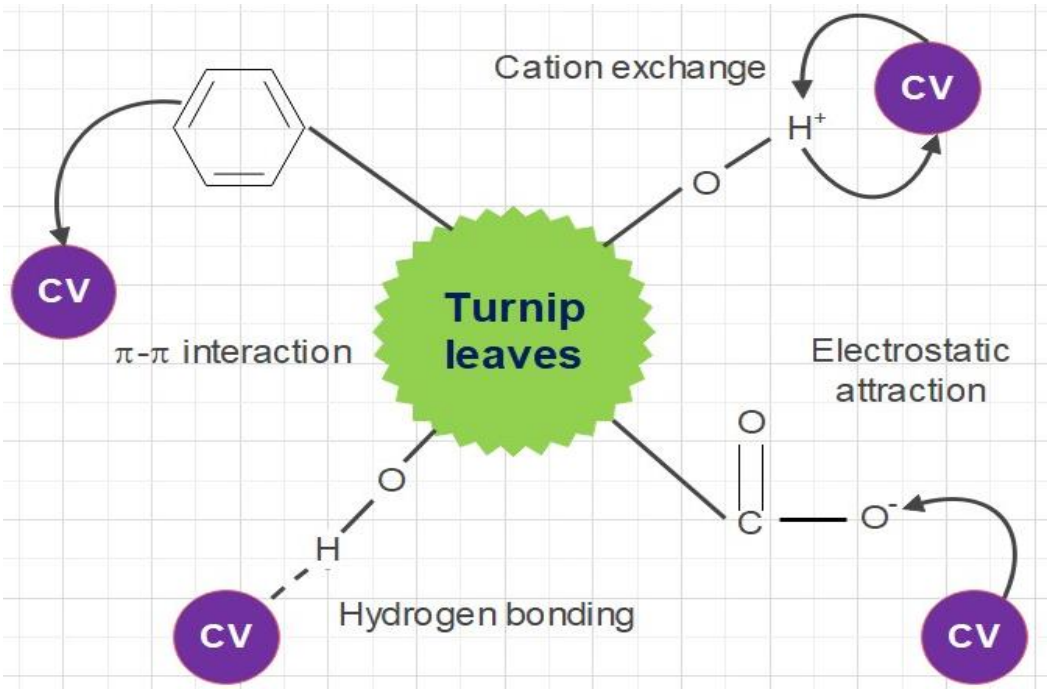

Figure III.16. The mechanism of interaction between the CV and turnip leaves.

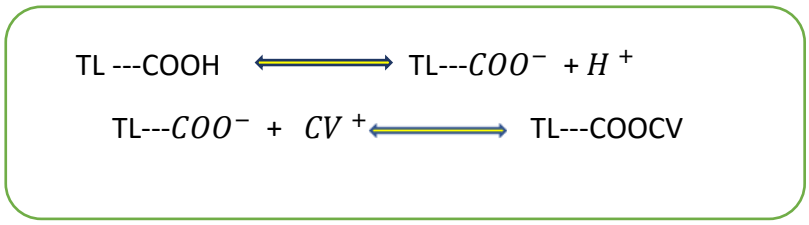

Figure III.17. Explanatory Shema on the exchange of ions between the dye and the hydrogen.

III.3.7. Desorption and regeneration studies

The results of the TLA regeneration tests Figure III.18 demonstrate remarkable reuse efficiency, with the possibility of repeating the adsorption cycles more than 4 times without observing a significant decrease in the adsorption yield. Indeed, a decrease in adsorption is

observed from 3.51 to 10% between the first and the fourth cycles, which suggests a slightly increased efficiency for TLA.

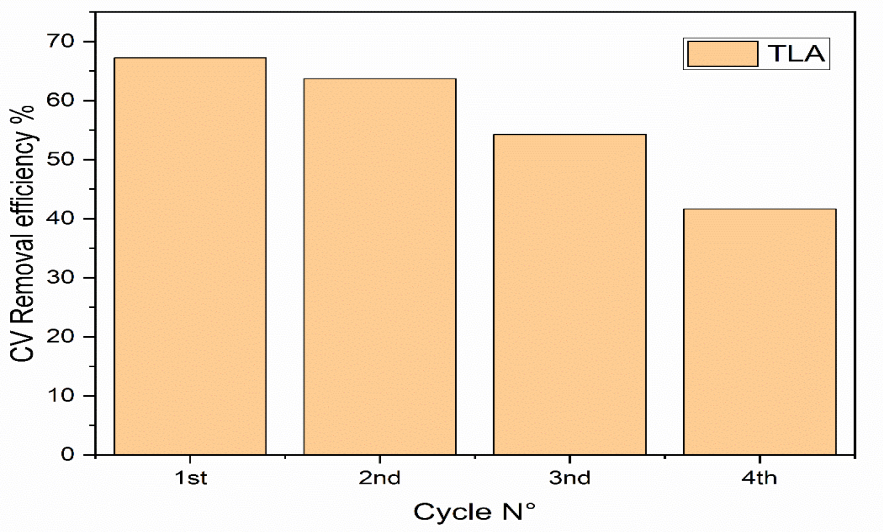

Figure 0.18. Regeneration of TLA after adsorption of CV.

III.3.8. Comparison of the adsorption capacities of the different adsorbents used for the removal of CV dyes.

The maximum adsorption capacity is a property that measures the effectiveness of an adsorbent in adsorbing organic pollutants. Because there is a rising need for inexpensive adsorbents with large adsorption capacities, in this study we compared the maximum adsorption capacities of the different biomass which eliminates the CV, Table III.7 displays the comparison's findings.

Table III.7. Comparison of maximum monolayer adsorption capacity on various adsorbents.

Adsorbent	Dose adsorbent (mg/l)	$V_{adsorbat}$ (ml)	Concentration (mg/l)	Qmax (mg/ g)	Equilibrium time (min)	Reference
Cedar cones	2500	100	50	13.64	Not given	[47]
Arundo donax L.	4400	Not given	100	19.60	60	[48]
Pinus bark powder	1g	50	20	32.78	120	[49]
Papaya seeds powder	12000	50	50	85.90	60	[50]
Almond shells (AS)	5000	40	30	12.2	90	[51]
Raw turnip leaves	1000	20	10	635.54	180	This work
Activated turnip leaves	1000	20	10	621.76	120	This work

in the event that the crystal violet dye is retained. When compared to other comparable adsorbents, the Raw turnip leaves TL biomass has a higher adsorption capability[52].

II.3.9. Optimization of Support Vector Regression Model using Dragonfly Algorithm

The support vector regression (SVR) model was optimized using the Dragonfly algorithm to fine-tune its hyperparameters within their specified ranges. The Dragonfly algorithm, coded with 50 search agents and a maximum of 100 iterations, was employed to explore the hyperparameter space efficiently.

The optimization process aimed to identify the optimal combination of hyperparameters that minimizes the error of the SVR model while maximizing its predictive performance. The hyperparameters considered in the optimization included the penalty parameter C, sigma (σ), the size of the insensitive zone (ε), and the choice of kernel function (Gaussian RBF, linear, and polynomial).

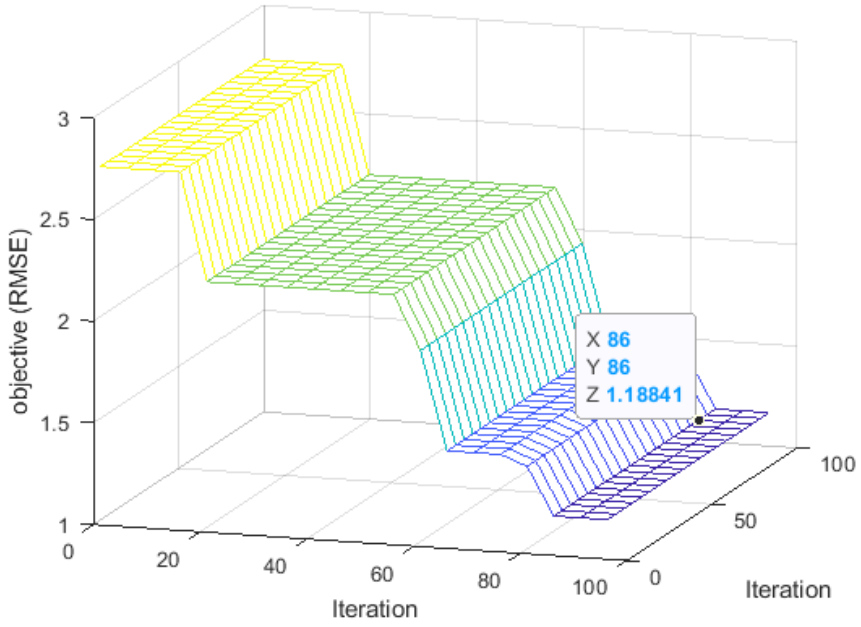

Figure III.19. Visual representation of the optimization process, showcasing the convergence of the Dragonfly algorithm towards the optimal solution over successive iterations.

After conducting multiple iterations, the best result was achieved at the 86th iteration, as depicted in Figure III.19. This iteration yielded the optimal set of hyperparameters that resulted in the highest accuracy and lowest error for the SVR model. Table III.8 presents the results of the hyperparameter optimization process conducted using the Dragonfly algorithm for the support vector regression model.

Table III.8. Hyperparameters Results.

Hyperparameter	Penalty parameter $C > 0$	Sigma σ	Size of the insensitive zone (ε)	Kernel function	Quantity of support vectors
Optimal Value	2.0e+05	2.3233	1.1684	Gaussian RBF	109

The results of correlation and additional metrics for the support vector regression model are summarized in Table III.9. These metrics provide insights into the performance and accuracy

of the support vector regression model on the training set, testing set, and the entire dataset. The Root Mean Square Error (RMSE) indicates the average deviation between the predicted and actual values, while the determination coefficient (R^2) represents the proportion of the variance in the dependent variable that is predictable from the independent variables.

Table III.8. Performance statistic criteria.

Data	RMSE	R^2	r	b	slop
Train	0.97338	0.9999	0.9999	0.2065	0.9995
Test	1.0809	0.9977	0.9989	0.0973	0.9910
All	0.99565	0.9998	0.9999	0.15197	0.9995

Additionally, the correlation coefficient (r) illustrates the strength and direction of the linear relationship between the predicted and actual values. The parameters 'b' and 'slope' describe the intercept and slope of the regression line, respectively.

The high values of R^2 and correlation coefficients demonstrate the excellent fit of the support vector regression model to the data, both in the training and testing phases. see Figure III.20.

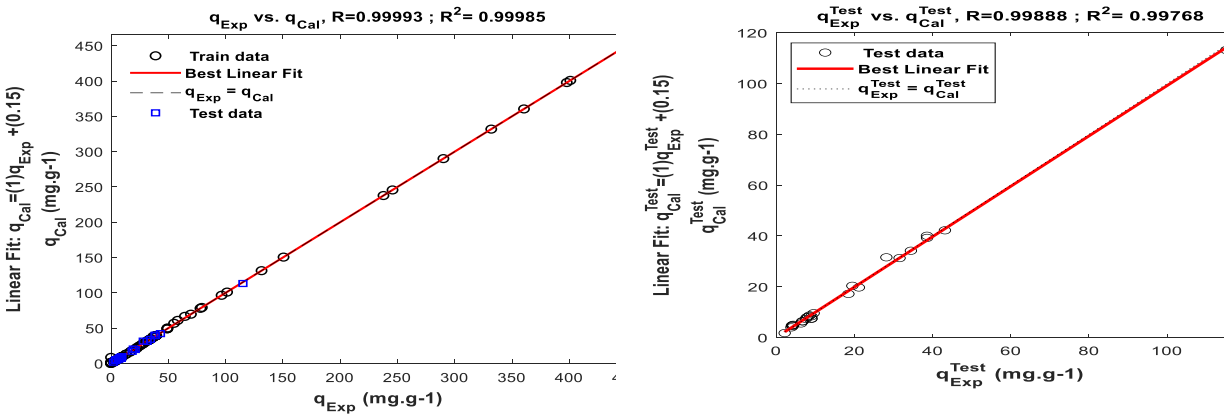

a **b**

Figure III.20. -a- Correlation between actual and predict of all data, -b- Correlation between actual and predict of test data.

Figure III.20 illustrates the correlation between the actual and predicted data obtained from the support vector regression model. This plot provides a visual representation of the relationship between the observed values and the model's predictions. A strong correlation between the actual and predicted data points indicates the efficiency of the regression model in capturing the underlying patterns in the dataset.

III.3.10. Model Deployment in Graphical User Interface (GUI)

The developed support vector regression model has been successfully deployed into a user-friendly Graphical User Interface (GUI), allowing for intuitive and accessible interaction with the predictive tool. Leveraging the capabilities of modern software development, the GUI provides a seamless platform for users to input their data and obtain predictions based on the trained model. Through the GUI, users can easily navigate through the various functionalities, including data input, model prediction, and result visualization

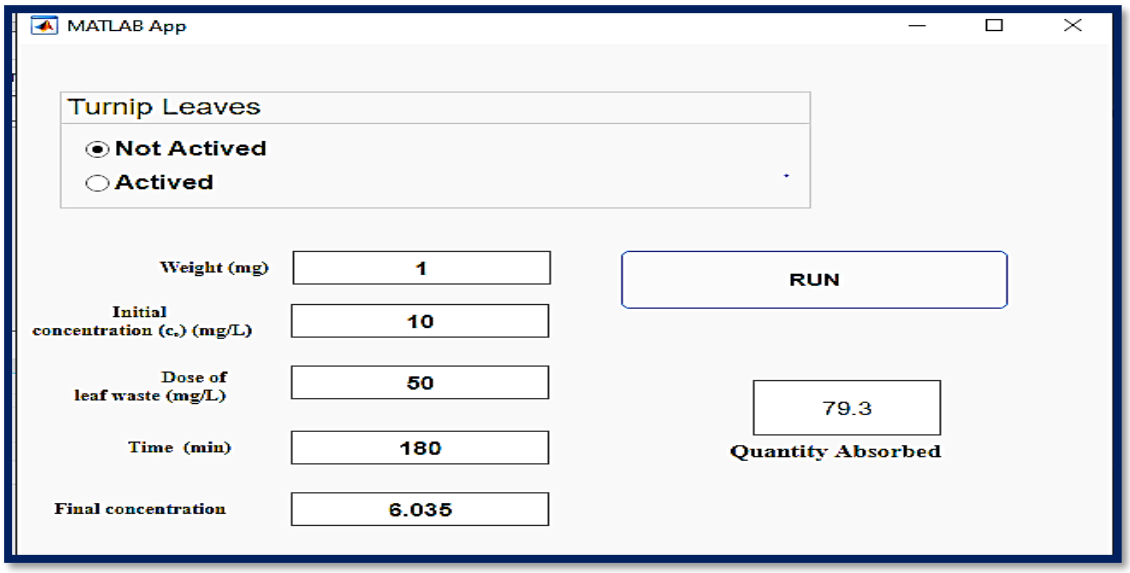

Figure III.21. Graphical User Interface (GUI) of DA_SVM model.

III.4. Conclusion

Raw and activated turnip leaves, an inexpensive and readily available biomass, have proven to be very effective in removing crystal violet from aqueous solutions. the optimal mass of TL and TLA is 20 mg, the maximum adsorption capacity was 635.54 mg/g for TL and 621.76mg /g for TLA. The mathematical modeling of the adsorption

isotherms has established that the Sips model is adequate to accurately represent the adsorption data for TL and TLA. The kinetic results were consistent with the pseudo-second-order model for TLA and TL. In addition, it has been found that intraparticular transport is the main factor governing the adsorption kinetics of the dye studied. The negative values of ΔG, ΔH and ΔS indicate that the adsorption process is spontaneous and favorable, the exothermic nature of the adsorption process and that there is a random decrease during adsorption. The developed DA-SVM model demonstrates versatility for the prediction of adsorption capacity in various systems of ternary pollutants, including heavy metals, dyes, pharmaceuticals, hydrocarbons, as well as organic and inorganic materials, relevant for water treatment and purification. To facilitate its practical use, a unique graphical interface based on MATLAB has been developed, using the parameters of the optimal model for accurate prediction of responses. In our study, a significantly elevated ESRM of 1.0809 mg/g was observed. turnip leaves are feasible, effective, and economical. in addition, this adsorbent is a promising candidate for wastewater treatment.

References

[1] I.O. Saheed, W.-D. Oh, F.B.M. Suah, Enhanced adsorption of acid Blue-25 dye onto chitosan/porous carbon composite modified in 1-allyl-3-methyl imidazolium bromide ionic liquid, Int. J. Biol. Macromol. 183 (2021) 1026–1033.

[2] T.A. Altalhi, M.M. Ibrahim, G.A. Mersal, M.H.H. Mahmoud, T. Kumeria, M.G. El-Desouky, A.A. El-Bindary, M.A. El-Bindary, Adsorption of doxorubicin hydrochloride onto thermally treated green adsorbent: Equilibrium, kinetic and thermodynamic studies, J. Mol. Struct. 1263 (2022) 133160.

[3] X. Jiang, W. Pan, Z. Xiong, Y. Zhang, L. Zhao, Facile synthesis of layer-by-layer decorated graphene oxide based magnetic nanocomposites for β-agonists/dyes adsorption removal and bacterial inactivation in wastewater, J. Alloys Compd. 870 (2021) 159414.

[4] K. Nadarajah, Y. Jeganathan, S.L. Ramakrishnan, E.R. Bandala, Understanding the interaction between selected microplastics and the toxic dye" Congo red" in water, Chemosphere 372 (2025) 144097.

[5] L. Chen, Y. Jiao, Preparation of activated carbon from sunflower straw through H3PO4 activation and its application for acid fuchsin dye adsorption, Water Sci. Eng. 16 (2023) 192–202.

[6] N. Hamri, A. Imessaoudene, A. Hadadi, S. Cheikh, A. Boukerroui, J.-C. Bollinger, A. Amrane, H. Tahraoui, H.N. Tran, A.O. Ezzat, Enhanced adsorption capacity of methylene blue dye onto kaolin through acid treatment: batch adsorption and machine learning studies, Water 16 (2024) 243.

[7] L.M.R. Lima, A.H. de Albuquerque Alves, D. Tavares, L.M.R. Lima, A.M.S. Paiva, Comparative study of influence of molecular structure of hydrogenocarbonate contaminants in adsorption process, using cactus pear forage (Opuntia fícus) as biomass, Braz. J. Dev. 9 (2023) 21487–21501.

[8] R. Moumen, M. Laidi, S. Hanini, M. Hentabli, A. Ibrir, Multicomponent Adsorption Capacity Forecasting Based on Support Vector Machine with Dragonfly Algorithm, Kem. U Ind. Časopis Kemičara Kem. Inženjera Hrvat. 72 (2023) 169–178.

[9] C. Djama, A. Bouguettoucha, D. Chebli, A. Amrane, H. Tahraoui, J. Zhang, L. Mouni, Experimental and theoretical study of methylene blue adsorption on a new raw material, Cynara scolymus—A statistical physics assessment, Sustainability 15 (2023) 10364.

[10] H. Khelili, S. Achour, K. KONAN, Kinetic and isotherm study of Methylene blue adsorption on orange peel activated carbon, LARHYSS J. P-ISSN 1112-3680E-ISSN 2521-9782 (2024) 89–103.

[11] M. Kebir, H. Tahraoui, M. Chabani, M. Trari, N. Noureddine, A.A. Assadi, A. Amrane, N. Ben Hamadi, L. Khezami, Water cleaning by a continuous fixed-bed column for Cr (VI) eco-adsorption with green adsorbent-based biomass: an experimental modeling study, Processes 11 (2023) 363.

[12] W. Zhang, W. Huang, J. Tan, D. Huang, J. Ma, B. Wu, Modeling, optimization and understanding of adsorption process for pollutant removal via machine learning: Recent progress and future perspectives, Chemosphere 311 (2023) 137044.

[13] A. El Bey, M. Laidi, A. Yettou, S. Hanini, A. Ibrir, M. Hentabli, H. Ouldkhaoua, Praktični alat umjetne neuronske mreže za predvi\djanje kompetitivne adsorpcije bojila na polimernoj nanoarhitekturi gemini, Kem. U Ind. Časopis Kemičara Kem. Inženjera Hrvat. 70 (2021) 481–488.

[14] P.S. Pauletto, S.F. Lütke, G.L. Dotto, N.P.G. Salau, Forecasting the multicomponent adsorption of nimesulide and paracetamol through artificial neural network, Chem. Eng. J. 412 (2021) 127527.

[15] Y. Mesellem, A.A.E. Hadj, M. Laidi, S. Hanini, M. Hentabli, Computational intelligence techniques for modeling of dynamic adsorption of organic pollutants on activated carbon, Neural Comput. Appl. 33 (2021) 12493–12512. https://doi.org/10.1007/s00521-021-05890-2.

[16] H. Xue, X. Wang, Q. Xu, F. Dhaouadi, L. Sellaoui, M.K. Seliem, A.B. Lamine, H. Belmabrouk, A. Bajahzar, A. Bonilla-Petriciolet, Adsorption of methylene blue from aqueous solution on activated carbons and composite prepared from an agricultural waste biomass: A comparative study by experimental and advanced modeling analysis, Chem. Eng. J. 430 (2022) 132801.

[17] C. Djilani, R. Zaghdoudi, F. Djazi, B. Bouchekima, A. Lallam, A. Modarressi, M. Rogalski, Adsorption of dyes on activated carbon prepared from apricot stones and commercial activated carbon, J. Taiwan Inst. Chem. Eng. 53 (2015) 112–121.

[18] L. Chunlan, X. Shaoping, G. Yixiong, L. Shuqin, L. Changhou, Effect of pre-carbonization of petroleum cokes on chemical activation process with KOH, Carbon 43 (2005) 2295–2301.

[19] S. Gupta, H.W. Kua, S. Dai Pang, Effect of biochar on mechanical and permeability properties of concrete exposed to elevated temperature, Constr. Build. Mater. 234 (2020) 117338.

[20] S.I. Siddiqui, G. Rathi, S.A. Chaudhry, Acid washed black cumin seed powder preparation for adsorption of methylene blue dye from aqueous solution: thermodynamic, kinetic and isotherm studies, J. Mol. Liq. 264 (2018) 275–284.

[21] M. Ghaedi, H. Hossainian, M. Montazerozohori, A. Shokrollahi, F. Shojaipour, M. Soylak, M.K. Purkait, A novel acorn based adsorbent for the removal of brilliant green, Desalination 281 (2011) 226–233.

[22] A. Guediri, A. Bouguettoucha, H. Tahraoui, D. Chebli, J. Zhang, A. Amrane, L. Khezami, A.A. Assadi, The Enhanced Adsorption Capacity of Ziziphus jujuba Stones Modified with Ortho-Phosphoric Acid for Organic Dye Removal: A Gaussian Process Regression Approach, Water 16 (2024) 1208.

[23] K.M. Kifuani, A.K.K. Mayeko, P.N. Vesituluta, B.I. Lopaka, G.E. Bakambo, B.M. Mavinga, J.M. Lunguya, Adsorption d'un colorant basique, Bleu de Méthylène, en solution aqueuse, sur un bioadsorbant issu de déchets agricoles de Cucumeropsis mannii Naudin, Int. J. Biol. Chem. Sci. 12 (2018) 558–575.

[24] S. Jebahi, M. Hidouri, K. Boughzala, Kinetic and thermodynamic study of the retention of textile effluent by co-products from the phosphate industry., RHAZES Green Appl. Chem. 14 (2022) 76–94.

[25] A. Benhouria, H. Zaghouane-Boudiaf, R. Bourzami, F. Djerboua, B.H. Hameed, M. Boutahala, Cross-linked chitosan-epichlorohydrin/bentonite composite for reactive orange 16 dye removal: Experimental study and molecular dynamic simulation, Int. J. Biol. Macromol. 242 (2023) 124786.

[26] N.D. Shooto, P.M. Thabede, B. Bhila, H. Moloto, E.B. Naidoo, Lead ions and methylene blue dye removal from aqueous solution by mucuna beans (velvet beans) adsorbents, J. Environ. Chem. Eng. 8 (2020) 103557.

[27] A. Benhouria, H. Zaghouane-Boudiaf, R. Bourzami, F. Djerboua, B.H. Hameed, M. Boutahala, Cross-linked chitosan-epichlorohydrin/bentonite composite for reactive orange 16 dye removal: Experimental study and molecular dynamic simulation, Int. J. Biol. Macromol. 242 (2023) 124786.

[28] A.S. Abdulhameed, A.H. Jawad, A.-T. Mohammad, Synthesis of chitosan-ethylene glycol diglycidyl ether/TiO2 nanoparticles for adsorption of reactive orange 16 dye using a response surface methodology approach, Bioresour. Technol. 293 (2019) 122071.

[29] A.H. Jawad, M.A. Islam, B.H. Hameed, Cross-linked chitosan thin film coated onto glass plate as an effective adsorbent for adsorption of reactive orange 16, Int. J. Biol. Macromol. 95 (2017) 743–749.

[30] S. Jebahi, M. Hidouri, K. Boughzala, Kinetic and thermodynamic study of the retention of textile effluent by co-products from the phosphate industry., RHAZES Green Appl. Chem. 14 (2022) 76–94.

[31] F. Granados-Correa, E. Gutiérrez-Bonılla, M. Jiménez-Reyes, G. Roa-Morales, P. Balderas-Hernández, CO_2 adsorption behavior of a highly-microporous KOH-activated carbon obtained from rice husk waste: kinetic and equilibrium studies, Int. J. Chem. React. Eng. 22 (2024) 181–187. https://doi.org/10.1515/ijcre-2023-0052.

[32] F. Benamraoui, H. Boudiaf, R. Bourzami, A. Gil, M. Boutahala, Methylene Blue Removal Using Black Cumin Seeds Waste: Experimental and Theoretical Investigations, Available SSRN 4386961 (n.d.).

[33] S. Shahriar, X. Han, H. Lin, Y. Zheng, Adsorptive Removal of Nitrogen and Sulfur Containing Compounds by SBA15 Supported Nickel (II) and Tungsten Phosphides and the Adsorption Mechanisms, Int. J. Chem. React. Eng. 14 (2016) 823–830. https://doi.org/10.1515/ijcre-2015-0107.

[34] G. Limousin, J.-P. Gaudet, L. Charlet, S. Szenknect, V. Barthes, M. Krimissa, Sorption isotherms: A review on physical bases, modeling and measurement, Appl. Geochem. 22 (2007) 249–275.

[35] T.C. Andrade Siqueira, I. Zanette da Silva, A.J. Rubio, R. Bergamasco, F. Gasparotto, E. Aparecida de Souza Paccola, N. Ueda Yamaguchi, Sugarcane bagasse as an efficient biosorbent for methylene blue removal: kinetics, isotherms and thermodynamics, Int. J. Environ. Res. Public. Health 17 (2020) 526.

[36] A.H. Jawad, R.A. Rashid, M.A.M. Ishak, L.D. Wilson, Adsorption of methylene blue onto activated carbon developed from biomass waste by H_2SO_4 activation: kinetic, equilibrium and thermodynamic studies, Desalination Water Treat. 57 (2016) 25194–25206. https://doi.org/10.1080/19443994.2016.1144534.

[37] H.S. Benammar, S. Guergazi, S. Youcef, L. Youcef, Removal of Congo red and Naphthol blue black dyes from aqueous solution by adsorption on activated carbon. Characterization, kinetic and equilibrium in nonlinear models studies, Deslin Water Treat 221 (2021) 396–405.

[38] P. Atheba, P. Drogui, A. Trokourey, Adsorption kinetics and thermodynamics study of butylparaben on activated carbon coconut based, J. Encapsulation Adsorpt. Sci. 8 (2018) 39.

[39] A.K.K. Mayeko, P.N. Vesituluta, J.N. Di Phanzu, D.M.W. Muanda, G.E. Bakambo, B.I. Lopaka, J.M. Mulangala, Adsorption de la quinine bichlorhydrate sur un charbon actif peu coûteux à base de la Bagasse de canne à sucre imprégnée de l'acide phosphorique, Int. J. Biol. Chem. Sci. 6 (2012) 1337–1359.

[40] M. Radjai, H. Ferkous, Z. Jebali, H. Majdoub, R. Bourzami, G. Raffin, M. Achour, A. Gil, M. Boutahala, Adsorptive removal of cationic and anionic dyes on a novel mesoporous adsorbent prepared from diatomite and anionic cellulose nanofibrils: Experimental and theoretical investigations, J. Mol. Liq. 361 (2022) 119670.

[41] A.-C. Enache, P. Samoila, C. Cojocaru, R. Apolzan, G. Predeanu, V. Harabagiu, An eco-friendly modification of a walnut shell biosorbent for increased efficiency in wastewater treatment, Sustainability 15 (2023) 2704.

[42] A.-C. Enache, C. Cojocaru, P. Samoila, V. Ciornea, R. Apolzan, G. Predeanu, V. Harabagiu, Adsorption of brilliant green dye onto a mercerized biosorbent: kinetic, thermodynamic, and molecular docking studies, Molecules 28 (2023) 4129.

[43] P.S. Ghosal, A.K. Gupta, Determination of thermodynamic parameters from Langmuir isotherm constant-revisited, J. Mol. Liq. 225 (2017) 137–146.

[44] S. Azizian, S. Eris, L.D. Wilson, Re-evaluation of the century-old Langmuir isotherm for modeling adsorption phenomena in solution, Chem. Phys. 513 (2018) 99–104.

[45] A.A. Khan, R.P. Singh, Adsorption thermodynamics of carbofuran on Sn (IV) arsenosilicate in H+, Na+ and Ca2+ forms, Colloids Surf. 24 (1987) 33–42.

[46] M. Aazza, H. Ahlafi, H. Moussout, H. Maghat, Adsorption of metha-nitrophenol onto alumina and HDTMA modified alumina: Kinetic, isotherm and mechanism investigations, J. Mol. Liq. 268 (2018) 587–597.

[47] M. Zamouche, A. Habib, K. Saaidia, M. Bencheikh Lehocine, Batch mode for adsorption of crystal violet by cedar cone forest waste, SN Appl. Sci. 2 (2020) 198. https://doi.org/10.1007/s42452-020-1976-0.

[48] F. Krika, A. Krika, A. Azizi, Arundo donax L. as a low-cost and promising biosorbent for the removal of crystal violet from aqueous media: kinetic, isotherm and thermodynamic investigations, Chem. Rev. Lett. 2 (2019) 59–68.

[49] R. Ahmad, Studies on adsorption of crystal violet dye from aqueous solution onto coniferous pinus bark powder (CPBP), J. Hazard. Mater. 171 (2009) 767–773.

[50] F.A. Pavan, E.S. Camacho, E.C. Lima, G.L. Dotto, V.T. Branco, S.L. Dias, Formosa papaya seed powder (FPSP): preparation, characterization and application as an alternative adsorbent for the removal of crystal violet from aqueous phase, J. Environ. Chem. Eng. 2 (2014) 230–238.

[51] I. Loulidi, F. Boukhlifi, M. Ouchabi, A. Amar, M. Jabri, A. Kali, S. Chraibi, C. Hadey, F. Aziz, Adsorption of crystal violet onto an agricultural waste residue: kinetics, isotherm, thermodynamics, and mechanism of adsorption, Sci. World J. 2020 (2020). https://www.hindawi.com/journals/tswj/2020/5873521/ (accessed October 20, 2023).

[52] G. Mosoarca, C. Vancea, S. Popa, M. Dan, S. Boran, Crystal violet adsorption on eco-friendly lignocellulosic material obtained from motherwort (Leonurus cardiaca L.) biomass, Polymers 14 (2022) 3825.

Chapter IV
Characterization and application of pumpkin peels as an alternative adsorbent for congo red removal from aqueous solutions

IV.1. Introduction

Water polluted with a variety of contaminants, such as toxic heavy metals and dyes, can lead to harmful consequences for human health[1]**.** Azo dyes, such as congo red, represent one of the main categories of synthetic dyes. Their use is widespread in the textile sector due to their advantageous characteristics, such as a wide range of colors, good resistance to fading and low energy consumption during dyeing operations. These dyes may contain one or more azo chromophore groups (-N=N-) as well as aromatic rings. Their stability in the face of light and aggressive chemical environments is attributed to their π-conjugated bonds and their molecular resonance[2,3]. Every year, a quantity of up to 10^8 tons of dyes is manufactured on a global scale, of which 60 to 70% are azo dyes. This intensive use leads to the production of a large amount of wastewater containing azo compounds. The congo red azoic dye causes particular concern due to the presence of aromatic amine groups in its structure, recognized for their carcinogenic potential. The stability of its aromatic structure gives this dye resistance to natural degradation, which contributes to its persistence in the environment and leads to adverse consequences on aquatic fauna and flora[4,5]. Thus, the treatment of water contaminated with the Congo Red dye is essential to mitigate its environmental and health impacts. Adsorption represents one of the most effective methods to eliminate this contaminant[6].

This chapter analyzes the various factors that impact the adsorption process of congo red (CR) by the biosorbents APP (activated pumpkin peels) and PP (pumpkin peels), particularly highlighting the impact of the amount of adsorbent, the initial concentration of the dye and the pH of the solution. The analysis of the adsorption capacity of these materials with respect to CR was carried out with the aim of evaluating their effectiveness as sustainable substitutes for conventional adsorbents.[7]. The produced materials were analysed utilising various techniques, including FTIR, XRD, SEM, TGA/DTA, and isoelectric point determination. The kinetics of adsorption have been examined and modelled by several methodologies, including pseudo-first-order (PFO), pseudo-second-order (PSO), Elovich models, and intraparticle diffusion. Models were chosen for their simplicity and relevance to the examined adsorption process [8]. The results of the adsorption isotherms of CR were analyzed using the classical models of Langmuir, Freundlich and Sips. This analysis aimed to elucidate the nature of the interaction mechanisms between the dyes and the prepared biomass[9].

IV.2. Results and Discussions

IV.2.1. Characterization of the PP and APP

The FTIR spectra of the PP and activated PPA from pumpkin peels are displayed in Figure IV.1.showing very similar spectra for the two samples, The pyridine group's olefinic = CH– groups can be recognized by the band at 1457 cm^{-1}, while the –C–N stretching vibrations are linked to the band at 1381 cm^{-1}[10].Similarly, the combination of elongation and distortion of the water molecule adsorbed on the surface produced the bands of H−O−H deformation (bending) seen in the 1950 cm^{-1} range[11].The main cause of the two absorption bands at 2850 and 2932 cm^{-1} is the aliphatic vibration sof the elongation CH[12].The peaks at 1044 cm^{-1} correspond to the C–O stretching vibrations of the carboxylic, phenolic and alcoholic groups, Additionally, this band confirms the lignin structure of APP and PP[13].. peaks denoting 2300, 2373, and 2150 cm^{-1} indicate the alkyne groups' C stretching vibration[14].This figure also shows changes in the intensity of some peaks, the displacement of others, and the disappearance of some, suggesting that the PP's surface has been modified by the orthophosphoric acid treatment, most likely due to widespread oxidation that formed oxygenated acid complexes.

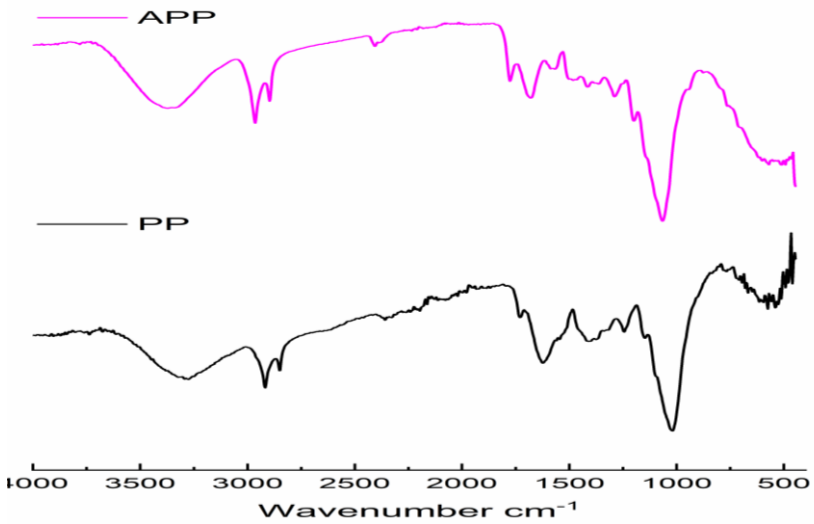

Figure IV.1. FTIR spectra of PP and APP.

Figure IV.1 and Figure IV.2 shows the structure and morphology of our biomass, Raw and activated. We can see that the surface looks quite neglected with irregular shapes and a large

amount of compacted organic matter. Propose a relatively dense structure. These particles seem to have spherical structures. Such zones may consist of fragments of an intact organic matrix or of non-biodegradable components of the block. there are well-defined micropores or mesopores can be seen. Which indicates that it is a raw (inactive) biomass in operation. on the other hand, the activated biomass surface is more porous and better organized due to the chemical treatment with H_3PO_4[15].

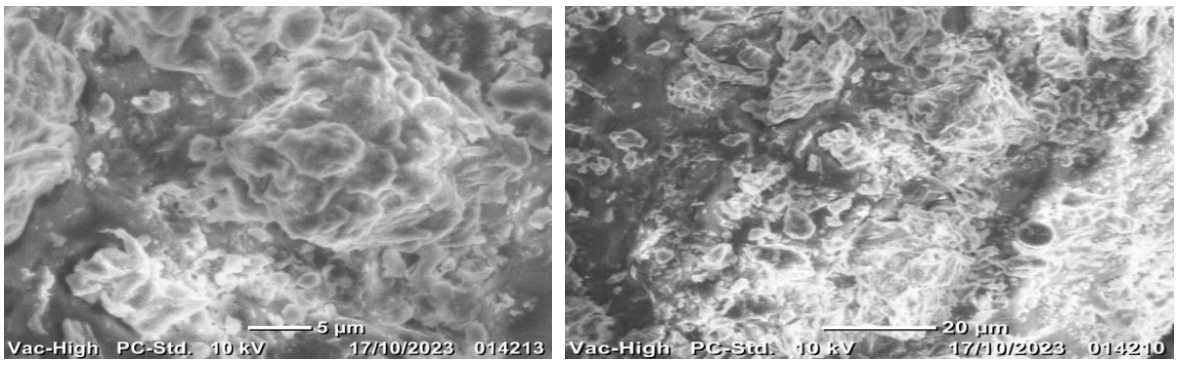

Figure IV.3. Scanning electron micrographs of the raw surface of the pumpkin peel (PP).

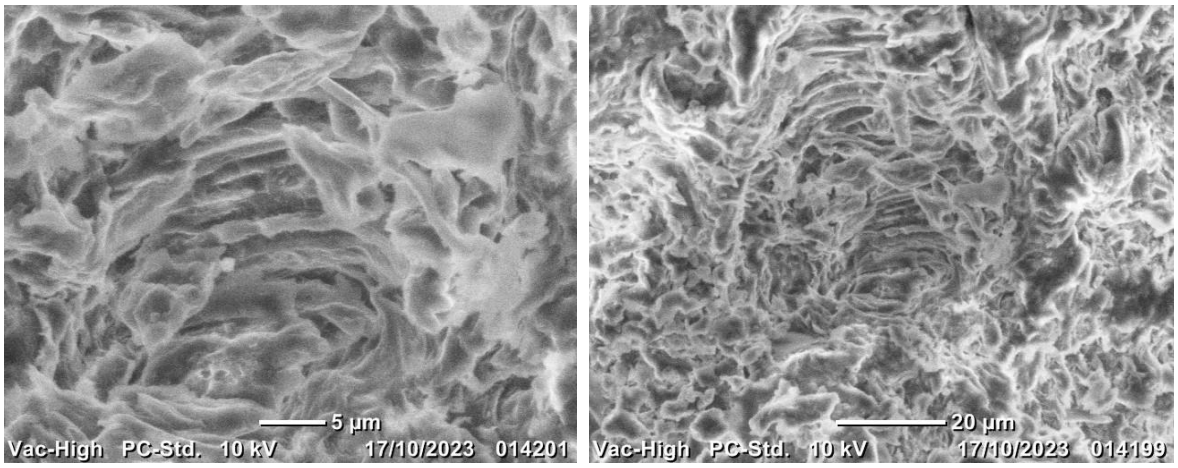

Figure IV.4. Scanning electron micrographs of the Activated surface of the pumpkin peel (APP).

Figure IV.5 illustrates the X-ray diffraction patterns (XRD) of the raw biomass (PP) and the biomass activated with H_3PO_4 (APP). The two materials share a similar structure, which is distinguished by its amorphous character. This configuration is characterized by two wide peaks observed at approximately 23° and 43°, which suggests the presence of compounds possessing an aromatic structure.

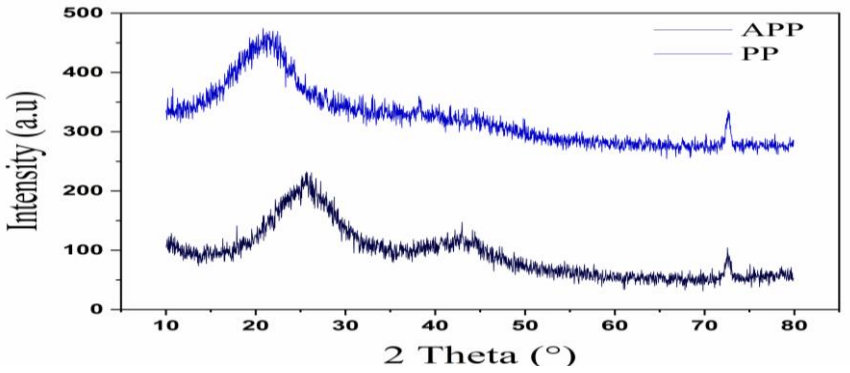

Figure IV.6. XRD data of PP, APP.

The thermogravimetric study (TGA) of (PP) and (APP) was carried out over a temperature range extending from 10 to 1200 °C., as illustrated in Figure IV.7. The graphs obtained show that the two materials undergo desorption of water molecules as well as degradation of volatile compounds in the temperature range from 30 to 220° C for PP and APP [16]. Both materials have good thermal stability in the first heating steps, with mass losses of about 10% for PP and APP. The second stage of degradation, observed between 220 and 380 ° C., is characterized by a significant loss of mass, attributable mainly to the thermal decomposition of the cellulose[17]. The last degradation step (380 °C. until the end of the analysis) is manifested by the rupture of the C-O and C-H bonds, accompanied by the transformation of the carbon residue formed previously. This process probably corresponds to the decomposition of the remaining aromatic structures and the partial graphitization of the material[18].

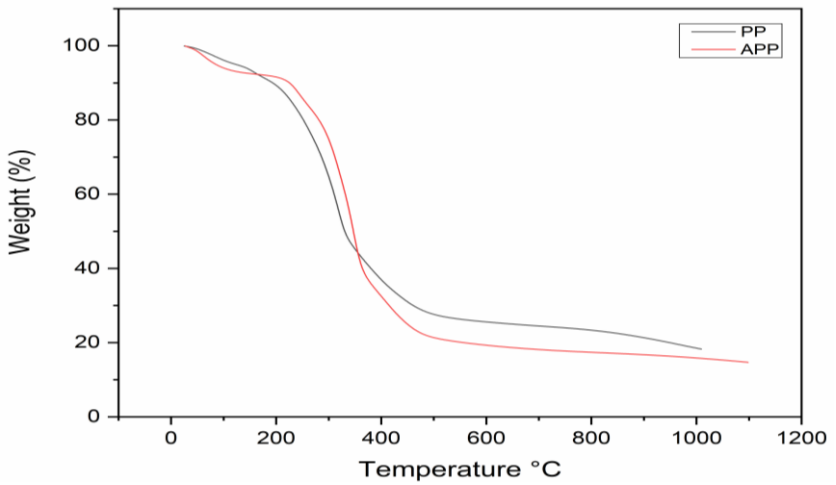

Figure IV.8. Thermogravimetric analysis of PP and APP.

The adsorption of the anionic dye such as congo red occurred at pH<pH_{PZC}, the biomasses used in this experiment had a pH_{PZC} of 4.1 of APP and 3.6 of PP, as shown in Figure IV.9. This indicates that when the pH of the medium is lower than pH_{PZC}, the surface of the adsorbent is positively charged which promotes electrostatic attraction with the anions of the dye therefore facilitating adsorption on the other hand when the pH is higher than pH_{PZC} the adsorbent is negatively charged, which causes a repulsion between the surface and the anions of the RC which reduces the adsorption[19].

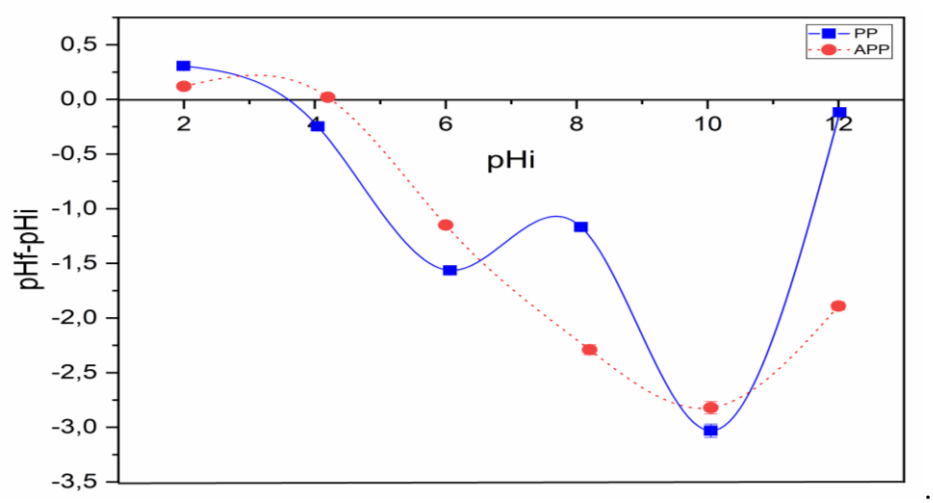

Figure IV.10. Isoelectric points of PP and APP.

IV.2.2. Adsorption experiments results

IV.2.2.1. Effect of adsorbent dosage

The adsorbent dosage significantly impacts the adsorption process, as it establishes the adsorption capability for a specific quantity of adsorbent Figure IV.7. Generally, an increase in the quantity of adsorbent results in a greater availability of sorption sites on the surface, hence enhancing the percentage of dye removal[20].The impact of different doses of adsorbent on the elimination % was examined using six 20 mL samples, each containing a solution of congo red at a concentration of 10 mg/L .Amounts of adsorbent ranging from 200 to 2800 mg/l for PP and from 200 to 2500 mg/l for APP were included in each sample. The solutions were then stirred for 24hours. After stirring, the samples were filtered and examined by a UV-Visible spectrophotometer to determine the percentage of removal of the dye. When the dosage is increased from 200 mg / L to 2500 mg / L for the two adsorbents, as shown in Figure IV.7, the percentage of adsorption for the PP increases from 26.73% to

82.83% and for the PPA from 65.35% to 93.39% with a decrease in the amount adsorbed for the PP from 33.41 to 7.39 mg/g and from 81.72 to 9.33 mg/g for the APP due to of the decrease in active sites. After reaching this value, stabilization is observed. One possible explanation is that the surface of the adsorbent is already saturated with dye molecules[21].Thus, the ideal adsorbent dosage for subsequent experiments was 2500 mg/L, which resulted in high adsorption while maintaining a high elimination rate.

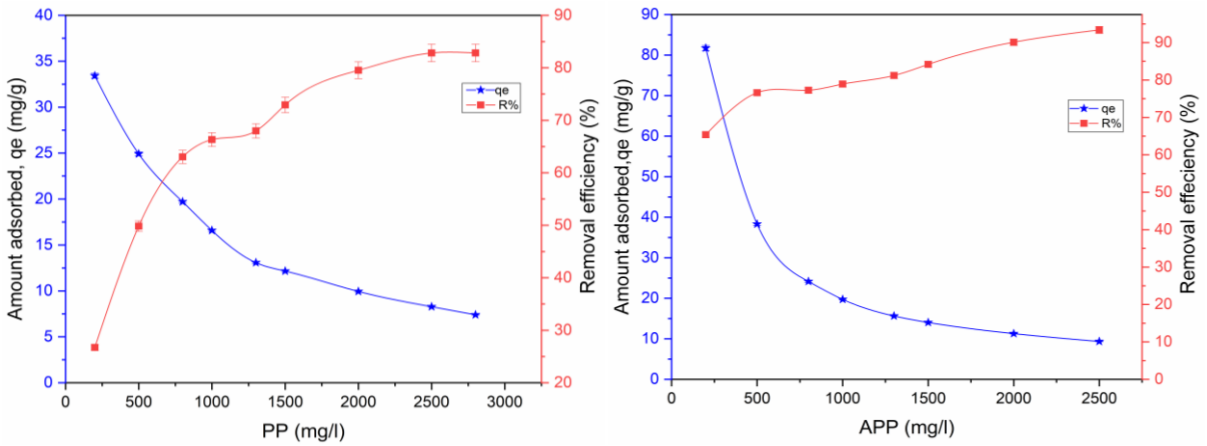

Figure IV.11. Effect of the dose of PP and APP on the elimination of CR.

IV.2.2.2. Effect of initial concentration

The impact of the dye concentration on the adsorption of CR by PP and APP was examined. By adjusting the initial dye concentration from 3 to 1000 mg / L and by studying the relationship between the amount of dye adsorbed and the initial CR concentration as shown in Figure IV.8. observing that when the initial CR concentration was increased from 3 to 450 mg / L for PP and from 3 to 400 mg/L for APP, the adsorbed amount (Q_{ads}) increased from 2.63 to 205.28 mg / g for PP and from 2.89 to 282.83 mg / g for APP. A greater adsorption is finally made possible by this increase in the initial dye concentration, because of the strengthening of the driving force and the decrease in the resistance between the aqueous and solid phases[22].

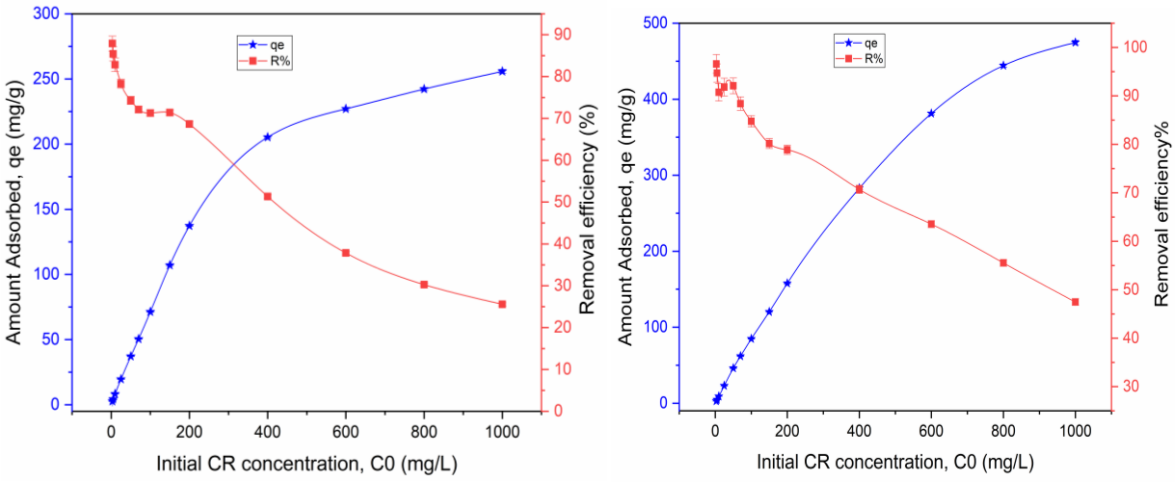

(a) (b)

Figure IV.12. Effect of concentration of PP (a), APP (b)

IV.2.2.3. Effect of PH

The adsorption of the dye particles was examined over a pH range of 2 to 12, revealing a peak at pH 5, with an elimination efficiency of 91.47% for PP and 97.85% for APP Figure IV.13 At this pH, a robust electrostatic interaction exists between the positively charged surface of the adsorbent and the anionic dye. As the pH of the system increases, the amount of negatively charged sites increases, while the amount of positively charged sites decreases. In addition, the reduction in the adsorption of CR at alkaline pH is attributed to the abundant presence of OH^- ions, which compete with the coloring anions for the adsorption sites[19]. Comparable results have been documented with the adsorption of CR on orange peel waste [23]and activated carbon [24].

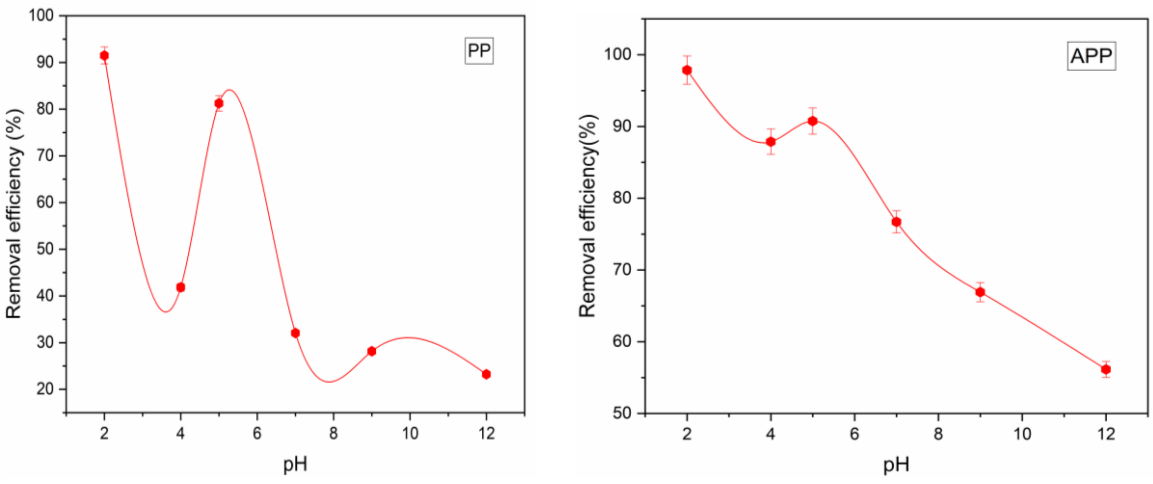

Figure IV.14. Effect of pH of PP, APP

IV.2.3. Kinetic Study

The adsorption kinetics as a function of time were evaluated in this work using discontinuous adsorption tests carried out at a pH of 5. Congo red (CR) at three initial concentrations of 3.5 and 10 mg/L was tested. 50 mL of each solution were brought into contact with a constant amount of 125 mg of adsorbent at ambient temperature (25 ± 2 °C.). the adsorption rate of CR dye on PP and APP materials has been examined Figure IV.15 [25]. In all the tests, rapid adsorption was observed during the 3 hours and 5 hours for APP and PP respectively, explained by the high availability of active sites on the surface of the APP at the beginning of the process compared to that of PP, due to chemical activation by H_3PO_4, which improved the specific surface of the biomass[26]. An equilibrium was established after this period, which made the adsorption process constant. Because the remains of active sites are difficult to complete, After the contact time, PP and APP achieved CR elimination rates of 86.79% and 95.59%, with q_{ads} reaching 8.14 and 9.07 mg/g, respectively. The pseudo-1st order , the pseudo-2nd t order, the Elovich and the models of intra-particle diffusion (table I.5) were used to adjust the adsorption kinetic data[27].The parameters obtained for these kinetic models are presented in Table IV.1.The adjustment of the experimental data to the kinetic models indicates that the pseudo-second-order (PSO) model has a higher coefficient of determination (R^2) than those of the pseudo-first-order (PFO) and Elovich models. In addition, the modeling curves generated with the pseudo-second-order model have a higher nonlinear adjustment compared to the PFO and Elovich models (Figure IV.10). These observations indicate that the mechanism of adsorption of Congo red (CR) on PP and App particles seems to follow a pseudo-second-order kinetic process. Therefore, the results suggest that the adsorption of the dye by our biomass is essentially due to a chemical process[28]. On the curves presented in Figure IV.11, three distinct steps have been identified for the different concentrations analyzed. The first step corresponds to the transport of the dye (CR) from the solution to the surface of the bioadsorbents. The second step is linked to the diffusion of the dye inside the pores of the adsorbent. Finally, the third step represents the equilibrium phase, during which the intraparticular diffusion slows down, due to the low residual concentration of the adsorbate in the aqueous solution. Moreover, the straight lines coming from the curves of Figure IV.11 do not pass through the origin for all concentrations, which indicates that intraparticular diffusion is not the limiting step of the adsorption process[29].

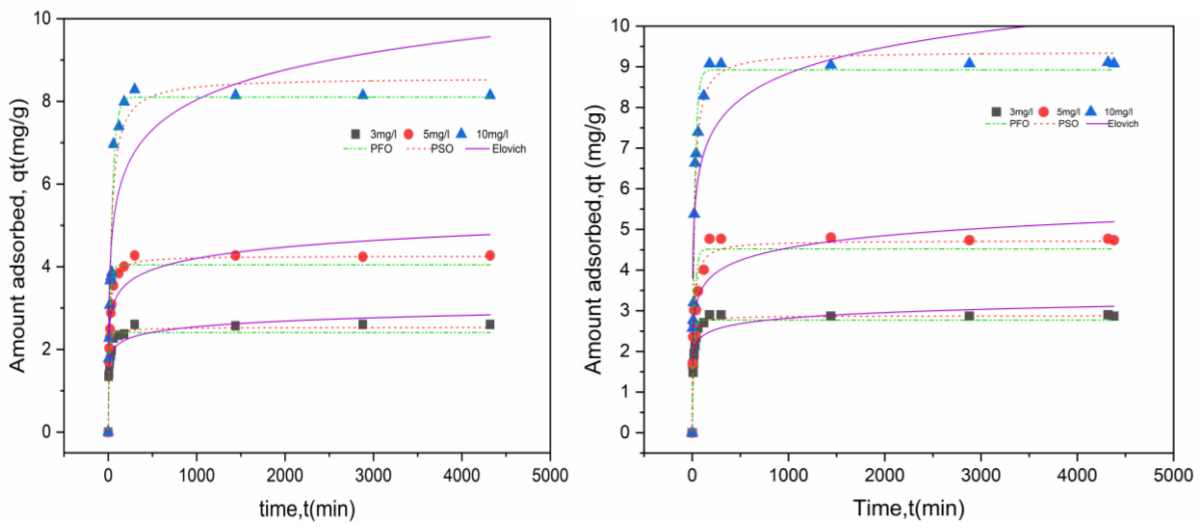

(a) (b)

Figure IV.16. Nonlinear compounds of PFO, PSO and Elovich for the kinetics of adsorption of CR by PP (a) and APP (b).

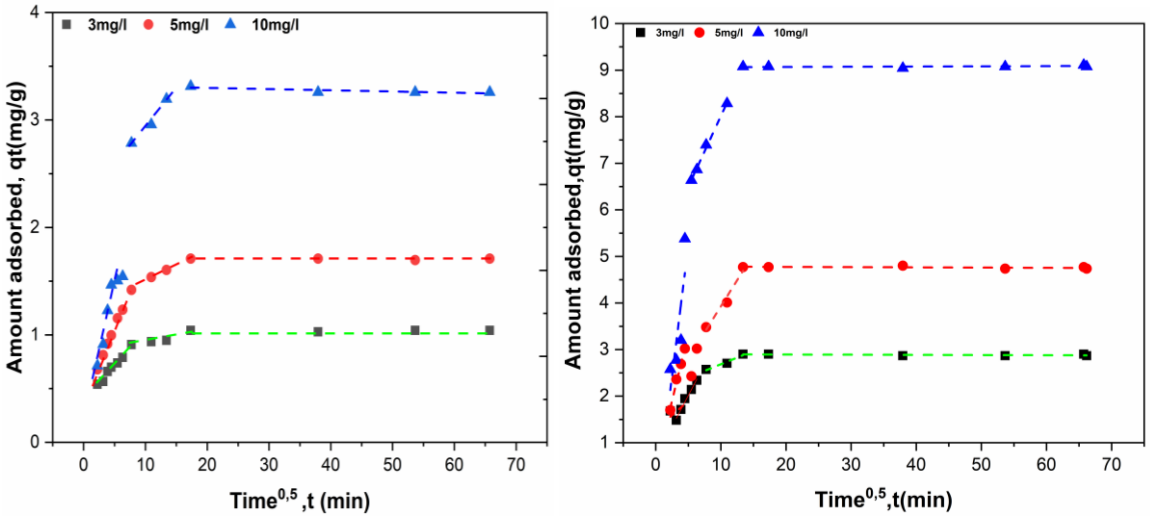

(a) (b)

Figure IV.17. Intraparticular diffusion model of the adsorption of CR on PP (a), APP (b)

Table IV.1. Kinetic model parameters of PP**.**

$C0$ (mg/L)	3			5			10		
qe,exp(mg/g)	2.60			4.27			8.14		
Pseudo-first-order									
qe (mg/g)	2.40			4.04			8.10		
k_1 (min^{-1})	0.078			0.052			0.025		
R^2	0.88041			0.92644			0.9616		
x^2	0.06161			0.11763			0.32256		
Pseudo-second-order model									
qe (mg/g)	2.53			4.26			8.57		
k_2(g/mg·min)	0.052			0.019			0.004		
R^2	0.96435			0.98233			0.95654		
x^2	0.01837			0.02825			0.36509		
Elovich									
α (mg/g.min)	89.97			17.11			2.30		
β (mg/g)	5.11			2.54			0.95		
R^2	0.93548			0.90669			0.82936		
x^2	0.03324			0.1492			1.43348		
Intraparticular diffusion model									
	Step1	Step2	Step3	Step1	Step2	Step3	Step1	Step2	Step3
K_3(mg/g·$min^{0.5}$)	0.013	0.064	0.001	0.029	0.138	0.001	0.05	0.21	0.001
C	0.79	0.39	**0.97**	1.19	**0.37**	1.64	2.35	0.30	**3.32**
R^2	0.847	0.957	0.167	0.988	0.995	0.087	0.937	0.847	0.556

Table IV.2. Kinetic model parameters of APP.

*C*0 (mg/L)	3			5			10		
***qe*,exp(mg/g)**	2.86			4.73			9.07		
Pseudo-first-order									
***qe* (mg/g)**	2.77			4.51			8.92		
k_1 **(min^{-1})**	0.072			0.043			0.039		
R^2	0.87728			0.8494			0.97444		
x^2	0.0798			0.30987			0.233		
Pseudo-second-order model									
***qe* (mg/g)**	2.87			4.72			9.37		
k_2**(g/mg·min)**	0.0453			0.0151			0.0062		
R^2	0.94902			0.93467			0.9745		
x^2	0.03315			0.13443			0.25035		
Elovich									
α **(mg/g.min)**	312.77			14.37			12.74		
β **(mg/g)**	5.06			2.28			1.077		
R^2	0.89393			0.8932			0.81619		
x^2	0.06897			0.21976			1.67579		
Intraparticular diffusion model									
	Step1	Step2	Step3	Step1	Step2	Step3	Step1	Step2	Step3
K_3**(mg/g·$min^{0.5}$)**	0.267	0.057	-0.0003	0.583	0.223	-0.0004	1.12	0.303	0.0004
C	0.67	2.11	2.9	0.43	1.69	4.78	-0.38	4.97	**9.05**
R^2	0.978	0.928	0.037	0.986	0.937	0.0029	0.554	0.994	-0.08

IV.2.4. Isotherm Study

The link between the residual concentration of congo red (CR) in aqueous solution and the adsorption capacity of PP and APP materials was investigated by examining the adsorption isotherms for a range of CR concentrations, from 5 to 1000 mg/L. These investigations used a pH of 5, a dosage of 20 mg/L of APP and PP, and a three-hour contact period [30]. The

nonlinear regression models from Langmuir, Freundlich, and sips were used to examine the isothermal adsorption data at various temperatures (25, 30, and 40 °C). (Table I.6) provides an overview of the equations related to these models.

The curves of adsorption isotherms of CR on PP and APP materials are shown in Figure IV.18. According to the Giles classification, the L-shape shows a significant affinity between the dye and the surface of the adsorbents, especially at low concentrations.

The nonlinear adaptations of the Freundlich, Langmuir and Sips models are also shown in Figure IV.19, with the respective parameters grouped in Table IV.3. The quality of the adjustments was evaluated using the correlation coefficients R^2 and the values of the error χ^2. Based on the high coefficients of determination (R^2) and the low values of the chi-squared coefficient (χ^2), it has been demonstrated that the Sips model was the most appropriate to describe the phenomenon of adsorption of CR on PP and APP.

revealing that this process takes place in a heterogeneous system. Unlike the Freundlich isotherm, which has a major limitation by not making it possible to predict the formation of monolayers, the Sips model offers a more complete and adapted approach to characterize this adsorption phenomenon. Thus, it makes it possible to better understand the mechanisms involved, in particular the heterogeneity of the adsorbent surface. The maximum adsorption capacities according to the Sips model are 265.52mg/g for PP and 698.20 mg/g for APP. On the other hand, the values estimated by the Langmuir model are 277.49mg/g for PP and 569.15 mg/g for APP.

In addition, the values of the separation coefficient (R_L) obtained from the Langmuir model, as well as the values of the parameter 1/n from the Freundlich model (which translates the adsorption intensity), suggest that the adsorption of Congo red on PP and APP is favorable and of a physical type[31].

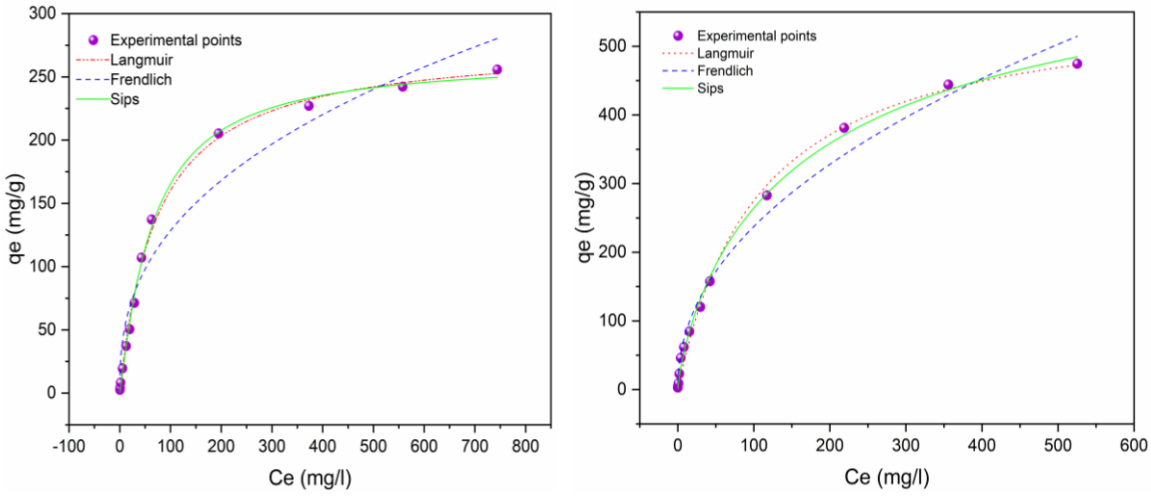

Figure IV.20. Nonlinear compounds of Langmuir, Frendlich and Sips for the kinetics of adsorption of CR by PP (a) and APP (b).

Table IV.4. Isotherm model parameters of PP.

Two-parameter isotherm models		Three-parameter isotherm models
Langmuir	Freundlich	Sips
q_m=277.49	K_F =21.42	q_m= 265.52
K_L= 0.013	n_f=2.57	ks=0.009 ns=0.892
R^2 = 0.99713	R^2 = 0.94787	R^2 = 0.99763
$\boldsymbol{x^2}$ =27.20577	x^2 = 493.32913	x^2= 22.44537

Tableau IV.5. Isotherm model parameters of APP.

Two-parameter isotherm models		Three-parameter isotherm models
Langmuir	Freundlich	Sips
q_m= 569.15	K_F =27.77	qm = 698.20
K_L= 0.009	n_f= 2.14	ks= 0.015 ns= 1.26
R^2 = 0.99462	R^2 = 0.9838	R^2 = 0.99751
$\boldsymbol{x^2}$ = 163.15876	$\boldsymbol{x^2 = 491.2459}$	$\boldsymbol{x^2 = 75.42641}$

IV.2.5. Adsorption Thermodynamics

The Van't Hoff plot Figure IV.21 relating to the adsorption of the CR dye was obtained from the equations described in Chapter I [32]. The thermodynamic parameters Table IV.6 and Table IV.6 indicate a negative enthalpy ($\Delta H°$ = -68.1 kJ.mol⁻1, -106,3 kJ.mol⁻1) and a negative entropy change (ΔS = -103.3 J·mol⁻1·K⁻, -226.05 J·mol⁻1·K⁻) for PP and APP respectively. The values of $\Delta H°$ are negative, which indicates that the adsorption of CR on the two samples is an exothermic process, favored at low temperature. Moreover, the chemical nature of this adsorption is confirmed by the values of $\Delta H°$, greater than 40 KJ/mol. the reduction of the disorder at the solid-solution interface is also suggested by these results.[33].

Moreover, the negative values of the Gibbs free energy (ΔG) confirm the spontaneous character of the adsorption. The decrease in ΔG with the increase in temperature indicates that the adsorption becomes more favorable at high temperature.

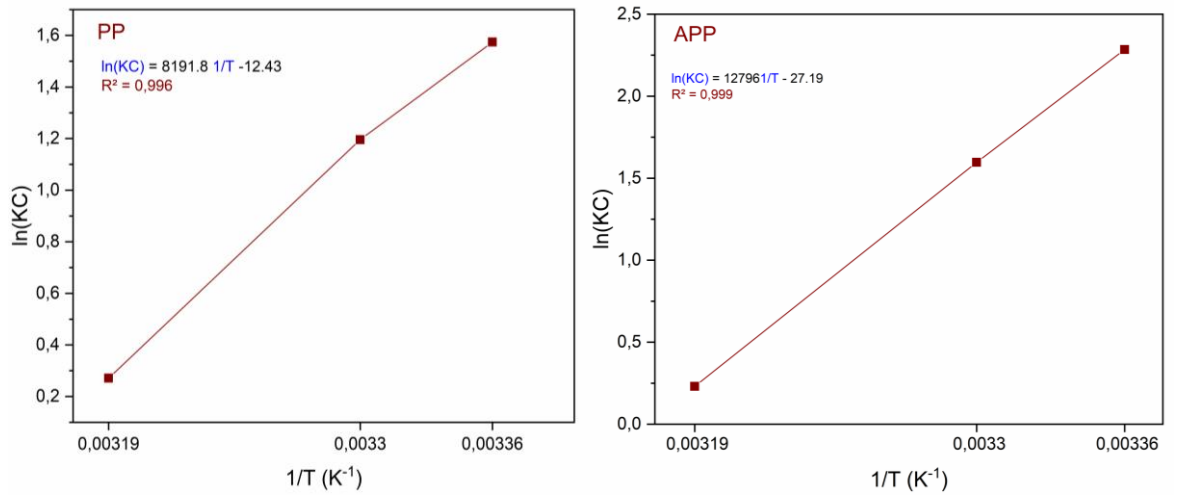

Figure IV.22. Thermodynamic of PP and APP.

Table IV.7. Thermodynamic parameters of PP.

Temperature (K)	ΔH° (kJ.mol^{-1})	ΔS° (J.mol^{-1}.K^{-1})	ΔG° (kJ.mol^{-1})	R^2
298	-68.1	-103.3	-37.310405	0.996
303			-36.79369	
313			-35.76026	

Table IV.8. Thermodynamic parameters of APP.

Temperature (K)	ΔH° (kJ.mol^{-1})	ΔS° (J.mol^{-1}.K^{-1})	ΔG° (kJ.mol^{-1})	R^2
298	-106.3	-226.05	-39.020761	0.999
303			-37.890473	
313			-35.629896	

IV.3. Conclusion

The study highlights the potential of pumpkin peels as an effective precursor in the elimination of congo red (CR) from aqueous solutions. The experimental data concerning the adsorption kinetics were examined using different models, among which the pseudo-second-order model (PSO) proved to be the most appropriate to characterize the phenomenon. In addition, the analysis carried out using the intraparticular diffusion model indicates that diffusion through the boundary layer (film) is not the step that limits adsorption. The Sips model is more suitable for describing the adsorption isotherms, revealing that this process takes place in a heterogeneous system on PP and APP surfaces. Thermodynamic analysis reveals that adsorption is a spontaneous and exothermic phenomenon, These results indicate that the use of pumpkin peels could constitute an economical and ecological solution for wastewater treatment.

References

[1] A. M. A. Adam et al., « Preparation and characterization of new CrFeO3-carbon composite using environmentally friendly methods to remove organic dye pollutants from aqueous solutions », Crystals, vol. 11, nº 8, p. 960, 2021.

[2] N. M. Mahmoodi, U. Sadeghi, A. Maleki, B. Hayati, et F. Najafi, « Synthesis of cationic polymeric adsorbent and dye removal isotherm, kinetic and thermodynamic », J. Ind. Eng. Chem., vol. 20, nº 5, p. 2745-2753, 2014.

[3] K. Mohajershojaei, N. M. Mahmoodi, et A. Khosravi, « Immobilization of laccase enzyme onto titania nanoparticle and decolorization of dyes from single and binary systems », Biotechnol. Bioprocess Eng., vol. 20, nº 1, p. 109-116, févr. 2015, doi: 10.1007/s12257-014-0196-0.

[4] N. M. Mahmoodi, « Photocatalytic Degradation of Dyes Using Carbon Nanotube and Titania Nanoparticle », Water. Air. Soil Pollut., vol. 224, nº 7, p. 1612, juill. 2013, doi: 10.1007/s11270-013-1612-3.

[5] B. Hayati et N. M. Mahmoodi, « Modification of activated carbon by the alkaline treatment to remove the dyes from wastewater: mechanism, isotherm and kinetic », Desalination Water Treat., vol. 47, nº 1-3, p. 322-333, 2012.

[6] A. Afkhami et R. Moosavi, « Adsorptive removal of Congo red, a carcinogenic textile dye, from aqueous solutions by maghemite nanoparticles », J. Hazard. Mater., vol. 174, nº 1-3, p. 398-403, 2010.

[7] S. I. Siddiqui et al., « Investigation of Congo red toxicity towards different living organisms: a review », Processes, vol. 11, nº 3, p. 807, 2023.

[8] L. Sellaoui, T. Depci, A. R. Kul, S. Knani, et A. B. Lamine, « A new statistical physics model to interpret the binary adsorption isotherms of lead and zinc on activated carbon », J. Mol. Liq., vol. 214, p. 220-230, 2016.

[9] M. B. Manaa, N. Bouaziz, B. Schmaltz, F. T. Van, et A. B. Lamine, « Study of the effect of variation in temperature and pH on the adsorption process of natural Gardenia yellow dye into TiO2 mesoporous for dye sensitized solar cells using the statistical physics formalism: Physicochemical and thermodynamic investigation », Microporous Mesoporous Mater., vol. 270, p. 82-92, 2018.

[10] K. Qiu, X. Song, G. Tang, L. Wu, et S. Min, « Determination of Fipronil in Acetamiprid Formulation by Attenuated Total Reflectance-Mid-Infrared Spectroscopy Combined

with Partial Least Squares Regression », Anal. Lett., vol. 46, nº 15, p. 2388-2399, oct. 2013, doi: 10.1080/00032719.2013.800537.

[11] N. Hamri et al., « Enhanced adsorption capacity of methylene blue dye onto kaolin through acid treatment: batch adsorption and machine learning studies », Water, vol. 16, nº 2, p. 243, 2024.

[12] M. S. Reddy, L. Sivaramakrishna, et A. V. Reddy, « The use of an agricultural waste material, Jujuba seeds for the removal of anionic dye (Congo red) from aqueous medium », J. Hazard. Mater., vol. 203, p. 118-127, 2012.

[13] F. Benamraoui et al., « Methylene blue removal using black cumin seeds waste: experimental study and molecular dynamic simulation », Desalination Water Treat., vol. 300, p. 167-177, 2023.

[14] V. O. Njoku et B. H. Hameed, « Preparation and characterization of activated carbon from corncob by chemical activation with H3PO4 for 2, 4-dichlorophenoxyacetic acid adsorption », Chem. Eng. J., vol. 173, nº 2, p. 391-399, 2011.

[15] L. Das, P. Das, A. Bhowal, et C. Bhattachariee, « Treatment of malachite green dye containing solution using bio-degradable Sodium alginate/NaOH treated activated sugarcane baggsse charcoal beads: Batch, optimization using response surface methodology and continuous fixed bed column study », J. Environ. Manage., vol. 276, p. 111272, 2020.

[16] A. Ü. Metin, D. Doğan, et M. Can, « Novel magnetic gel beads based on ionically crosslinked sodium alginate and polyanetholesulfonic acid: Synthesis and application for adsorption of cationic dyes », Mater. Chem. Phys., vol. 256, p. 123659, 2020.

[17] A. Guediri, A. Bouguettoucha, H. Tahraoui, D. Chebli, A. Amrane, et J. Zhang, « Thermodynamic study and the development of a support vector machine model for predicting adsorption behavior of orange peel-derived beads in wastewater treatment », J. Mol. Liq., vol. 403, p. 124860, 2024.

[18] R. Ahmad et R. Kumar, « Synthesis and Properties of Cellulose Carbon Encapsulated ZnO for Dye Removal », J. Dispers. Sci. Technol., vol. 32, nº 5, p. 737-740, avr. 2011, doi: 10.1080/01932691.2010.480869.

[19] S. Secrain et al., « REMOVAL OF CONGO RED DYE USING ENTODON PROREPENS (MITT.) JAEG.(A MOSS) BIOMASS: KINETICS, ISOTHERMS AND THERMODYNAMICS STUDY », Consulté le: 22 octobre 2024. [En ligne]. Disponible

sur:https://www.plantarchives.org/article/226%20Removal%20of%20Congo%20red%20dye%20using%20Entodon%20prorepens%20(Mitt.)%20Jaeg.%20(a%20moss)%20biomass%20Kinetics,%20isotherms%20and%20thermodynamics%20study.pdf

[20] M. A. M. Salleh, D. K. Mahmoud, W. A. W. A. Karim, et A. Idris, « Cationic and anionic dye adsorption by agricultural solid wastes: a comprehensive review », Desalination, vol. 280, nº 1-3, p. 1-13, 2011.

[21] P. Barooah, N. Mushahary, B. Das, et S. Basumatary, « Waste biomass-based graphene oxide decorated with ternary metal oxide (MnO-NiO-ZnO) composite for adsorption of methylene blue dye », Clean. Water, p. 100049, 2024.

[22] S. Banerjee et M. C. Chattopadhyaya, « Adsorption characteristics for the removal of a toxic dye, tartrazine from aqueous solutions by a low cost agricultural by-product », Arab. J. Chem., vol. 10, p. S1629-S1638, 2017.

[23] Z. Hua, Y. Pan, et Q. Hong, « Adsorption of Congo red dye in water by orange peel biochar modified with CTAB », RSC Adv., vol. 13, nº 18, p. 12502-12508, 2023.

[24] C. Namasivayam et D. Kavitha, « Removal of Congo Red from water by adsorption onto activated carbon prepared from coir pith, an agricultural solid waste », Dyes Pigments, vol. 54, nº 1, p. 47-58, 2002.

[25] A. Guediri, A. Bouguettoucha, H. Tahraoui, D. Chebli, A. Amrane, et J. Zhang, « Thermodynamic study and the development of a support vector machine model for predicting adsorption behavior of orange peel-derived beads in wastewater treatment », J. Mol. Liq., vol. 403, p. 124860, 2024.

[26] E. Errais et al., « Efficient anionic dye adsorption on natural untreated clay: Kinetic study and thermodynamic parameters », Desalination, vol. 275, nº 1-3, p. 74-81, 2011.

[27] B. Li, J. Guo, K. Lv, et J. Fan, « Adsorption of methylene blue and Cd (II) onto maleylated modified hydrochar from water », Environ. Pollut., vol. 254, p. 113014, 2019.

[28] X. Wang et al., « Core-shell alginate beads as green reactor to synthesize grafted composite beads to efficiently boost single/co-adsorption of dyes and Pb (II) », Int. J. Biol. Macromol., vol. 206, p. 10-20, 2022.

[29] S. Sharma, A. Hasan, N. Kumar, et L. M. Pandey, « Removal of methylene blue dye from aqueous solution using immobilized Agrobacterium fabrum biomass along with

iron oxide nanoparticles as biosorbent », Environ. Sci. Pollut. Res., vol. 25, n° 22, p. 21605-21615, août 2018, doi: 10.1007/s11356-018-2280-z.

[30] J. Sharma, M. Sharma, S. Nigam, et M. Joshi, « Environmental-friendly algal-mediated magnetic activated carbon for adsorptive removal of contaminants from water », Chem. Phys. Impact, vol. 6, p. 100169, 2023.

[31] D. Kaboub, H. Khelili, M. Guellal, K. G. Konan, M. Hentabli, et A. Amrane, « Enhanced bio-adsorbent derived from turnip leaves for crystal violet removal in aqueous solutions: experimental investigation, characterization, and machine learning modeling », Int. J. Chem. React. Eng., avr. 2025, doi: 10.1515/ijcre-2024-0206.

[32] L. Giraldo et J. C. Moreno-Piraján, « Synthesis of Activated Carbon Mesoporous from Coffee Waste and Its Application in Adsorption Zinc and Mercury Ions from Aqueous Solution », J. Chem., vol. 9, n° 2, p. 938-948, janv. 2012, doi: 10.1155/2012/120763.

[33] J. A. Akande, A. I. Adeogun, et A. S. Uzosike, « Removal of Congo Red Dye from Simulated Wastewater Using Activated Carbon Derived from Corn Cobs; Kinetics and Equilibrium Studies », Glob J Pure Appl Chem Res, vol. 11, p. 1-19, 2023.

Chapter V
Characterization and application of pomegranate crusts as an alternative adsorbent for the removal of methyl red from aqueous solutions

V.1. Introduction

The increasing development of science and technology is accompanied by a significant industrial expansion, especially in the textile production sector [1]. The discharge of effluents from this industry into waterways has harmful effects on aquatic life, human health, as well as a negative impact on environmental sustainability [2]. Methyl red is an azo dye commonly used in textile dyeing [3]. This dye contains an azo group (-N=N-) linked to an aromatic nucleus, forming a chromophore characteristic of synthetic dyes [4]. It is particularly reactive in textile dyeing processes.

Methyl red is highly toxic to living organisms due to the difficulty of its degradation in liquid effluents. If inhaled or swallowed, it can cause irritation to the skin, eyes and digestive system. It is also recognized as mutagenic, toxic for cell division (mitotoxic), and potentially carcinogenic [5]. Its non-biodegradable nature, combined with its toxicity, makes it imperative to dispose of industrial wastewater [6].

Adsorption is recognized as one of the most effective methods for water purification, due to its simplicity of implementation, its easy design and its low cost [7]. Various materials have been explored as adsorbents to remove methyl red from aquatic environments. Among these materials are in particular zeolite [8], activated carbon [9], biomass [10] as well as biochar [11].

The objective of this study is to develop economical adsorbents from pomegranate crustal waste, with the aim of obtaining an effective material applicable to the treatment of wastewater, in particular for the decolorization of effluents from the textile industry. In this context, methyl red (MR) was used as a model dye (adsorbate), while pomegranate crusts, in the crude state (PC) and after chemical activation with phosphoric acid (APC), served as adsorbents. The method of preparation of these materials is detailed in Chapter II.

In this chapter, we have characterized the prepared materials (PC and APC) by various analytical techniques, in particular X-ray diffraction (XRD), infrared spectroscopy (FTIR) and the determination of the isoelectric point. These analyses made it possible to study their physicochemical properties, such as their crystal structure, their functional groups and their surface charge.

Moreover, the effectiveness of PC and APC for the elimination of methyl red in solution was evaluated according to several experimental parameters :

Initial concentration of the dye, powder mass of the pomegranate crusts, pH of the solution, Contact time and Temperature.

In addition, the adsorption mechanisms were analyzed using kinetic and isothermal models, in order to understand the dynamics of the process and the adsorbate-adsorbent interactions.

V.2. Results and discussions

V.2.1. Characterization of the PC and APC

Infrared (IR) spectrometry analysis of activated pomegranate crusts (APC) with phosphoric acid Figure V.1 reveals various specific bands corresponding to the functional groups present in the functionalized carbonaceous materials. The wide band centered around 3387 cm^{-1} is characteristic of the elongation of the O-H bonds, which suggests the presence of hydroxyl groups or water adsorbed on the surface [12]. The intense band at 1620 cm^{-1} is attributed to the stretching of the aromatic C=C bonds or the conjugated carbonyl groups (C=O) present in the degraded lignocellulosic structures following activation [13,14]. The band observed at 864 cm^{-1} is associated with out-of-plane vibrations of aromatic C-H bonds, indicating the presence of substituted aromatic rings, as frequently observed in activated carbons derived from plant materials [15]. In addition, the possible presence of phosphate groups (P–O–C or P=O) originating from activation with phosphoric acid is usually identified by bands located between 1100 and 900 cm^{-1} [16]. All these observations in infrared spectroscopy confirm the chemical transformation of the surface of the pomegranate crusts following activation, as well as the incorporation of polar groups favoring adsorption.

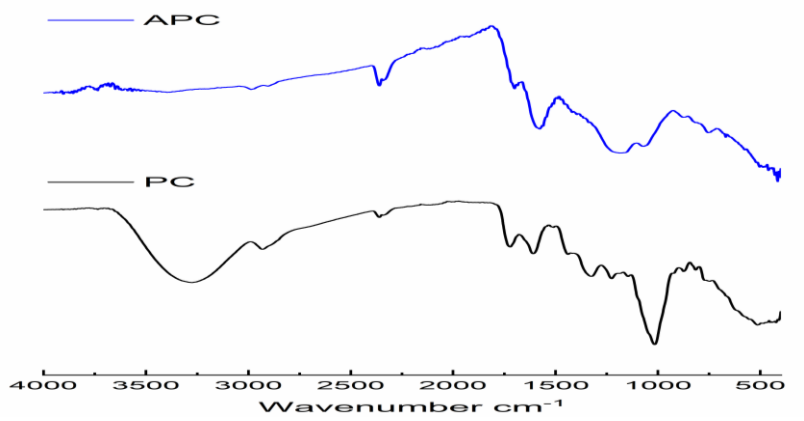

Figure V.2. FTIR spectra of APC and PC.

The zero charge point, denoted pH_{PZC}, corresponds to the pH where the surface charge density of the cations (positive ions) is equal to that of the anions (negative ions), thus leading to a surface neutrality. This parameter is of paramount importance, since the efficiency of many adsorption processes is closely related to pH. The values of the pH_{PZC} for the APC was measured at 6.5, as indicated in Figure V.2. These data reveal that the adsorbent surface charge is positive at pH values below the pH_{PZC}, and becomes negative beyond this threshold. Therefore, the adsorption capacity of anionic dyes such as methyl red (MR) is higher at pHs below 6.5, thus promoting the maximum electrostatic interaction between the dye molecules and the positively charged surface[17].

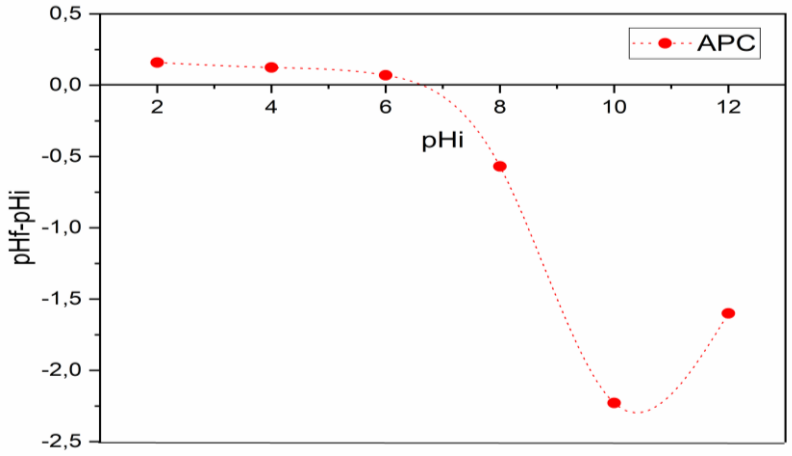

Figure V.3. Isoelectric points of PC and APC.

V.2.2. Adsorption experiments results

V.2.2.1. Effect of adsorbent dosage

The impact of the adsorbent dose (APC and PC) was examined by modifying the doses from 0 to 1500 mg/L to evaluate its effect on the elimination of methyl red (RM). The studies were carried out with an initial MR concentration of 5 mg/L at a pH of 5. The results obtained are illustrated in Figure V.3.The results indicate an increase in the removal rate of pollutants depending on the amount of bioadsorbent used. This improvement is due to the increase in the contact area between the adsorbent and the adsorbate, which favors the availability of active sites for adsorption [18]. A thorough analysis of the data showed that the maximum adsorption efficiency of methyl red is obtained with APC at a dose of 300 mg / l, and 500 mg / l for PC, with an adsorbed amount of 15.25 and 3.89 mg / g respectively and an elimination rate of 91.5% and 39.2% which confirms that the chemical activation increased the specific

surface of APC. Beyond these values, no significant improvement in the efficiency was observed, which suggests a saturation of the available active sites or a phenomenon of overlapping of the particles.

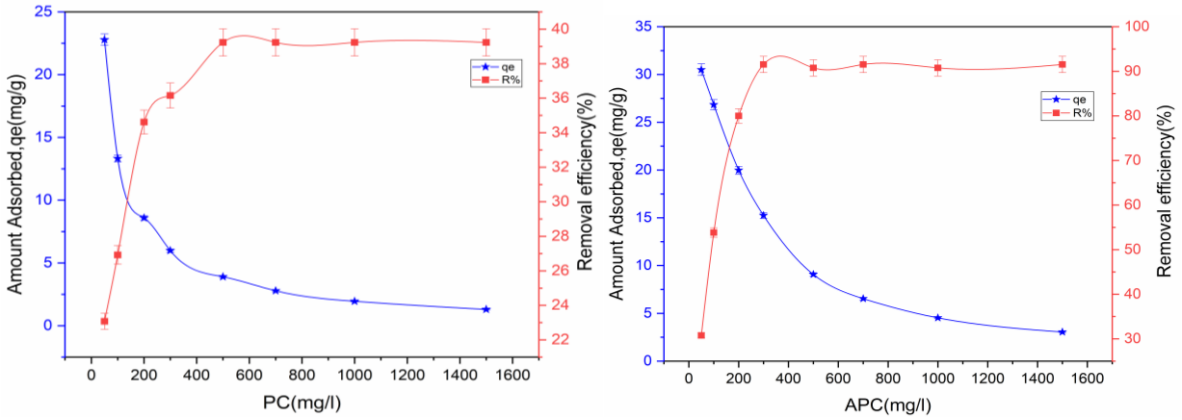

Figure V.4. Effect of the dose of PC and APC on the elimination of MR.

V.2.2.2. Effect of initial concentration

The initial concentration of the pollutant (MR) is a crucial factor that influences the elimination rate. To evaluate its impact, various concentrations of MR were experimented with: 4, 5, 10, 15 and 20 mg/L. For each test, a quantity of 50 mL of dye solution was used, with an APC concentration fixed at 300 mg/L and PC at 500 mg/L. The experiments were carried out under optimal conditions, with a pH of 5, a temperature of 24 °C. and a contact time of 48 hours. Figure V.4 depicts the correlation between the initial concentration of the pollutant (MR) and the adsorption capacity (Qe) of the examined adsorbent. The adsorption capacity is shown to increase with the initial concentration of the adsorbate. This phenomenon can be elucidated by an elevated frequency of successful collisions between the adsorbate molecules and the active sites of the adsorbent, hence promoting enhanced adsorption. The results indicate that this capacity attains a threshold at a concentration of 5 mg/L of MR, with a maximum adsorbed amount (Qads) of approximately 15.25 mg/g for APC and 3.89 mg/g for PC [10].

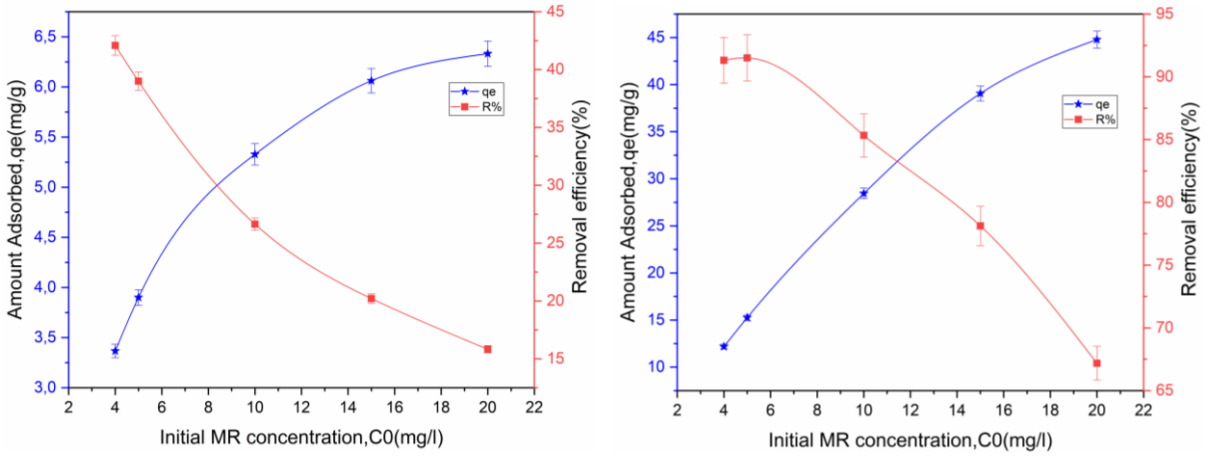

(a) (b)

Figure V.5. Effect of initial concentration of MR by PC (a) and APC (b).

V.2.2.3. Effect of pH

The influence of the pH, covering a range of values from 2 to 9, on the process of elimination of methyl red in solution was examined according to the following experimental parameters: an initial dye concentration of 5 mg/L, adsorbent concentrations of 300 mg/L for APC and 500 mg/L for PC, at a temperature maintained at 25 ± 2 ° C., with a contact time of 24 hours. The pH plays a crucial role in the adsorption phenomenon, by impacting both the surface charge of the adsorbent and the ionic speciation of the adsorbate. Figure V.5 shows the impacts of pH on the removal rate of the pollutant[19]. An increase in the yield of elimination of methyl red was observed with the increase in pH. This disparity in behavior can be attributed largely to the nature of the dyes used, in this case methyl red which is an anionic dye. Due to the high pH negative charge of PC and APC, their surfaces favor the electrostatic attraction of cationic species such as methylene blue, while repelling anionic species such as methyl red. The dye chosen for this study has a variety of functional groups (-NH_2, -ch_3) and aromatic rings that can interact with the adsorbent material. These interactions can encompass hydrogen bonds, electrostatic forces, as well as π–π interactions between the aromatic rings of the dye and the graphitic structures of the PCA. These interactions have been frequently documented in the scientific literature dealing with the adsorption of dyes on activated carbons derived from lignocellulosic biomass[20].

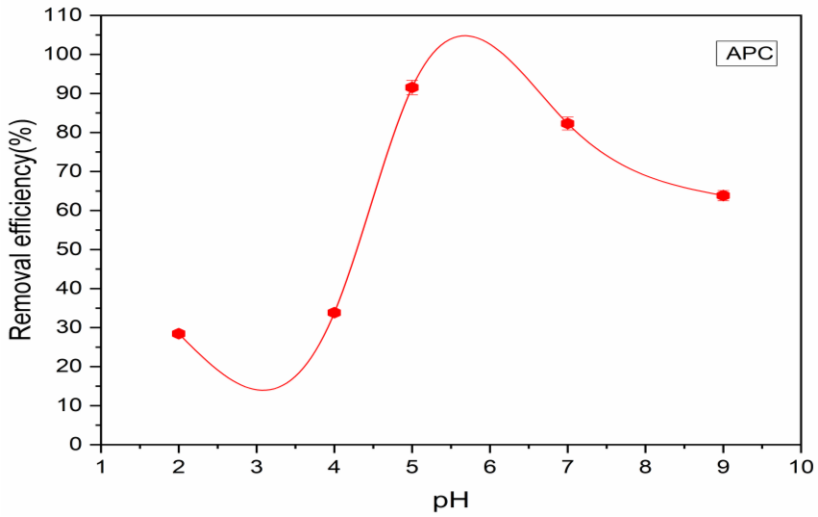

Figure V.6. Effect of pH of APC.

V.2.3. Kinetic Study

Three concentrations of MR (5, 10 and 20 mg/L) were used in order to study the influence of the contact time on the PC and APC adsorbents, at a pH of 5 and at ambient temperature, with respective doses of 500 mg/L for PC and 300 mg/L for APC. In order to evaluate the adsorption rate of MR at the APC surface and PC , Three kinetic models have been applied: the pseudo-first-order model, the pseudo-second-order model and the Elovich model (Table I.5). The adjustment of the experimental data to the nonlinear shapes of these models is presented in Figure V.6, while the corresponding kinetic parameters are grouped in Table V.1 and Table V.2 [21]. For the APC adsorbent, the pseudo-second-order kinetic model (PSO) has a better correlation coefficient (R^2) than the pseudo-first-order (PFO) and Elovich models. This result indicates that the adsorption of MR on APC mainly follows the PSO kinetic model, suggesting a mechanism dominated by chemisorptions [22,23]. On the other hand, for the PC, the Elovich model displays R^2 values greater than 0.95, which indicates that the adsorption is mainly governed by a chemisorption process on heterogeneous sites. Figure V.7 shows the linear plots of the intraparticle diffusion model for the APC and PC adsorbents. Three distinct phases can be observed: phase I, phase II and phase III, which suggests that adsorption takes place in three successive diffusion steps. These phases could correspond respectively to an electrostatic attraction, a diffusion in the macropores, then a diffusion in the micropores [22].

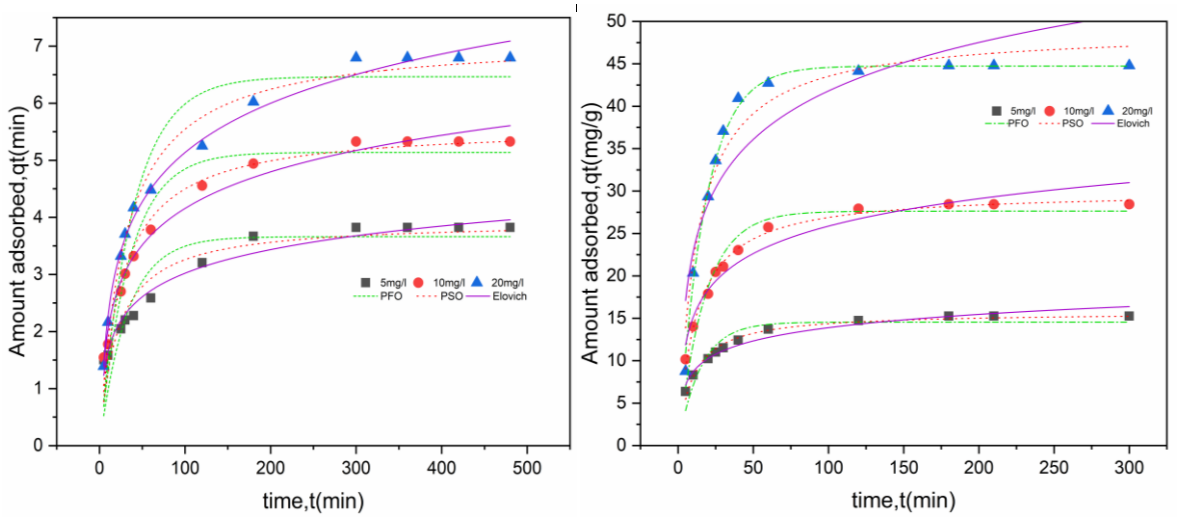

(a) **(b)**

Figure V.7. Nonlinear compounds of PFO, PSO and Elovich for the kinetics of adsorption of MR by PC (a) and APC (b).

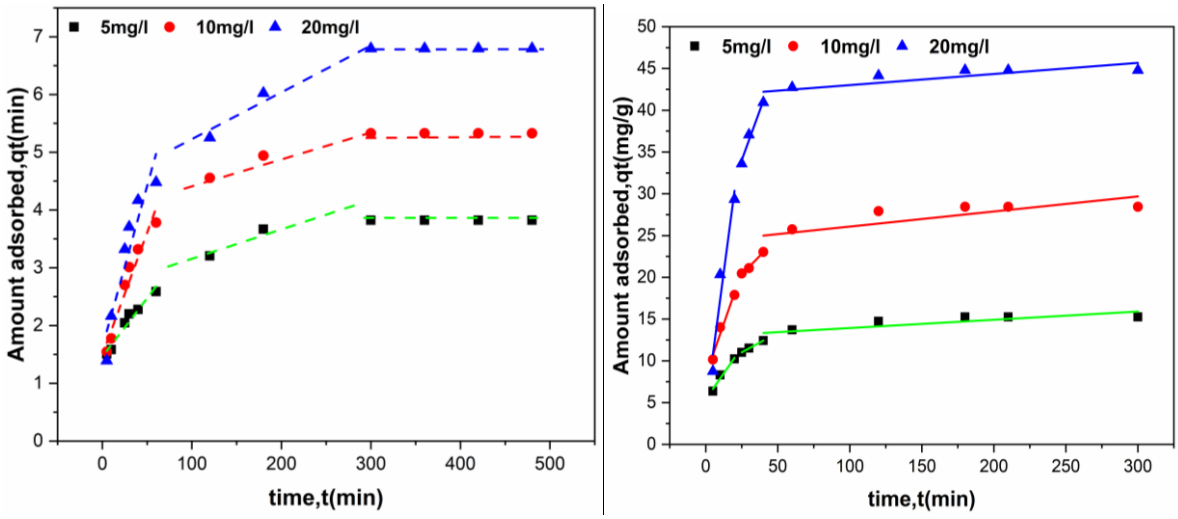

(a) **(b)**

Figure V.8. Intraparticular diffusion model of the adsorption of MR on PC(a), APC(b)

Table V.1. Kinetic model parameters of PC.

$C0$ (mg/L)	5			10			20		
qe,exp(mg/g)	3.8224			5.3282			6.7954		
Pseudo-first-order									
qe (mg/g)	3.66			5.13			6.46		
k_1 (min^{-1})	0.03			0.02			0.02		
R^2	0.79542			0.92309			0.92419		
x^2	0.17577			0.15596			0.27635		
Pseudo-second-order model									
qe (mg/g)	3.92			5.60			7.14		
k_2(g/mg·min)	0.012			0.007			0.004		
R^2	0.88822			0.97538			0.97963		
x^2	0.09604			0.04992			0.07426		
Elovich									
α (mg/g.min)	0.940			0.828			0.768		
β (mg/g)	1.67			1.08			0.80		
R^2	0.96476			0.98191			0.99221		
x^2	0.03027			0.03669			0.02838		
Intraparticular diffusion model									
	Step1	Step2	Step3	Step1	Step2	Step3	Step1	Step2	Step3
K_3(mg/g·$min^{0.5}$)	0.020	0.003	0	0.042	0.004	0	0 .055	0.008	0
C	1.45	2.93	3.82	1.49	4.11	5.32	1.622	4.36	6.79
R^2	0.9409	0.5879	--	0.9316	0.9285	--	0,8501	0.9285	--

Table V.2 Kinetic model parameters of APC

$C0$ (mg/L)	5			10			20		
qe,exp(mg/g)	15.25			28.44			44.78		
Pseudo-first-order									
qe (mg/g)	14.55			27.63			44.73		
k_1 (min^{-1})	0.06			0.05			0.05		
R^2	0.85894			0.93103			0.99323		
x^2	1.29247			2.73902			0.9503		
Pseudo-second-order model									
qe (mg/g)	15.71			30.00			49.04		
k_2(g/mg·min)	0.006			0.002			0.001		
R^2	0.97893			0.98942			0.95005		
x^2	0.19308			0.42008			7.01572		
Elovich									
α (mg/g.min)	10.54			11.87			13.11		
β (mg/g)	0.44			0.21			0.12		
R^2	0.9546			0.93784			0.81354		
x^2	0.41599			2.46829			26.19083		
Intraparticular diffusion model									
	Step1	Step2	Step3	Step1	Step2	Step3	Step1	Step2	Step3
K_3(mg/g·$min^{0.5}$)	0.24	0.09	0.009	0.49	0.17	0.018	1.30	0.47	0.01
C	5.4	8.67	12.94	8.23	16	24.2	4.24	22.17	41.67
R^2	0.9285	0.9977	0.6244	0.9285	0.9835	0.5522	0.8656	0.9493	0,6107

V.2.4. Isotherm Study

The adsorption isotherms provide essential information on the nature of the interactions between the adsorbate and the surface of the adsorbent[24]. In this study, we evaluated the mechanisms of MR absorption on APC and PC by applying three theoretical models:

Langmuir (for homogeneous surfaces), Freundlich (for heterogeneous surfaces) and Sips (hybrid model combining the two approaches). As illustrated in Figure V.8, Table V.3 and table V.4, The values of the separation factor R_L, calculated for different initial concentrations of dye MR, are between 0 and 1, which indicates a favorable adsorption on the PC and APC adsorbents. The adjustment of the isotherms by a nonlinear analysis using the Microcal Origin 2018 software highlights distinct adsorption mechanisms :

For the PC: the Langmuir model (R^2 = 0.9989 ; X^2=0.001) provides the best fit compared to the Sips and Freundlich models, suggesting a monolayer adsorption on a homogeneous surface. The maximum adsorption capacity (qm) reaches 7.39 mg/g. For APC: the Sips model (R^2 =0.996; X^2=0.67), which combines the characteristics of the Langmuir and Freundlich models, fits best to the data, indicating adsorption on a heterogeneous surface. The maximum adsorption capacity (qm) is 55.74 mg/g[25]. These results underline the high efficiency of APC for the elimination of dyes, with adsorption mechanisms influenced by the molecular structure of the compounds.

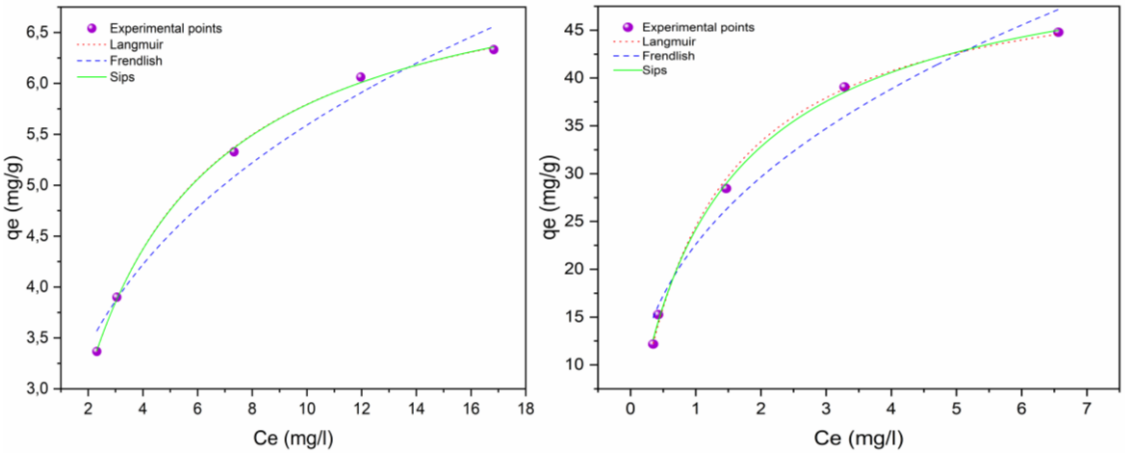

(a) **(b)**

Figure V.9. Nonlinear modeling of MR adsorption isotherms by PC (a), APC (b).

Table V.3. Isotherm model parameters of PC

Two-parameter isotherm models		Three-parameter isotherm models
Langmuir	Freundlich	Sips
q_m= 7.39	K_F =2.75	qm = 7.44
K_L= O.361	n_f= 3.26	ks= 0.363 ns= 1.015
R^2 = 0.9891	R^2 = 0.96584	R^2 =0.99839
$\boldsymbol{x^2}$ = 0.00187	$\boldsymbol{x^2 = 0.5882}$	$\boldsymbol{x^2 = 0.00277}$

Table V.4. Isotherm model parameters of APC.

Two-parameter isotherm models		Three-parameter isotherm models
Langmuir	Freundlich	Sips
q_m= 52.31	K_F =22.60	qm = 55.74
K_L= 0.879	n_f= 2.55	ks= 0.764 ns= 1.10
R^2 = 0.99641	R^2 = 0.95344	R^2 = 0.99669
$\boldsymbol{x^2}$ = 0.73269	$\boldsymbol{x^2 = 9.1416}$	$\boldsymbol{x^2 = 0.67717}$

V.2.5. Adsorption Thermodynamics.

The thermodynamic study of the adsorption process involves key parameters such as the Gibbs free energy change (ΔG⁰), the enthalpy change (ΔH⁰) and the entropy change (ΔS ⁰).

Figure V.9 shows the linear relationship between 1/T and ln Kc, obtained from the Van't Hoff equation. The thermodynamic parameters derived from this analysis are grouped in Table V.5 and table V.6. The enthalpy values (ΔH°) are : -66.99 kJ.mol-1 for PC and -64.05 kJ.mol-1 for APC These negative values confirm that the adsorption of methyl red on these adsorbents is an exothermic process, releasing energy during the attachment of the molecules[26]. In addition, The negative value of ΔS ° confirms a chemisorption, where the dye molecules lose their disorder by fixing in an oriented manner on the surface, possibly with an organized displacement of the water molecules. The negative Gibbs free energy values (ΔG°) demonstrate the spontaneous nature of the process at the optimum temperature of 298 K. In

particular, the increasing negativity of ΔG ° with increasing temperature indicates an increased favorability of the process at higher temperatures.These thermodynamic results collectively suggest that, although adsorption occurs spontaneously in the studied temperature range, the process becomes even more favorable as the temperature increases, despite its exothermic character[27,28]. These findings collectively confirm that the dye molecules form strong chemical bonds with the APC and PC surfaces, resulting in an efficient and thermodynamically favorable removal process.

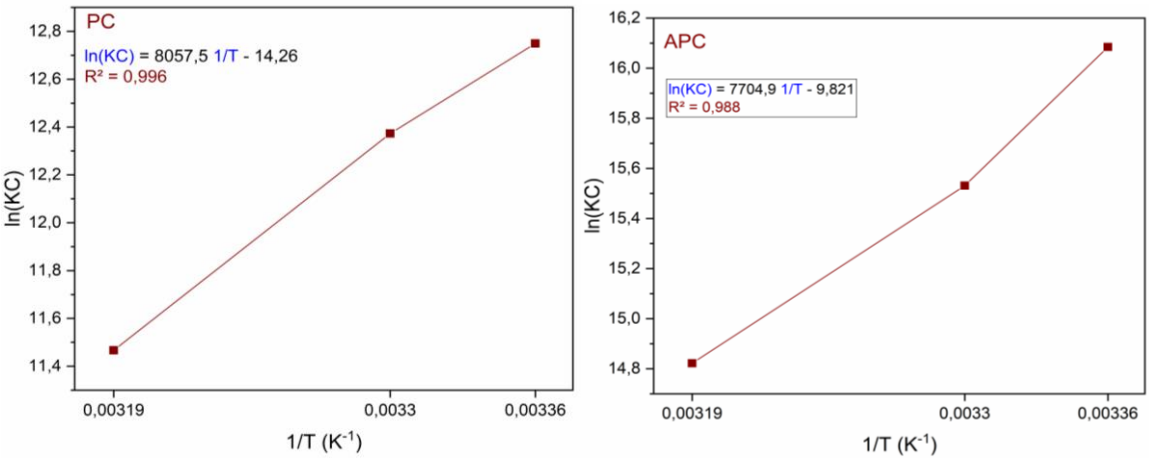

Figure V.10. Thermodynamic of PC and APC.

Table V.5. Thermodynamic parameters of PC.

Temperature (K)	ΔH° (kJ.mol^{-1})	ΔS° (J.mol^{-1}.K^{-1})	ΔG° (kJ.mol^{-1})	R^2
298	-66.99	-118.55	-31.659878	0.996
303			-31.06709	
313			-29.881514	

Table V.6. Thermodynamic parameters of APC.

Temperature (K)	ΔH° (kJ.mol^{-1})	ΔS° (J.mol^{-1}.K^{-1})	ΔG° (kJ.mol^{-1})	R^2
298	-64.05	-81.65	-39.726304	0.988
303			-39.318045	
313			-38.501527	

V.3. Conclusion

In this study, the adsorption of methyl red (MR) on adsorbents derived from biomass of pomegranate crusts, whether crude (PC) or chemically activated (APC), was examined. The interactions between the dye in aqueous solution and the adsorbents were studied, and a thorough characterization of the materials was carried out using the FTIR, XRD, TGA/DTA techniques, as well as by determining the zero charge point (pH_{pzc}).The characterization results revealed significant structural differences between the two adsorbents. The FTIR and XRD analyses revealed that the thermal and chemical treatment leads to the rupture of chemical bonds, a loss of mass and the formation of clusters, thus modifying the structure of the materials. These structural modifications, induced by chemical activation, allowed an improvement in the adsorption properties, reinforcing the efficiency of the PCA in the elimination of dyes. The point of zero charge was determined to be 6.5 for the APC. The adsorption of the MR showed a progressive increase over time, reaching equilibrium after 3 hours for the APC and 5 hours for the PC. The maximum adsorption capacity was observed with APC, reaching 44.78 mg/L, which is attributed to its higher specific surface area. The optimal adsorption conditions were obtained at a pH of 5 and a temperature of 25 °C. Under these conditions, a maximum yield of 91.5% was recorded with an initial MR concentration of 5 mg/L, an adsorbent dose of 300 mg/L for PCA and 500 mg/L for PC. However, lower adsorption capacities have been observed under certain experimental conditions, probably due to unfavorable electrostatic interactions between the negatively charged surface of the adsorbent and the anionic nature of the dye. The thermodynamic study revealed that the adsorption of MR is an exothermic process of the chemisorption type, as indicated by the negative values of the enthalpy ($\Delta H°$). In addition, the negative values of the Gibbs free energy (ΔG^{0}) confirm the spontaneity of the process. Thus, pomegranate crusts, in particular after chemical activation, prove to be very effective adsorbents for the elimination of methyl red.

References

[1] E. A. Khan et T. A. Khan, « Adsorption of methyl red on activated carbon derived from custard apple (Annona squamosa) fruit shell: equilibrium isotherm and kinetic studies », J. Mol. Liq., vol. 249, p. 1195-1211, 2018.

[2] T. A. Altalhi et al., « Adsorption of doxorubicin hydrochloride onto thermally treated green adsorbent: equilibrium, kinetic and thermodynamic studies », J. Mol. Struct., vol. 1263, p. 133160, 2022.

[3] M. Ikram et al., « Biodegradation of azo dye methyl red by Pseudomonas aeruginosa: optimization of process conditions », Int. J. Environ. Res. Public. Health, vol. 19, n° 16, p. 9962, 2022.

[4] Z. Zaheer, A.-A. Aisha, et E. S. Aazam, « Adsorption of methyl red on biogenic Ag@ Fe nanocomposite adsorbent: Isotherms, kinetics and mechanisms », J. Mol. Liq., vol. 283, p. 287-298, 2019.

[5] N. T. Nandhini, S. Rajeshkumar, et S. Mythili, « The possible mechanism of eco-friendly synthesized nanoparticles on hazardous dyes degradation », Biocatal. Agric. Biotechnol., vol. 19, p. 101138, 2019.

[6] E. Yılmaz, E. Sert, et F. S. Atalay, « Synthesis, characterization of a metal organic framework: MIL-53 (Fe) and adsorption mechanisms of methyl red onto MIL-53 (Fe) », J. Taiwan Inst. Chem. Eng., vol. 65, p. 323-330, 2016.

[7] R. Ahmad et K. Ansari, « Fabrication of alginate@ silver nanoparticles (Alg@ AgNPs) bionanocomposite for the sequestration of crystal violet dye from aqueous solution », Int. J. Biol. Macromol., vol. 218, p. 157-167, 2022.

[8] D. F. Romdhane, Y. Satlaoui, R. Nasraoui, A. Charef, et R. Azouzi, « Adsorption, Modeling, Thermodynamic, and Kinetic Studies of Methyl Red Removal from Textile-Polluted Water Using Natural and Purified Organic Matter Rich Clays as Low-Cost Adsorbent », J. Chem., vol. 2020, p. 1-17, mai 2020, doi: 10.1155/2020/4376173.

[9] M. Ghaedi, R. Hassani, K. Dashtian, G. Shafie, M. K. Purkait, et H. Dehghan, « Adsorption of methyl red onto palladium nanoparticles loaded on activated carbon: experimental design optimization », Desalination Water Treat., vol. 57, n° 47, p. 22646-22654, 2016.

[10] S. Gul et al., « Efficient removal of methyl red dye by using bark of hopbush », Water, vol. 14, n° 18, p. 2831, 2022.

[11] M. A. Ahmad, N. Ahmad, et O. S. Bello, « Modified durian seed as adsorbent for the removal of methyl red dye from aqueous solutions », Appl. Water Sci., vol. 5, nº 4, p. 407-423, déc. 2015, doi: 10.1007/s13201-014-0208-4.

[12] T. Tay, S. Ucar, et S. Karagöz, « Preparation and characterization of activated carbon from waste biomass », J. Hazard. Mater., vol. 165, nº 1-3, p. 481-485, 2009.

[13] A. C. Lua et T. Yang, « Characteristics of activated carbon prepared from pistachio-nut shell by zinc chloride activation under nitrogen and vacuum conditions », J. Colloid Interface Sci., vol. 290, nº 2, p. 505-513, 2005.

[14] W. M. A. W. Daud et W. S. W. Ali, « Comparison on pore development of activated carbon produced from palm shell and coconut shell », Bioresour. Technol., vol. 93, nº 1, p. 63-69, 2004.

[15] N. A. Rashidi et S. Yusup, « A review on recent technological advancement in the activated carbon production from oil palm wastes », Chem. Eng. J., vol. 314, p. 277-290, 2017.

[16] M. Jagtoyen et F. Derbyshire, « Activated carbons from yellow poplar and white oak by H3PO4 activation », Carbon, vol. 36, nº 7-8, p. 1085-1097, 1998.

[17] M. D. Teweldebrihan et M. O. Dinka, « Methyl red adsorption from aqueous solution using Rumex Abyssinicus-derived biochar: Studies of kinetics and isotherm », Water, vol. 16, nº 16, p. 2237, 2024.

[18] R. Foroutan, S. J. Peighambardoust, S. S. Hosseini, A. Akbari, et B. Ramavandi, « Hydroxyapatite biomaterial production from chicken (femur and beak) and fishbone waste through a chemical less method for Cd2+ removal from shipbuilding wastewater », J. Hazard. Mater., vol. 413, p. 125428, 2021.

[19] A. Khalfaoui, E. M. Bouchareb, K. Derbal, S. Boukhaloua, B. Chahbouni, et R. Bouchareb, « Uptake of Methyl Red dye from aqueous solution using activated carbons prepared from Moringa Oleifera shells », Clean. Chem. Eng., vol. 4, p. 100069, 2022.

[20] A. Bazan-Wozniak et R. Pietrzak, « Adsorption of cationic dye on nanostructured biocarbons: kinetic and thermodynamic study », Appl. Nanosci., vol. 13, nº 10, p. 6787-6801, oct. 2023, doi: 10.1007/s13204-023-02775-9.

[21] A. Benhouria, H. Zaghouane-Boudiaf, R. Bourzami, F. Djerboua, B. H. Hameed, et M. Boutahala, « Cross-linked chitosan-epichlorohydrin/bentonite composite for reactive orange 16 dye removal: Experimental study and molecular dynamic simulation », Int. J. Biol. Macromol., vol. 242, p. 124786, 2023.

[22] M. Sharma et al., « ZnO tetrapods and activated carbon based hybrid composite: Adsorbents for enhanced decontamination of hexavalent chromium from aqueous solution », Chem. Eng. J., vol. 358, p. 540-551, 2019.

[23] M. Sharma et al., « Efficient oil removal from wastewater based on polymer coated superhydrophobic tetrapodal magnetic nanocomposite adsorbent », Appl. Mater. Today, vol. 17, p. 130-141, 2019.

[24] N. O. Rubangakene, A. Elwardany, M. Fujii, H. Sekiguchi, M. Elkady, et H. Shokry, « Biosorption of Congo Red dye from aqueous solutions using pristine biochar and ZnO biochar from green pea peels », Chem. Eng. Res. Des., vol. 189, p. 636-651, 2023.

[25] M. Radjai et al., « Adsorptive removal of cationic and anionic dyes on a novel mesoporous adsorbent prepared from diatomite and anionic cellulose nanofibrils: Experimental and theoretical investigations », J. Mol. Liq., vol. 361, p. 119670, 2022.

[26] P. Doondani, V. Gomase, D. Saravanan, et R. M. Jugade, « Chitosan coated cotton-straw-biochar as an admirable adsorbent for reactive red dye », Results Eng., vol. 15, p. 100515, 2022.

[27] W. Konicki, M. Aleksandrzak, et E. Mijowska, « Equilibrium, kinetic and thermodynamic studies on adsorption of cationic dyes from aqueous solutions using graphene oxide », Chem. Eng. Res. Des., vol. 123, p. 35-49, 2017.

[28] N. Hassan, A. Shahat, A. El-Didamony, M. G. El-Desouky, et A. A. El-Bindary, « Mesoporous iron oxide nano spheres for capturing organic dyes from water sources », J. Mol. Struct., vol. 1217, p. 128361, 2020.

General conclusion and Prospects

General conclusion and prospects

The industry consumes considerable amounts of water. Industrial discharges, loaded with dyes and highly toxic and poorly biodegradable organic compounds, seriously disturb aquatic ecosystems. The treatment of effluents containing dyes is therefore crucial to preserve the environment. In addition, the search for inexpensive, locally available and effective materials could offer an alternative to commercial activated carbon for the removal of dyes from contaminated water. Developing new efficient, ecological, renewable and economical adsorbents remains a major challenge in the field of water treatment.

In this study, we used inexpensive plant biomass: turnip leaves (TL), pumpkin peels (PP) and pomegranate crusts (PC). These materials were used in the raw state and chemically activated, for the removal of crystal violet (CV), congo red (CR) and methyl red (MR) from aqueous solutions. We have developed a chemical activation protocol using phosphoric acid (H_3PO_4), leading to the formation of activated biomass (TLA, APP and APC). the APC was calcined at 450°C to obtain activated carbon.

The selected biomasses were characterized using various analytical techniques, including Fourier-transform infrared spectroscopy (FTIR), X-ray diffraction (XRD), scanning electron microscopy (SEM), and thermogravimetric analysis (TGA/DTG). The physicochemical characterization of these materials yielded the following results:

Fourier transform infrared spectroscopy (FTIR) revealed that the adsorbents tested present a great diversity of functional groups (-OH, C≡C, C-C, C=C and C-H), capable of interacting with the CV, CR and MR dyes in solution. The images obtained by scanning electron microscopy (SEM) revealed the presence of numerous cavities, testifying to the development of a porous structure. The surface of the activated biomass appears more porous and better organized, thanks to the chemical treatment with H_3PO_4. The X-ray diffraction (XRD) shows an amorphous structure for all the samples, whether they are raw or activated, indicating that the treatment with orthophosphoric acid has not modified their crystalline organization. The thermogravimetric study (TGA) of PP and APP shows a good initial thermal stability, followed by several successive degradation steps, linked to the loss of water, to the decomposition of the cellulose, then to the transformation of the residual carbon structures. Finally, the determination of the pH at the zero charge point (pH_{PZC}) showed values below 7, reflecting the slightly acidic nature of the surface of the materials.

However, the following conclusions have been drawn from the results obtained during tests carried out with synthetic solutions in distilled water:

- Our results demonstrate that an increase in the adsorbent mass leads to an improvement in the dye removal yields, reaching up to 90%.
- The results of the study of the effect of the initial concentration of CV, CR and MR demonstrate a significant influence of the concentration of dyes on the bleaching efficiency. In accordance with expectations, the higher the initial concentration of pollutants, the more the decolorization process is slowed down.
- The study of the influence of the pH has shown that the adsorption of the CV, CR and MR dyes strongly depends on the pH of the solution, with high elimination rates, exceeding 80%, in particular for the CV dye.
- The best fit of the experimental data was obtained with a high correlation coefficient (R^2) and a low chi-squared value (χ^2). The pseudo-second-order kinetic model proved to be the most suitable for describing the dynamic adsorption process on TL, TLA, PP, APP and APC powders, while Elovich's model offered a good description of the behavior of the PC adsorbent.
- The thermodynamic analysis revealed that the adsorption of the CV, CR and MR dyes on the TL (turnip leaves), PP (pumpkin peel) and PC (pomegranate crusts) biomass, as well as on their activated forms (TLA, PPA, PCA), had a spontaneous ($\Delta G < 0$) and exothermic ($\Delta H < 0$) character. These results confirm the thermodynamic feasibility of the adsorption process.
- The absorption properties at equilibrium of the different adsorbents (TL, TLA, PP, APP, PC and APC) were evaluated by modeling the absorption isotherms of CV, CR and MR dyes. The results revealed that :
    - For the TL, TLA, PP, APP and APC adsorbents, the Sips model presented the best fit to the experimental data, with maximum respective adsorption capacities of : 635.54 mg/g (TL), 621.76 mg/g (TLA), 265.52 mg/g (PP), 698.20 mg/g (APP) et 55.74 mg/g (APC). indicating adsorption on a heterogeneous surface
    - Regarding the PC material, the Langmuir model proved to be more suitable, presenting a maximum adsorption capacity of 7.39 mg/g, suggesting a monolayer adsorption on a homogeneous surface.

This thesis has resulted in the development of new bio-based adsorbents with remarkable performances for the simultaneous elimination of cationic (Crystal Violet) and anionic dyes (Congo Red, Methyl Red). The high adsorption capacities, the reproducibility of the results and the low cost of the materials developed confirm their potential for industrial applications in the treatment of polluted water.

Prospects

- To evaluate the effectiveness of adsorbents for the elimination of other priority contaminants, in particular heavy metals ($Pb2^{+}$, $Cd2^{+}$, $Hg2^{+}$) and pharmaceutical residues (antibiotics, anti-inflammatories, hormones).
- Synthesize new adsorbent composites (for example based on conductive polymers or nanomaterials) and evaluate their performance in systems: Unicomponent (selective adsorption of a single contaminant), Binary (competition between two simultaneous pollutants).

Abstract

This thesis focused on the valorization of local plant biomass, in the raw state and after chemical treatment with H_3PO_4, as economic and ecological adsorbents for the treatment of water contaminated with toxic dyes. Turnip leaves (TL and TLA) were used for the elimination of crystal violet CV, pumpkin peels (PP and APP) for congo red CR, and pomegranate crusts (PC and APC) for methyl red MR. The prepared adsorbents are characterized by several methods such as: XRD, textural analysis by, FTIR, TGA / DTG and SEM. The adsorbents were subjected to various elimination tests for crystal violet (CV), congo red (CR) and methyl red (MR) dyes under different experimental conditions: contact time, temperature, pH, initial dye concentration and adsorbent dose. The adsorption of the dyes by the different materials increases with the contact time. The pseudo-second-order kinetic model proved to be the most suitable for describing the dynamic adsorption process on TL, TLA, PP, APP and APC powders, while Elovich's model described the behavior of the PC adsorbent well. Regarding the adsorption isotherm, the Sips model showed the best fit for TL, TLA, PP, APP and APC. On the other hand, for the PC material, it is the Langmuir model which has proved to be the most suitable, with maximum adsorption capacities (q_max) of 635.54 mg/g, 621.76 mg/g, 265.52 mg/g, 698.20 mg/g, 55.74 mg/g and 7.39 mg/g respectively. Thermodynamic studies have demonstrated that the process of adsorption of dyes (CV, CR, MR) on our biomass is spontaneous and exothermic.

In conclusion, this study demonstrated that agricultural waste constitutes effective adsorbents for the elimination of anionic (CR, MR) and cationic (CV) dyes, thus offering a promising solution for the treatment of contaminated industrial water. It should be emphasized that the biomasses chemically activated with H_3po_4 have adsorption performances superior to those of the crude biomasses.

Keywords: Adsorption**;** Turnip leaves; pumpkin peels; pomegranate crusts; organic dyes; Chemical activation; phosphoric acid H_3PO_4.

Résumé

Cette thèse a porté sur la valorisation de la biomasse végétale locale, à l'état brut et après traitement chimique au H_3PO_4 comme adsorbants économiques et écologiques pour le traitement des eaux contaminées par des colorants toxiques. Des feuilles de navet (TL et TLA) ont été utilisées pour l'élimination du CV cristal violet, des écorces de citrouille (PP et APP) pour le CR rouge congo et des croûtes de grenade (PC et APC) pour le MR rouge méthyle. Les adsorbants préparés sont caractérisés par plusieurs méthodes telles que: DRX, analyse texturale par, FTIR, TGA / DTG et SEM. Les adsorbants ont été soumis à divers tests d'élimination des colorants cristal violet (CV), rouge congo (CR) et rouge méthyle (MR) dans différentes conditions expérimentales: temps de contact, température, pH, concentration initiale en colorant et dose d'adsorbant. L'adsorption des colorants par les différents matériaux augmente avec le temps de contact. Le modèle cinétique de pseudo-second ordre s'est avéré le plus approprié pour décrire le processus d'adsorption dynamique sur les poudres TL, TLA, PP, APP et APC, tandis que le modèle d'Elovich décrivait bien le comportement de l'adsorbant PC. En ce qui concerne l'isotherme d'adsorption, le modèle Sips a montré le meilleur ajustement pour TL, TLA, PP, APP et APC. En revanche, pour le matériau PC, c'est le modèle de Langmuir qui s'est avéré le plus adapté, avec des capacités d'adsorption maximales (q_max) de 635,54 mg/g, 621,76 mg/g, 265,52 mg/g, 698,20 mg/g, 55,74 mg/g et 7,39 mg/g respectivement. Des études thermodynamiques ont démontré que le processus d'adsorption des colorants (CV, CR, MR) sur notre biomasse est spontané et exothermique.

En conclusion, cette étude a démontré que les déchets agricoles constituent des adsorbants efficaces pour l'élimination des colorants anioniques (CR, MR) et cationiques (CV), offrant ainsi une solution prometteuse pour le traitement des eaux industrielles contaminées. Il convient de souligner que les biomasses activées chimiquement avec H_3PO_4 ont des performances d'adsorption supérieures à celles des biomasses brutes.

Mots clés: Adsorption; Feuilles de navet; Pelures de citrouille; croûtes de grenade; colorants organiques; Activation chimique; acide phosphorique H_3PO_4.

الملخص

ركزت هذه الأطروحة على تثمين الكتلة الحيوية النباتية المحلية ، في الحالة الخام وبعد المعالجة الكيميائية بـ H_3PO_4 كممتزات اقتصادية وبيئية لمعالجة المياه الملوثة بالأصباغ السامة. وقد استخدمت أوراق اللفت (TL و TLA) للقضاء على الكريستال البنفسجي CV، قشور اليقطين (PP و APP) للكونغو الأحمر CR والقشور الرمان (PC و APC) للميثيل الأحمر MR وقد تم تمييز الممتزات المعدة بعدة طرق مثل : DRX ، تحليل التكوينية من قبل ، FTIR، TGA / DTG و SEM. خضعت الممتزات لاختبارات التخلص المختلفة للأصباغ الكريستال البنفسجي والأحمر الكونجو وأحمر الميثيل في ظل ظروف تجريبية مختلفة: وقت التلامس ودرجة الحرارة ودرجة الحموضة وتركيز الصبغة الأولي وجرعة الممتزات. يزداد امتصاص الأصباغ بواسطة المواد المختلفة مع وقت التلامس. أثبت النموذج الحركي من الدرجة الثانية الزائفة أنه الأنسب لوصف عملية الامتزاز الديناميكي على مساحيق ، TL, TLA, PP, APP ,APC، في حين وصف نموذج إلوفيتش سلوك الممتزات PCجيدا. وفيما يتعلق إيسوثرم الامتزاز ، أظهر نموذج سيبس أفضل تناسب ل .TL, TLA, PP, APP ,APCمن ناحية أخرى ، بالنسبة لمواد PC ، أثبت نموذج لانجموير أنه الأنسب ، بقدرات امتصاص قصوى تبلغ 635.54 مجم/جم ، 621.76 مجم/جم ، 265.52 مجم/جم ، 698.20 مجم/جم ، 55.74 مجم/جم و 7.39 مجم/جم على التوالي. وقد أظهرت الدراسات الديناميكية الحرارية أن عملية امتصاص الأصباغ (CR, MR,CV) على الكتلة الحيوية لدينا هي عفوية وطاردة للحرارة.

في الختام ، أظهرت هذه الدراسة أن النفايات الزراعية تشكل مواد ماصة فعالة للتخلص من الأصباغ الأنيونية والكاتيونية ، مما يوفر حلا واعدا لمعالجة المياه الصناعية الملوثة. يجب التأكيد على أن الكتل الحيوية التي يتم تنشيطها كيميائيا لها أداء امتزاز أعلى من تلك الخاصة بالكتل الحيوية الخام

الكلمات المفتاحية: الامتزاز ؛ أوراق اللفت ؛ قشور اليقطين ؛ قشور الرمان ؛ الأصباغ العضوية ؛ التنشيط الكيميائي ؛ حمض الفوسفوريك